NIST Internal Report
NIST IR 8538

In-process monitoring and non-destructive evaluation for metal additive manufacturing processes

Alkan Donmez
Jason Fox
Felix Kim
Brandon Lane
Maxwell Praniewicz
Vipin Tondare
Jordan Weaver
Paul Witherell

This publication is available free of charge from:
https://doi.org/10.6028/NIST.IR.8538

NIST NATIONAL INSTITUTE OF STANDARDS AND TECHNOLOGY
U.S. DEPARTMENT OF COMMERCE

NIST Internal Report
NIST IR 8538

In-process monitoring and non-destructive evaluation for metal additive manufacturing processes

Alkan Donmez
Jason Fox
Felix Kim
Brandon Lane
Vipin Tondare
Jordan Weaver
Intelligent Systems Division
Engineering Laboratory

Maxwell Praniewicz
Sensor Science Division
Physical Measurement Laboratory

Paul Witherell
Systems Integration Division
Engineering Laboratory

This publication is available free of charge from:
https://doi.org/10.6028/NIST.IR.8538

September 2024

U.S. Department of Commerce
Gina M. Raimondo, Secretary

National Institute of Standards and Technology
Laurie E. Locascio, NIST Director and Under Secretary of Commerce for Standards and Technology

NIST IR 8538
September 2024

Certain equipment, instruments, software, or materials, commercial or non-commercial, are identified in this paper in order to specify the experimental procedure adequately. Such identification does not imply recommendation or endorsement of any product or service by NIST, nor does it imply that the materials or equipment identified are necessarily the best available for the purpose.

Note: All figures in this report are used and referenced with permission from the original publisher.

Publication History
Approved by the NIST Editorial Review Board on 2024-09-13

How to Cite this NIST Technical Series Publication
Donmez A, Fox J, Kim F, Lane B, Praniewicz M, Tondare V, Weaver J, Witherell P (2024) In-process monitoring and non-destructive evaluation for metal additive manufacturing processes. (National Institute of Standards and Technology, Gaithersburg, MD), NIST Internal Report (IR) NIST IR 8538. https://doi.org/10.6028/NIST.IR.8538

Author ORCID iDs
Alkan Donmez: 0000-0002-1324-1642
Jason Fox: 0000-0002-4585-8284
Felix Kim: 0000-0002-1042-9500
Brandon Lane: 0000-0001-5153-1678
Maxwell Praniewicz: 0000-0001-8800-4126
Vipin Tondare: 0000-0002-0483-1990
Jordan Weaver: 0000-0003-4857-5164
Paul Witherell: 0000-0002-6375-9482

Abstract

The rapid pace of maturation of metal additive manufacturing (AM) technologies makes them an excellent candidate for the fabrication of nuclear power plant (NPP) components. However, the current levels of process variations create numerous challenges for industrial acceptance of AM for NPP applications. One of those challenges is associated with the qualification and certification of fabricated components for safety-significant NPP applications. To reduce the cost of qualification and certification, in-process monitoring and in-process non-destructive evaluation (NDE) are considered essential tools. This report aims to support the efforts of the U.S. Nuclear Regulatory Commission (NRC) to meet the challenges of regulating NPP components fabricated by AM technologies. It provides a review of the current state-of-the-art in the areas of in-process monitoring and in-process NDE methods, instruments, and relevant standards. It also identifies gaps in knowledge, technologies, and standards to achieve the goal of using them as robust tools for AM process and part qualification.

Keywords

Additive manufacturing; directed energy deposition; in-process monitoring; non-destructive evaluation; powder bed fusion.

Table of Contents

List of Tables

List of Figures

Preface

This report was prepared as part of the interagency agreement (IAA) between the U.S. Nuclear Regulatory Commission (NRC) and the National Institute of Standards and Technology (NIST). The purpose of this report is to provide the NRC staff with the information to assess the technologies associated with in-process monitoring and non-destructive evaluation of the two most mature additive manufacturing processes used in manufacturing components for nuclear power plant applications. It also provides the standardization landscape associated with the in-process monitoring and non-destructive evaluation of these AM processes and resulting components, along with the gaps in related standards.

Acknowledgments

The authors acknowledge the support of S. Moylan and K. Jurrens of NIST and A. Hull of NRC in establishing the Inter Agency Agreement (IAA) to include the generation of this report. They also acknowledge the technical and editorial reviews of the following members of NIST and NRC staff: K. Jurrens, D. Deisenroth and A. Jones of NIST, A. Hull, E. Focht, M. Bayssie, C. Fairbanks, R. Tregoning, I. Anchondo-Lopez, J. Wise, C. Nove, and D. Rudland of NRC.

Executive Summary

With its capability for cost-effective fabrication of complex high-value components with significantly reduced lead times, metal additive manufacturing (AM) is considered as an alternative to conventional manufacturing technologies for small batch manufacturing applications, including aerospace, medical instruments and implants, and power generation. Manufacturing of components for nuclear power plants (NPPs) are among the emerging applications for this technology. However, due to the physical complexities of metal AM processes and the large number of influencing factors, it is difficult to estimate and obtain consistent properties of resulting printed parts. The variability of printed part properties and the lack of comprehensive standards associated with AM processes often require lengthy, expensive, and component-specific qualification for safety-significant applications making AM difficult to economically justify for small-batch production.

In-process monitoring and non-destructive evaluation (NDE) methods are used to reduce the qualification cost and lead times.

The objectives of this report are to review the state-of-the-art of in-process monitoring of AM processes and in-process NDE methods, identify technology readiness levels and their current use cases, as well as identify technology gaps for qualification of AM processes and components used in NPP applications.

To provide a proper context for the in-process monitoring and NDE methods analyzed, the report first describes (in Section 2) two metal AM processes, which are the most mature and common processes used in NPP applications. They are powder bed fusion (PBF) and directed energy deposition (DED) processes. For each process, Section 2 provides the general description of the process, the factors influencing printed part defects, and finally the process signatures, anomalies, and flaws observable by NDE methods that could result in printed part defects. Since this chapter is meant to provide a comprehensive learning tool about these two AM processes, not focusing on in-process NDE methods and the gaps, the readers who are familiar with these technologies can skip this chapter and directly go to remainder chapters. They describe the available in-process NDE methods (Section 3), related industry standards for these methods (Section 4), associated classification and considerations for the data generated by these methods (Section 5), and the use of such data for AM process and part qualification applications (Section 6). It should be noted that standards explicitly discussing in-process NDE for AM are few. Therefore, Section 4 provides the standards which have relevance to in-process NDE.

Section 7 describes the knowledge gaps and the recommendations to enable wide-spread use of the AM in-process monitoring and NDE methods in terms of technology readiness levels (TRLs) as well as the gaps in industry standards. These gaps and recommendations mostly extract higher-level gaps that span all in-process NDE technologies from existing industrial efforts, especially the reports by ASTM Additive Manufacturing Center of Excellence (CoE) and Additive Manufacturing Standardization Collaborative (AMSC), in which co-authors of this report have been active participants. In general, TRLs for in-process NDE methods are much lower than post-process NDE methods, many of them are currently under investigation by research institutes or small companies. Naturally, such low TRL levels result in the lack of adequate industry standards

for in-process NDE applications in the qualification of AM processes and parts. Therefore, in-process monitoring and NDE are currently not relied on as the principal sources of evidence for qualification in mission-critical applications.

List of Symbols, Abbreviations, and Acronyms

ABS
American Bureau of Shipping

AE
Acoustic Emission

AI
Artificial Intelligence

AIA
Aerospace Industries Association

AM
Additive Manufacturing

AMSC
Additive Manufacturing Standardization Collaborative

ANN
Artificial Neural Network

AWS
American Welding Society

BC
Bragg Cell

BV
Bureau Veritas

CAD
Computer Aided Design

CCD
Charge Coupled Device

CMOS
Complementary Metal-Oxide Semiconductor

CMT
Cold Metal Transfer

CoE
Center of Excellence

DED
Directed Energy Deposition

DEM
Discrete Element Method

DNV
Det Norske Veritas

DTR
Draft Technical Report (ISO)

EB-DED
Electron Beam Directed Energy Deposition

EB-PBF
Electron Beam Powder Bed Fusion

EBSD
Electron Backscatter Diffraction

EC
Eddy Current

ECT
Eddy Current Testing

EFCP
Equipment and Facility Control Plan

EHLA
Extreme High-Speed Laser Material Deposition

FAA
Federal Aviation Administration

FBH
Flat-bottom Hole

FDA
Food and Drug Administration

FMC
Full Matrix Capture

GMA-DED
Gas Metal Arc Directed Energy Deposition

GTA-DED
Gas Tungsten Arc Directed Energy Deposition

IR
Infrared

ISO
International Organization for Standardization

KED
Knife Edge Detector

L-DED
Laser Directed Energy Deposition

LIPA
Laser Induced Phased Array

LMD
Laser Metal Deposition

LOF
Lack of Fusion

L-PBF
Laser Powder Bed Fusion

LS
Laser source

LU
Laser ultrasonics

ML
Machine Learning

MPM
Melt Pool Monitoring

MSFC
Marshall Space Flight Center

MV
Machine Vision

NASA
National Aeronautics and Space Administration

NDE
Non-destructive Evaluation

NDT
Non-destructive Testing

NPP
Nuclear Power Plant

NRC
Nuclear Regulatory Commission

OCT
Optical Coherence Tomography

OEM
Original Equipment Manufacturer

OT
Optical Tomography

PA-DED
Plasma Arc Directed Energy Deposition

PAUT
Phased Array Ultrasonic Transducer

PBF
Powder Bed Fusion

PBS
Polarized Beam Splitter

PD
Photodetector

POD
Probability of Detection

PSD
Particle Size Distribution

PSPP
Process-Structure-Property-Performance

PWI
Preliminary Work Item (ISO)

QWP
Quarter Wave Plate

R&D
Research and Development

R&R
Repeatability and Reproducibility

SAW
Surface Acoustic Wave

SDO
Standards Development Organization

SD-OCT
Spectral-Domain Optical Coherence Tomography

SEM
Scanning Electron Microscopy

SNL
Sandia National Laboratories

SL
Structured Light

SLR
Single Lens Reflex

SPC
Statistical Process Control

SRAS
Spatially Resolved Acoustic Spectroscopy

TFM
Total Focusing Method

TOT
Time over Threshold or Time over Temperature

TR
Technical Report (ISO)

TRA
Technology Readiness Assessment

TRL
Technology Readiness Level

TTR
Transient Thermoreflectance

UL
Underwriter Laboratories

XCT
X-ray Computed Tomography

WAAM
Wire Arc Additive Manufacturing

WA-DED
Wire Arc Directed Energy Deposition

WEAM
Wire Electron Beam Additive Manufacturing

WLAM
Wire Laser Additive Manufacturing

1. Introduction

Metal additive manufacturing (AM) has been developed and improved as an alternative to conventional manufacturing technologies over the last several decades. It has reached a maturity level that makes it a feasible and cost-effective alternative for many critical industrial applications, such as aerospace, medical implants, and automotive [1]. Since the main advantages of AM include the cost-effective fabrication of complex high-value components in small batches with significantly reduced lead times, it is an excellent candidate for the fabrication of complex components of new-generation nuclear power plants (NPPs) as well as replacing components of the current designs [2, 3]. However, there are numerous challenges for industrial acceptance of AM for safety-significant NPP applications.

One of the most critical technical challenges facing the AM industry in general, and the NPP industry in particular, is the substantial material microstructure and geometric inconsistencies in the parts produced by AM processes. There are a large number of factors influencing the AM processes. While some of those are user selected/controlled such as programmed process parameters (e.g., thermal power density, layer thickness, hatch spacing, etc.), other factors, such as variations in feedstock characteristics, inert gas flow, disturbances due to molten metal spatter, and plume of evaporated metal and other contaminants generated during the process, are hard to control by the AM operators. Such a significant number of influencing factors and the complex interactions among them cause unforeseen short-term (within a single build) and day-to-day variations in the outcomes of these AM processes as well as lack of adequately robust process-structure-property-performance (PSPP) relationships lead to potential difficulties in predicting the quality of the fabricated components.

The variability of part properties and the lack of comprehensive standards often require lengthy, expensive, and component-specific qualification for safety-significant applications, making it difficult to economically justify for small-batch production. Therefore, the AM research community spends significant effort to improve the understanding of the cause-and-effect relationships among the influencing factors and the resulting process variations [4]. In parallel to these efforts, monitoring and assessing the process variations to predict their impact on final product quality are of the highest priorities within the AM development and application community, as well as within the scope of the recent roadmaps for the improvement of AM technologies [5]. For example, the Additive Manufacturing Standardization Collaborative (AMSC) has recently completed the third version of its Standardization Roadmap for Additive Manufacturing, confirming the high priority of needs for process monitoring [5].

In view of these ongoing developments, the objectives of this report are to review the state-of-the-art in in-process monitoring of AM processes and in-process non-destructive evaluation (NDE) methods, identify technology readiness levels and their current use cases, as well as identify technology gaps for qualification of AM processes and components used in NPP applications.

There are several types of AM processes used with metals, the most common, NPP-relevant, and advanced AM processes are powder bed fusion (PBF) and directed energy deposition (DED).

Therefore, this report covers in-process NDE methods applicable only to these two types of AM processes. Both PBF and DED processes as well as factors influencing these processes will be described in Sec. 2.

Although there are some common techniques used, in-process NDE is categorically different from post-process NDE, or more commonly known simply as just "NDE." Multiple NDE methods to inspect and qualify manufactured products have existed for decades [6]. Most of them are applicable to AM-fabricated components as well [7]. NDE methods help reduce the cost of final product qualification (i.e., conformance to specifications) without altering the characteristics of the components under test. These methods are most useful in checking the integrity and condition of internal features (such as microstructures, pores, cracks, or deformations) of the components.

For mature conventional manufacturing processes, where the variations of the resulting products are within a known set of limits, NDE methods along with other post-process measurements applied to a sampling of the manufactured products would provide robust statistics for the quality assurance of the whole batch of the products. Statistical process control (SPC) methods are used to monitor the performance of manufacturing processes in terms of critical quality metrics of the manufactured products, such as dimensional, surface finish, and material characteristics, to detect significant variations that result in product quality degradations. Traditionally, such quality metrics are obtained by post-process inspection and the trends in variations of these metrics are determined by statistical control charts. Necessary adjustments in manufacturing process parameters are implemented based on these control charts to avoid producing parts not conforming to their specifications [8].

In conventional manufacturing processes, SPC is used as a complementary control scheme along with other system control methods. For example, in metal cutting applications, machine tools have their own control systems relying on real-time sensor information to implement feedback and feedforward control algorithms to generate accurate motion of the cutting tool [9]. To enable such real-time control, sensor data must be provided to the controller at high update rates (on the order of 10 kHz or higher). Similar control algorithms are also applied in PBF and DED machines. However, due to the very high speeds of moving energy sources in PBF machines, data rates for sensors must be at least an order of magnitude higher. On the other hand, since AM processes generate parts layer-by-layer, there may be opportunities to adjust process parameters intermittently (between each layer), which relaxes the requirements of high sensor data update rates.

Although there are some efforts described in the literature, SPC is not widely used for AM processes [10]. For AM processes, as mentioned earlier, excessive process variability resulting from a large number of influencing factors causes unexpected defects in the fabricated products reducing part quality. The complexity of interactions between the influencing factors and the AM process makes SPC based on post-process inspection of product quality characteristics generally ineffective. Furthermore, since part defects are detected only after the completion of the build process, they increase the scrap rates, leading to a further increase in the cost of metal AM applications.

In contrast with post-process NDE, in-process NDE is an emerging technology comprising various methods that are used to qualify the fabricated part while it is being built. While in-process NDE is used to detect any imperfections in observed printed layers, in-process monitoring is used to detect any AM process anomalies potentially leading to flaws in the printed layers. However, it is important to note that cause-and-effect relationships between process anomalies and part flaws are currently not well established and are the subject of ongoing research. In the absence of such clearly defined relationships, in-process monitoring can be used for assessing process stability, which is the first step of the qualification of the AM processes. Qualification of AM processes is a means to confirm that the particular process will operate consistently, producing parts with quality characteristics within acceptable limits established for a given application. AM process qualification will significantly reduce the cost of qualification of the resulting products. Furthermore, the information obtained from in-process monitoring and in-process NDE is also useful to identify the regions of the final product suspected of having defects, on which to focus the post-process NDE tests, reducing the overall inspection effort and the cost of product qualification. However, for NPP applications, required post-process NDE of a part will likely be dictated by nuclear code, potentially limiting the flexibility to focus only on certain areas.

An additional future benefit of in-process monitoring and in-process NDE is the ability to implement layer-wise process control by adjusting the programmable process parameters once the deviations from normal process conditions are detected. There is even potential to implement real-time process control (e.g., by adjusting power levels, scan speed, and positions on the fly) within layers when data acquisition and analysis speeds are adequately increased in the future. Until such capabilities are readily available, information obtained from in-process monitoring and in-process NDE can be useful for statistical control purposes by identifying conditions beyond acceptable thresholds or trends towards those conditions [11].

Although there are standards providing terminology for general (post-process) NDE methods [12], due to the differences mentioned above, the terminology used in the context of in-process NDE differs from that of the post-process NDE. However, due to its emerging nature, there is no consensus in the AM community about the terminology related to in-process NDE. This is considered an important technical gap for reaching a common understanding of potential capabilities and impacts of in-process NDE. Therefore, a set of definitions applicable to in-process NDE covered in this report is provided below. In the proposed definitions, the difference between in-process monitoring and in-process NDE is based on the difference in their direct goals. In-process monitoring is first and foremost concerned with process qualification and process anomalies. When in-process monitoring methods become focused on detecting flaws and defects in the physical part, this becomes in-process NDE. The distinction between in-process monitoring and in-process NDE is not always clear in every scenario.

Definitions used in this report:

In-process monitoring – measurement or observation of process signatures during a build, including feedstock delivery and machine conditions.

In-process NDE – non-destructive detection and evaluation of *solidified part* properties, at any point in time during the build, without altering its characteristics. It

does not include the measurement of AM process (i.e., feedstock material delivery and melting/solidification of material).

Process qualification – acts of gaining objective evidence that the process is able to operate at a certain standard level during sustained operation and the output will meet specified requirements within a known confidence interval.

Part qualification – acts of gaining objective evidence that the part meets specified requirements within a known confidence interval.

Imperfection – a departure of a quality characteristic from its intended condition. [12]

Discontinuity – a lack of continuity or cohesion; an intentional or unintentional interruption in the physical structure or configuration of a material or component. [12]

Indication – the response or evidence from a non-destructive examination. An indication is determined by interpretation to be relevant, non-relevant, or false. [12]

Process Signature – observable (expected and unexpected) physical phenomenon associated with the selection of process parameters and other conditions. Process signatures are observed or measured before being characterized as anomalous (modified from ASTM E3353 [13]).

Process Anomaly – unexpected variation of signature. Process anomalies are characterized by measurement or observation. Observations may be indirectly quantified using various data processing tools. Interpreted indications of anomalies are used to assess false, relevant, and non-relevant process anomalies. Evaluations or classifications of relevant anomalies determine the critical and non-critical process anomalies based on the process specifications.

In-Process Flaw – an imperfection or discontinuity in the solidified part during the build process that may be detectable by in-process nondestructive testing (including in-process monitoring) and is not necessarily rejectable. (This is the ASTM E1316 definition with "in-process" added). In-process refers to the fact that the flaw exists in the part at a moment in time during the process. It may not be the same or exist during the final part inspection.

In-Process Defect – one or more in-process flaws whose aggregate size, shape, orientation, location, or properties do not meet specified acceptance criteria and are rejectable. (Modified from ASTM E1316 [12]). In-process refers to the fact that the defect exists in the part at a moment in time during the process. It may not be the same or exist during the final part inspection.

It should be noted that within the context of this report, in a multi-layer AM build process, the "process" has two distinct components: (1) feedstock delivery and (2) melting and solidification and consolidation of material by moving energy sources. *In-process flaw* and *in-process defect* are application-specific terms; critical thresholds for in-process flaw and acceptance criteria for in-process defect are determined by the end-use acceptable part performance criteria. Furthermore, in-process flaws/defects exist at a moment in time during the build process; however, due to remelting in the line-by-line and layer-by-layer process, they may be modified

or eliminated before the part fabrication is completed. This is referred to as the "self-healing" phenomenon (see Sec. 7.1). Therefore, the relationship between in-process flaws and defects and the final part flaws and defects are not always directly correlated. There is some probability that in-process flaws indicated by in-process NDE will be remelted and no longer exist in the final part, thus resulting in a "false positive" if post-fabrication NDE is used as a ground truth for defect identification. It should also be noted that the above definitions do not consider the correlations between process anomalies and product defects. Currently, limited knowledge exists related to such correlations.

The remainder of this report is organized as follows. Section 2 provides an overview of the two common laser-based metal AM processes: PBF and DED. For each process, this section provides the general description of the process, the factors influencing printed part defects, and finally the process signatures, anomalies, and flaws observable by NDE methods that could result in printed part defects. Section 3 provides descriptions of available in-process NDE methods, including melt pool monitoring methods, optical and machine vision methods, and acoustic and electromagnetic methods, and the current state-of-the-art of those, along with their associated technology readiness levels (TRLs). TRLs provide metrics to assess the maturity of a particular technology throughout its research, development, and deployment phases. TRLs, on a scale from 1 to 9, indicate the levels of technology maturity, 9 being the most mature technology ready for commercial deployment. Section 4 reviews the existing codes and standards for in-process NDE, including the ongoing efforts in relevant standardization. Section 5 reviews the classification of data obtained from in-process NDE for use in the AM process and part qualification. Section 6 describes use cases of in-process NDE along with modeling and test data for AM process and part qualifications. Section 7 discusses the knowledge gap analysis of in-process NDE to ensure part quality, as well as associated TRLs of various in-process NDE methods. It should be noted that this gap analysis has a limited scope involving only in-process NDE-related issues. Section 8 provides a summary and conclusions along with the recommended actions for further developments. It should be noted that the common theme running through the document is that measurements must be useful and practical for industrial applications. Measurement capabilities/requirements (e.g., required frequency, resolution, etc.) as well as data management/integration/fusion requirements are impacted by these criteria.

2. Overview of metal AM technologies

2.1. Laser powder bed fusion (L-PBF)

Powder bed fusion (PBF) is a category of an additive manufacturing process in which thermal energy selectively fuses regions of a powder bed [14]. PBF processes can be used to manufacture components made from multiple classes of materials including polymers and metals. **Figure 2.1** depicts the laser PBF process. During the process, a powder feedstock is spread over the build plate in a thin layer. The energy source then scans over the build area to fuse the powder feedstock, by melting and solidifying it as it passes over an area of powder on the build plate according to the path prescribed in the build file to fuse the first layer. Once the material is fused to the build plate, the build platform is lowered according to the prescribed layer thickness.

Powder feedstock is then spread over the previously fused layer and the fusion process is repeated using the path prescribed in the build file to fuse the second layer. This process is then continuously repeated with many newly spread powder layers until the prescribed component geometry is completed. The melting of powder creates a pool of molten metal, called a melt pool, which fuses to the adjacent solid regions during the solidification starting immediately after the energy source passes over. The two most common thermal energy sources used for the PBF of metals are high-power laser (L-PBF) and electron beams (EB-PBF). PBF processes are performed in controlled environments; inert gas, such as nitrogen or argon, for L-PBF processes and vacuum for EB-PBF. L-PBF systems are often capable of smaller feature sizes than EB-PBF processes due to a more concentrated energy source [2]. Compared to other additive manufacturing processes, such as directed energy deposition (DED), PBF processes are capable of producing much finer features and greater geometrical complexity due to the small layer sizes (20 µm to 150 µm) and smaller melt pool sizes (≈100 µm) [15]. The part sizes produced by PBF processes are limited by the size of the build chamber, which vary from system to system. Generally, PBF processes are able to produce small to medium size components and features (1 mm – 1 m).

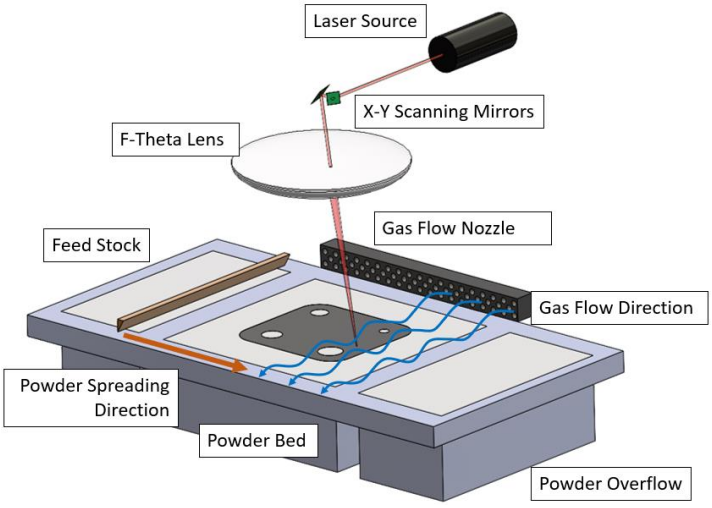

Figure 2.1 Schematic of the L-PBF process.

2.1.1. Factors influencing printed part defects

The L-PBF process is influenced by a multitude of parameters and conditions. These have been generally classified into four major categories: feedstock material, build preparation, process influences, and equipment influences.

2.1.1.1. Feedstock material

Similar to many other manufacturing processes, the quality of feedstock material utilized in PBF processes greatly affects the quality of the final components. Bulk powder properties such as flowability and packing density directly influence the powder layer characteristics, which contribute to the final component quality [16]. These two factors are largely attributed to the powder size distribution and the particle morphology. Smaller particle sizes can increase the

packing density but can also lead to poor flowability and cause irregular powder layer spreading and clumping [17]. Despite this poor performance in flowability, fine powders have been found to produce mechanical properties (e.g., density, hardness, strength) similar to coarse powder sizes [18, 19]. Powder particle morphology also has been shown to influence the spread powder layer characteristics. Powder with spherical particles can have the most efficient particle packing. This can create a denser powder layer, which can produce higher-density components [20, 21]. Improved methodologies for the characterization of powder feedstock are needed to ensure their quality [22]. Assessment of uncertainty in powder rheology and particle size distribution measurement are important areas of research [23, 24].

Metallic powders can also become contaminated with organics or other absorbed gasses. Oxide or nitride films can form on the surfaces of powder particles. Contamination from these sources can result in poor fusion of the material and degrade mechanical properties [25]. Studies on the reuse of powder feedstock have shown differing results in terms of mechanical properties, but feedstock reuse clearly influences particle size distribution and contamination [26 – 29]. Powder reuse can also be executed in various forms as defined in ASTM F3456 − 22 (no reuse, discrete reuse, continuous reuse, in-process powder reuse, continuous refreshing with virgin powder, etc.) to tailor the process to the requirements of the end product [30]. Gas entrapped within powder particles during their production can also remain present in the final component as gas pores [31].

AM feedstock also needs to be stored properly. If the powder is exposed to a humid environment, its properties can degrade due to moisture contamination. Such inappropriate powder storage can lead to poor part performance [32].

In the case of titanium alloys, it is recommended that powder should be stored in a metal container, which is backfilled with argon. The same is recommended for aluminum alloys. Further, a temperature and humidity-controlled location for storage of the containers may provide additional protection [32]. It should be noted that AlSi10Mg feedstock is particularly vulnerable to moisture and oxygen pick-up. It can degrade its spreadability causing a relatively poor powder bed density. It can also create porosity during the melting process [33]. Nickel-based alloys (IN718) can be stored in a sealed container made up of metal or plastic [32]. Steels and stainless steels can be stored in sealed containers made of metal or plastic and stored with inert desiccant materials to reduce moisture content in the container.

In general, any metal AM powder must be kept in a fully sealed container, preferably in a metal container and an inert atmosphere. Certain storage solutions may offer better protection to metal powders, but still, metal powders show slight changes in their properties if stored 6 months or longer [32]. However, the effects of storage and handling conditions on the L-PBF process are not well understood. Therefore, there is no general rule about the optimal length of time for storage of metal powders. So, prolonged storage time is not recommended.

2.1.1.2. Build preparation

The factors during the preparation of geometry files for a PBF process can also contribute to defects within finished components. The two main items to consider are the position and

orientation of components within the build volume and the design of support structures [34]. The layer-wise nature of PBF can create form and dimensional errors on critical features if not properly oriented within the build volume [35, 36]. The orientation of surfaces relative to the build direction has been shown to have a significant effect on the surface texture [37, 38]. Component orientation also has been shown to have a significant effect on the residual stress within components due to the buildup of thermal energy [39]. The position and orientation of components within the build volume influence microstructural anisotropy resulting in anisotropy in mechanical properties and fatigue life [40, 41]. The design of support structures is another aspect of the PBF process, which, if not designed carefully, can introduce errors into the process and the final component. Generally, supports should be able to prevent components from collapse/warping during the PBF process while maintaining minimal contact area and cross-section to allow for easy removal and using minimal material volume to minimize waste [42]. Inadequate support structure design could lead to significant internal stresses, geometric errors, and build failure due to binding with the recoater mechanism [39, 43]. Design guidelines have been developed to help mitigate these influences [44].

2.1.1.3. Process influences

The user-programmed parameters that dictate a PBF process arguably have the largest influence on the generation of defects. Although there are many process parameters that significantly influence the LPBF process, depending on the PBF system, only a limited set of these parameters may be available for the user to change. The laser power (for L-PBF) or electron beam energy (for EB-PBF), energy source scan velocity, layer thickness, and hatch spacing (the lateral distance between adjacent melt pool tracks) are the most common ***user-programed parameters***. While each of these parameters contributes individually to the quality, they are largely interconnected [45 – 49]. The relationship between these parameters is often described using energy density, a measure for the averaged applied energy per volume of material during the scanning of a layer [48]. While the energy density is a large contributor to the anticipated quality of a PBF process, there may not be a simple linear relationship to guarantee quality [46]. **Figure 2.2** provides examples of process maps, which show the connection between scan speed and laser power with other parameters held constant for various L-PBF processes. These maps are often divided into different processing windows with respect to defects or resultant component properties (e.g., porosity, residual stress). The range of parameters that produce an acceptable result in the PBF process is often bordered on both sides by unacceptable process results. High laser speeds and low laser powers do not introduce enough energy for the fusion of the feedstock material resulting in lack-of-fusion (LOF) type defects [50]. Low laser speeds and high power provide too much energy into the fusion process causing overheating of the heat-affected zone, resulting in keyhole porosity (deep cavities in the melt pool created by vaporization of liquid metal) and/or balling (a phenomenon when powders are either not sintered at all or completely melted and join into large droplets) [47, 51 – 53]. The optimal process window will change for different combinations of AM systems or materials. The component geometry may also influence the optimal process window [54]. Often, the AM system manufacturer-specified parameters for material will fall within the acceptable process window, though they can be optimized further based on the user's requirements to improve productivity while mitigating defects. Changes in

these parameters can lead to residual stresses/cracks, porosity, balling, and unfavorable microstructures [46, 47, 55].

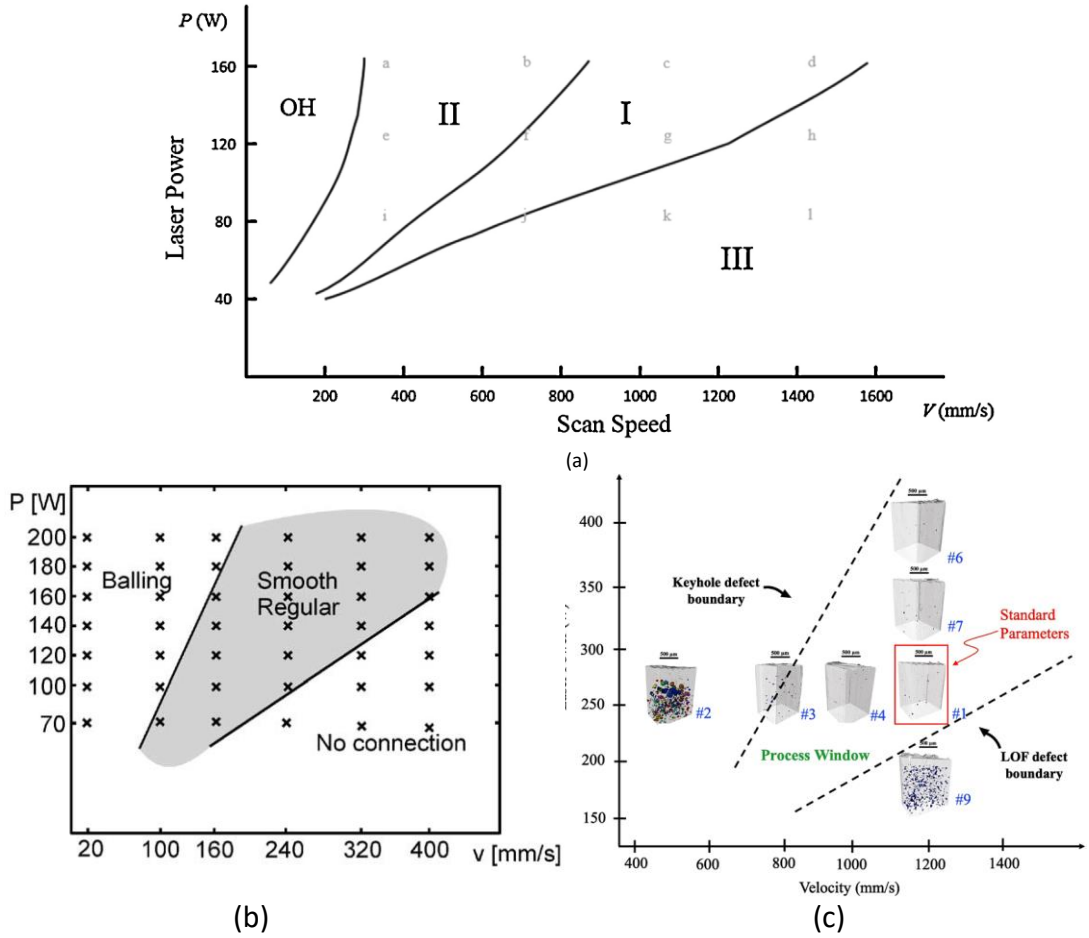

Figure 2.2 Examples of Process Maps for L-PBF processes: (a) Ti-6AL-4V process map divided into four melting zones: "fully dense" (Zone I), "over melting" (Zone II), "incomplete melting" (Zone III), and "over heating" (Zone OH) [46]; (b) iron process map optimized to mitigate balling (X's show sampling within the parameter space with the process regions defined as "smooth regular" weld tracks bordered by balling and poor interlayer connection) [47]; (c) EOS (AM system manufacturer) process map for identifying regions of Ti-6Al-4V defect types [49].

Because of the layer-wise nature of additive manufacturing, the geometry manufactured is always approximated by discrete slices instead of continuous surfaces along the vertical direction. Thus, larger layer thicknesses will lead to larger geometric imperfections and rougher surfaces due to a larger step size used to represent a continuous geometry [56]. As discussed above, a change in layer thickness will also necessitate changes in the other user parameters to keep the system within a "good" operating window. However, commercial PBF systems do not typically provide the flexibility of varying layer thickness within a build. Often, they provide the user with limited control over the details of the scan pattern. The scan parameters can also be modified for upskin (upward facing) or downskin (downward facing) surfaces to improve the surface quality and consistency of melt pool depth [44, 57]. Contour passes along the boundary of the solidified layer geometry can be used to improve geometric accuracy and surface quality [58]. Advanced planning of the scan path can also greatly reduce the residual stress and defects

[59 –61]. Advanced geometry-based laser power control can also increase the consistency of the melt pool withing L-PBF processes [59]. However, these advanced controls are not common in commercial PBF systems.

Intrinsic process characteristics, which cannot be directly controlled by the user, constitute another group of factors influencing the PBF process and its signatures that affect component quality. The ejection of particles or molten metal during the fusion process, commonly referred to as spatter, has an adverse effect on component quality. Spatter can be categorized into several types resulting from differing formation mechanisms [62 – 64]. Spatter (liquid or solid) can range in size and can be up to four times the size of the powder particles [65, 66]. Ejected spatter particles often differ in chemical composition from the original feedstock material due to oxidation, thus changing the local material composition if they are fused into the component [67, 68]. The ejection of spatter particles can come from several locations within the melt pool, but the general path of ejected particles often follows the flow pattern of the shielding gas used [69 – 71]. Thus, some of the effects of spatter can be mitigated by altering the order of component fabrication within a layer (when multiple components are fabricated on the same build plate). Components built within regions known to be spatter-rich (regions in which ejected spatter particles are more likely to be deposited) are typically fused first within a layer to reduce the possibility of spatter contamination from other components within the layer [72].

During the PBF process, thermal energy may vaporize part of the melt pool to create a metal vapor 'plume' [73]. The plume is affected by the beam diameter, beam power, beam velocity, scanning strategy, and inert gas flow [74]. This plume can attenuate the laser power transmitted to the melt pool through scattering and absorption, resulting in reduced energy density [64]. This becomes more problematic for multi-laser PBF systems, where the plume from one laser can affect the power applied by the other [75].

Rapid heating and cooling of regions with fast-moving energy sources cause significant thermal gradients in the parts being printed. This results in the buildup of internal stresses, which can lead to crack formation and propagation. To decrease the thermal gradient between the baseplate and the melted powder surface, the baseplate is pre-heated [76]. However, the baseplate pre-heating temperature needs to be set depending on the processed material and its phase transformations [76]. Long exposure to preheating temperature can affect the microstructure of some alloys [76].

2.1.1.4. Equipment influences

As with any manufacturing process, the quality of the produced components is highly dependent on the quality of the manufacturing equipment. Defects can come from inappropriate settings, poor performance, and improper system calibration.

Energy source and delivery system (optical chain) can lead to significant anomalies in L-PBF processes if they are improperly calibrated or controlled. In L-PBF processes, errors in the construction and alignment of the optical system used for laser delivery can lead to component geometric errors and losses in laser power [77]. The elliptical distortion of the laser spot at the edges of the working volume due to non-orthogonal incidence with the build plane also changes

the shape and energy density, potentially leading to lack-of-fusion [78]. Improper scaling of the laser-steering control system, laser following error and synchronization error, and incorrect settings of the beam offset can also lead to geometric errors and porosity within components [79 – 81]. Examples of these control errors can be seen in **Figure 2.3**. Fluctuations of the laser source from the commanded power, particularly at high power levels, can also lead to inconsistent melt pool geometries and cause excess plume and lack-of-fusion [82].

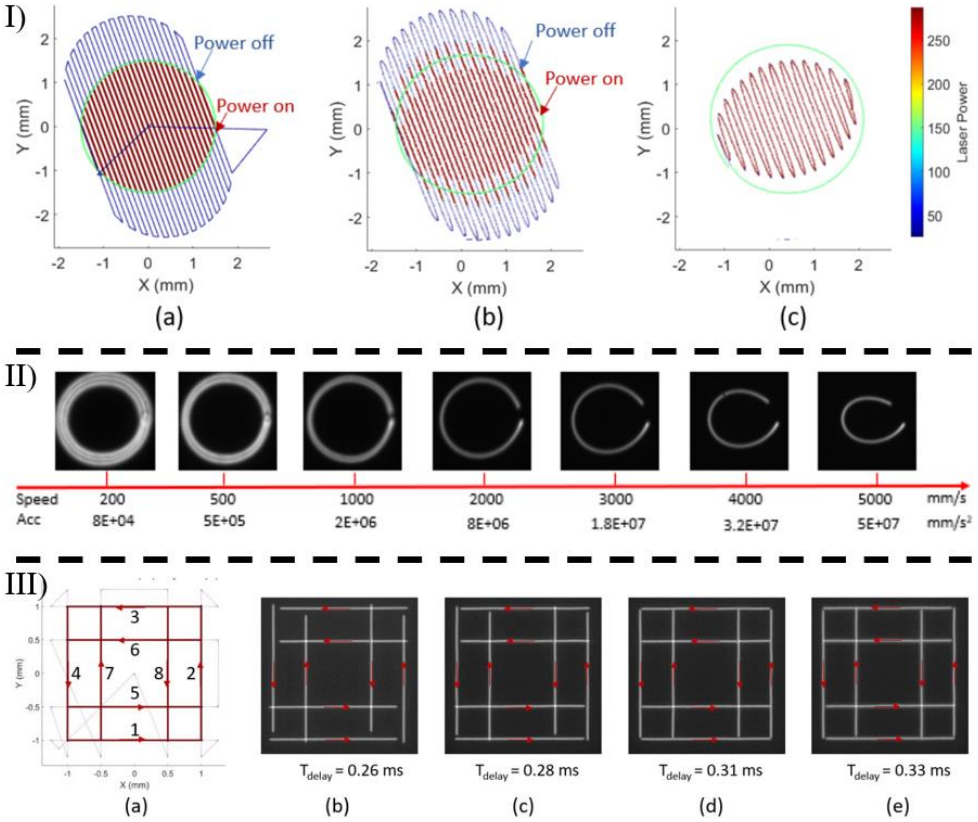

Figure 2.3 I) Laser delay time synchronization errors can lead to geometric errors (shown as incomplete circle geometry) II) Laser-steering acceleration limits can limit the maximum laser velocity, leading to positioning errors (shown as roundness errors).. III) Laser power-position synchronization calibration. Images taken at different delay times show overlapping / incomplete intersection of lines. [82]

Environmental factors within the L-PBF build chamber can contribute to process anomalies and the formation of defects. The preheat temperature of the build plate is critical to reducing residual stress, cracks, and delamination within completed components [83, 84]. Reduced residual stress also decreases component deflection [85]. The inert gas quality and flow pattern within the build chamber are large factors influencing the L-PBF process. Too low of inert gas velocity would be insufficient to clear the vapor plume of the melt pool and too high of gas velocities can disturb the spread powder layer [87]. Insufficient gas flow has also been found to cause asymmetric, shallow, and wide melt tracks that may cause lack-of-fusion defects [87]. The gas flow has been found to vary significantly throughout the build area, adding the potential for certain locations within the build volume to be more defect prone. [88].

Powder-spreading equipment is another important influencing factor. Usually, the powder is spread using a recoater blade or a roller. Recoater blades can be rigid steel, ceramic blades, or flexible silicone blades. A flexible blade is usually used for delicate and high aspect ratio parts. The geometry of the recoater blade or roller also plays an important role in achieving a good-quality spread layer. The effects of various blade-geometries on the powder spreading process have been examined by Wang et al. [89] using discrete element method (DEM) simulation, as shown in **Figure 2.4**. An appropriate powder-spreading mechanism for a specific powder particle size distribution (PSD) is required so that particles get deposited in front of the recoater blade or roller, or at the bottom of the advancing powder heap. The particles should not move upward to create a rotational motion within the advancing powder heap [89]. **Figure 2.4 f)** shows the most desirable outcome for the simulated PSD (D10 = 25.9 µm, D50 = 39.4 µm and D90=52.7 µm).

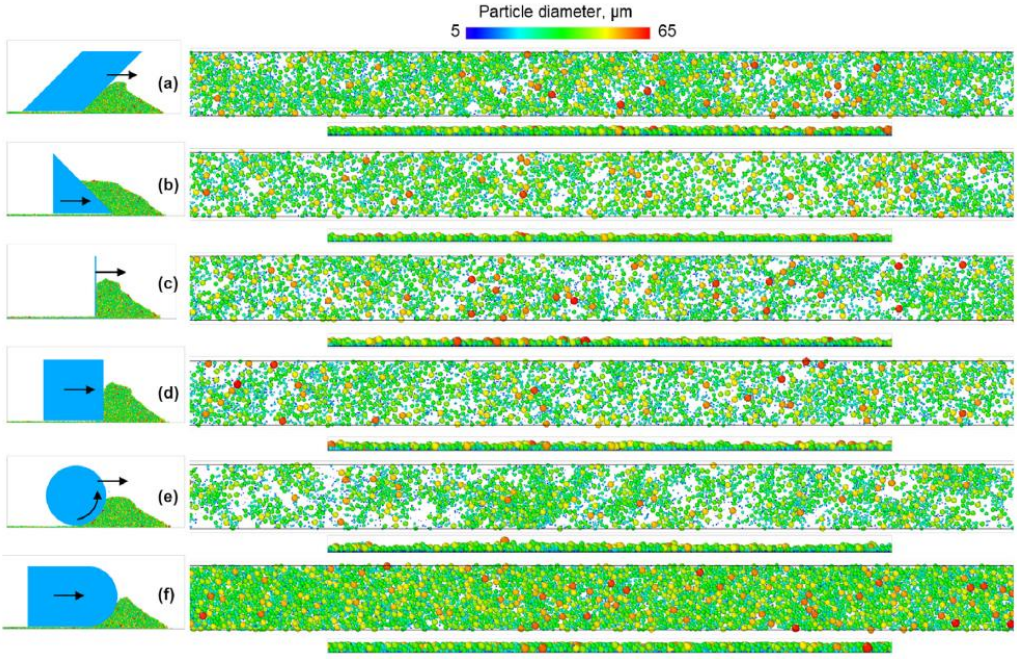

Figure 2.4 Simulated cross-sectional view of different spreaders and top-view and cross-sectional view of the corresponding spread layers: (a) inclined blade, (b) declined blade, (c) vertical blade, (d) wide blade, (e) roller, and (f) round blade. Ideally, the spread powder should form a uniform layer. Adapted from [89].

The goal is always to achieve a uniform and dense spread layer. For example, in contrast with the study described in [89], which used powder of relatively large particle sizes, small-particle cohesive powders may be spread better using rollers [90]. It should be noted that there is also an effort to develop a new method for contact-free powder spreading [91]. Apart from the quality of the feedstock, the selected layer thickness can impact the feature resolution of the built parts. The smaller the layer, the smaller the feature resolution in the layering (i.e., vertical or z-axis) direction. However, selecting a smaller layer thickness also affects spread layer quality, especially on rough surfaces. In general, a larger layer thickness can have a more uniformly spread layer. The speed of the recoater used can also affect the spread layer uniformity and powder bed density [92]. Further, the presence of fine particles can increase the powder bed density as they fill voids among bigger particles, but a high amount of fine (< 20 µm) particles in the feedstock can lead to agglomeration and a non-uniform powder spreading [93].

2.1.2. Process signatures, anomalies, and in-process flaws

While there are many signatures of the L-PBF process that can be monitored using in-process sensing, there are three main categories of process signatures that are investigated: the spread powder layer, the melt pool, and the fused layer. Each of these is described in more detail below.

2.1.2.1. Spread powder layer

L-PBF machines use metal powders with average particle sizes, typically in the range of 25 µm to 45 µm [94]. A dense and homogenous powder bed that is free from voids is essential for optimum thermal diffusivity, creating a uniform fusion of the powder bed and better performance of the finished parts [95]. Anomalies in the spread powder layer can occur during the powder-spreading stage of the process [96]. The quality of powder bed is monitored using machine vision systems as explained in Section 3.2. ASTM F3522-22 covers in detail the powder spreading process failure modes, causes, and effects on parts. **Figure 2.5** shows some of those examples. Insufficient powder coverage (short feed) can be caused by insufficient dosing or too high speed of powder spreading. Track lines may be caused by dragging of a spatter particle, a contaminant, or an agglomerate, etc. or by a damaged recoater. Non-uniform bed surface can be caused by cohesion, moisture in the powder, and electrostatic or magnetic effects. Non-uniform bed density can be caused by particle segregation due to different particle sizes. Wavy bed surface can be caused by vibrations or interactions or both. Additionally, the surface roughness of the melted region can lead to non-uniform powder coverage in some cases, resulting in increased porosity in the finished parts. Interestingly, the finer powders with reduced free-flowing ability can sometimes achieve better surface coverage on already melted powder surfaces [97]. Understanding the spreadability of a powder and defining the relevant metrics is still an ongoing topic of research [33, 92].

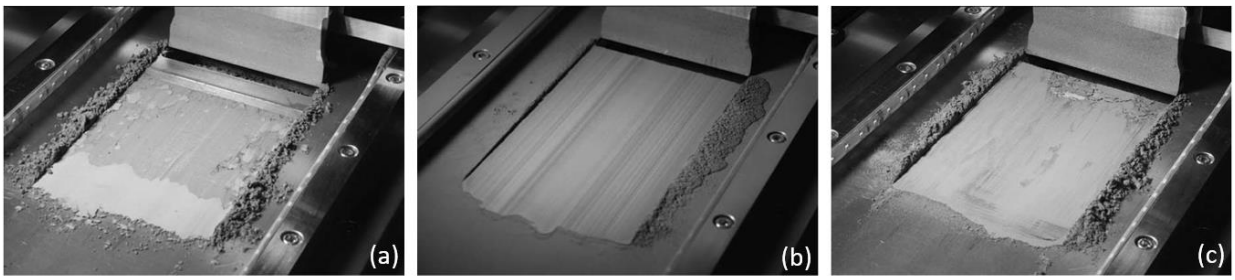

Figure 2.5 Failure modes as seen in powder bed spreading (Adapted from [98]).

2.1.2.2. Melt pool

As described above, changes in energy density can lead to changes in build quality. While the user-programmed parameters define the nominal settings for these values, in-process phenomena (e.g., spatter, melt plume, powder layer variation) can change them significantly. In-process monitoring allows for direct monitoring of the energy density. Measurement of the melt

pool temperature can directly show over or under heating of the melt pool, indicating areas where defects may form [99]. Overheated melt pools can indicate areas in which keyhole porosity may form while underheated melt pools can indicate areas in which lack-of-fusion porosity (see Sec. 2.1.1.3) may form [51, 82]. In-process measurements of the melt pool size can also provide insight into the quality of the L-PBF process (see Sec. 3.1). Melt pool widths insufficient compared to the hatch spacing can lead to lack-of-fusion porosity and crack initiation sites [50]. Spatter ejected from the melt pool can also be monitored and used as an indicator of build quality. A high amount of spatter that lands in the powder bed or on components can increase the likelihood of lack-of-fusion porosity within components caused by the nature of spatter particles (large, irregular, and/or oxidized), which may not be sufficiently melted [71].

2.1.2.3. Fused layer

The solidified layer can also provide rich insight into the L-PBF process. One of the most common ways to monitor the build quality is to take images of the build process after the fusion of each layer (layer-wise imaging) (see Sec. 3.2). Inspection of the fused surface layer-by-layer can reveal geometric distortions of components due to thermal stress, collision with the recoater mechanism, or overbuilding of geometry [100, 101]. Optical imaging of the fused layer can also be used to observe flaws that could point to potential locations of porosity [102, 103]. Thermography of the fused layer can also provide insight into the formation of material defects due to high cooling rates or the prediction of unexpected changes in residual stress due to heat accumulation [104]. Measurement of the fused layer geometry using various metrological techniques can also be used to identify flaws within the L-PBF process [105]. Depending on the sensors utilized, surface texture information can be extracted from the fused layer to investigate variation between individual melt pools [106]. Additionally, the data from multiple L-PBF signatures can be used in combination to improve anomaly detection capability [107, 108].

The summary of relationships between process signatures and in-process flaws is given in **Table 1** below. Descriptions of the in-process sensing technologies utilized to monitor these process signatures and categorization of the flaws they are potentially capable of detecting are provided in Sec. 3 (In-process monitoring and in-process NDE methods).

Table 1 Process signatures and in-process flaws

Process signatures	Related in-process flaw(s)
Spread powder layer	Porosity, geometry
Substrate/powder bed temperature	Geometry, microstructure
Meltpool temperature and shape	Porosity, geometry, cracking, microstructure
Spatter	Porosity, microstructure
Fused layer	Porosity, geometry, cracking, microstructure

2.2. Directed energy deposition

Directed energy deposition (DED) uses a focused thermal energy source to fuse materials layer by layer by melting them as they are deposited, in contrast to PBF where the material is fused after being deposited. The deposited material is applied in selected regions over multiple layers

until the prescribed component geometry is completed [14]. Directed energy deposition is almost exclusively used for metals [15]. Melting creates a pool of molten metal, called a melt pool, which fuses to the adjacent solid regions during the solidification, starting immediately after the energy source moves to a new position during scanning. There are three types of energy sources (laser, electron, and arc) and two types of feedstocks (powder and wire). Wire feedstocks are used in combination with all three energy sources, whereas powder feedstock is primarily used with laser-based DED [110]. Powder feedstock has been demonstrated with plasma arc [111, 112]; however, it is not widely used. Laser (L-DED) and arc typically operate in an inert and/or reducing (i.e., gas mixtures) atmosphere environment by injecting a shielding gas into the deposition region. In some cases, the entire build chamber may be in an inert environment or additional crossflow of the shielding gas may be applied across the part to provide shielding of the hot material outside the deposition region [113, 114]. Electron beam DED (EB-DED) operates in a high vacuum (10^{-4} Torr) environment for electron transport purposes. Wire feed arc DED is most closely related to welding processes and includes three different technologies: gas metal arc (GMA-DED), gas tungsten arc (GTA-DED), and plasma arc (PA-DED) [113, 115]. A further subset of GMA-DED is cold metal transfer (CMT) where metal is deposited drop by drop by oscillating the wire (advancing and retracting), which allows for faster cooling rates and smaller feature size compared to the continuous melt pool produced by GMA-DED [110, 113, 116]. Finally, there is a relatively new subcategory of powder feed L-DED, which is extreme high-speed laser material deposition (EHLA) [117]. This technology, initially limited to coatings of rotating components, uses the high-speed motion of the deposition head (energy source and feeding mechanism) and component to achieve smaller features while maintaining fast build rates [118]. One can also find combinations of feedstocks (powder and wire [111]) or energy sources (arc and laser [119]) in a single DED process, although this is not common. Naming conventions for DED are given in **Table 2**. The first column is the energy source followed by the feedstock types for each energy source. The remaining three columns are different naming conventions. The naming conventions are messy and don't map well to a specific energy source and feedstock combination. A larger table entry (multiple rows) in the gray columns is indicative of a broad naming convention. A general observation is that the naming conventions typically focus on energy sources and lack specificity about feedstock type. The American Welding Society (AWS) provides more specificity regarding arc energy sources. On the other hand, it is also convenient to have naming conventions that can refer to a sub-group of DED technologies (e.g., wire feedstock and arc energy sources are commonly referred to as wire-arc additive manufacturing – WAAM or wire-arc directed energy deposition – WA-DED). **Figure 2.6** illustrates how the different energy sources, feedstock materials, feeding methods, etc. are combined to deposit material during the DED process.

In addition to the review by Ahn [110], there are two ASTM standard guides [121, 122] that provide advantages and disadvantages of DED and a high-level comparison of the different types of DED. Here we note several unique attributes of DED compared to other AM technologies:

- Directed energy deposition provides higher build rates and larger components compared to powder bed fusion. Typical feedstock sizes for powder and wire range from 10 µm to 200 µm and 0.75 mm to 3.2 mm, respectively [121, 123, 16]. DED is readily capable of "large scale" additive manufacturing (parts greater than 1 m^3 or with the longest dimension greater than 1 m to 2 m). However, this comes at the expense of coarser feature resolution due to the

larger feedstock size and molten pools. The stair-step effect caused by layer-wise deposition is more pronounced with thicker layers. For example, wire feed DED geometry is generally 10× less accurate than LPBF [115]. The rough surfaces of as-built AM components can complicate post process NDE.

Table 2 Classification of DED methods based on feedstock type and thermal energy source. Other common names: Laser additive manufacturing (LAM), wire laser additive manufacturing (WLAM), wire electron beam additive manufacturing (WEAM), wire arc additive manufacturing (WAAM), wire arc directed energy deposition (WA-DED), laser metal deposition (LMD).

<table>
<tr><th>Thermal Energy Source</th><th>Feedstock Type</th><th>ISO/ASTM 52900-21 [109]</th><th>AWS D20.1/D20.1M: 2019 [120]</th><th colspan="2">Other common names [110]</th></tr>
<tr><td rowspan="2">Laser Beam</td><td>Powder</td><td rowspan="2">DED-LB</td><td rowspan="2">L-DED</td><td>LAM-DED</td><td rowspan="2">LMD</td></tr>
<tr><td>Wire</td><td>WLAM</td></tr>
<tr><td>Electron Beam</td><td>Wire</td><td>DED-EB</td><td>EB-DED</td><td colspan="2">WEAM</td></tr>
<tr><td rowspan="2">Arc-electric</td><td rowspan="2">Wire</td><td rowspan="4">DED-Arc</td><td>GMA-DED</td><td colspan="2" rowspan="3">WAAM
WA-DED</td></tr>
<tr><td>GTA-DED</td></tr>
<tr><td rowspan="2">Arc-plasma</td><td>Wire</td><td rowspan="2">PA-DED</td></tr>
<tr><td>Powder</td><td colspan="2"></td></tr>
</table>

- Directed energy deposition is readily able to produce parts with multiple materials and/or chemical composition gradients. The nature of DED allows for changing between feedstock materials during the process (e.g., multiple feedstock nozzles and hoppers). A review by Feenstra et al. [124] covers the state-of-the art in multi-material DED.
- Directed energy deposition, mainly laser and arc systems, is also advantageous for hybrid manufacturing (combination of additive and subtractive manufacturing in a single system) since the part is accessible for machining during the building process and the machine may already operate like a computer numerical control (CNC) machine. Davila et al. [125] provided a review of hybrid manufacturing using DED.
- Directed energy deposition is also suitable for repair, printing on three-dimensional (3D) substrates, and incorporating the substrate into the final part. Saboori et al. [126] reviewed DED for repairing applications.
- A DED system with five or more degrees of freedom allows for the avoidance of overhanging features and their support structures because the part can be reoriented relative to the deposition head. Overhanging features are generally a challenge for AM processes. The increased degrees of freedom make the slicing of a 3D model into layers more complicated with multiple slicing strategies [113].
- Wire feedstocks allow for a nearly 100 % efficient use of material (ratio of material deposited to material supplied) [127]. Powder efficiency for DED varies on process conditions and is typically less than wire feed DED (e.g., 30 % up to 90 % [128-130]). Recovering and reusing powders can improve the overall material efficiency; however, powder reuse adds complexity to qualification and certification.

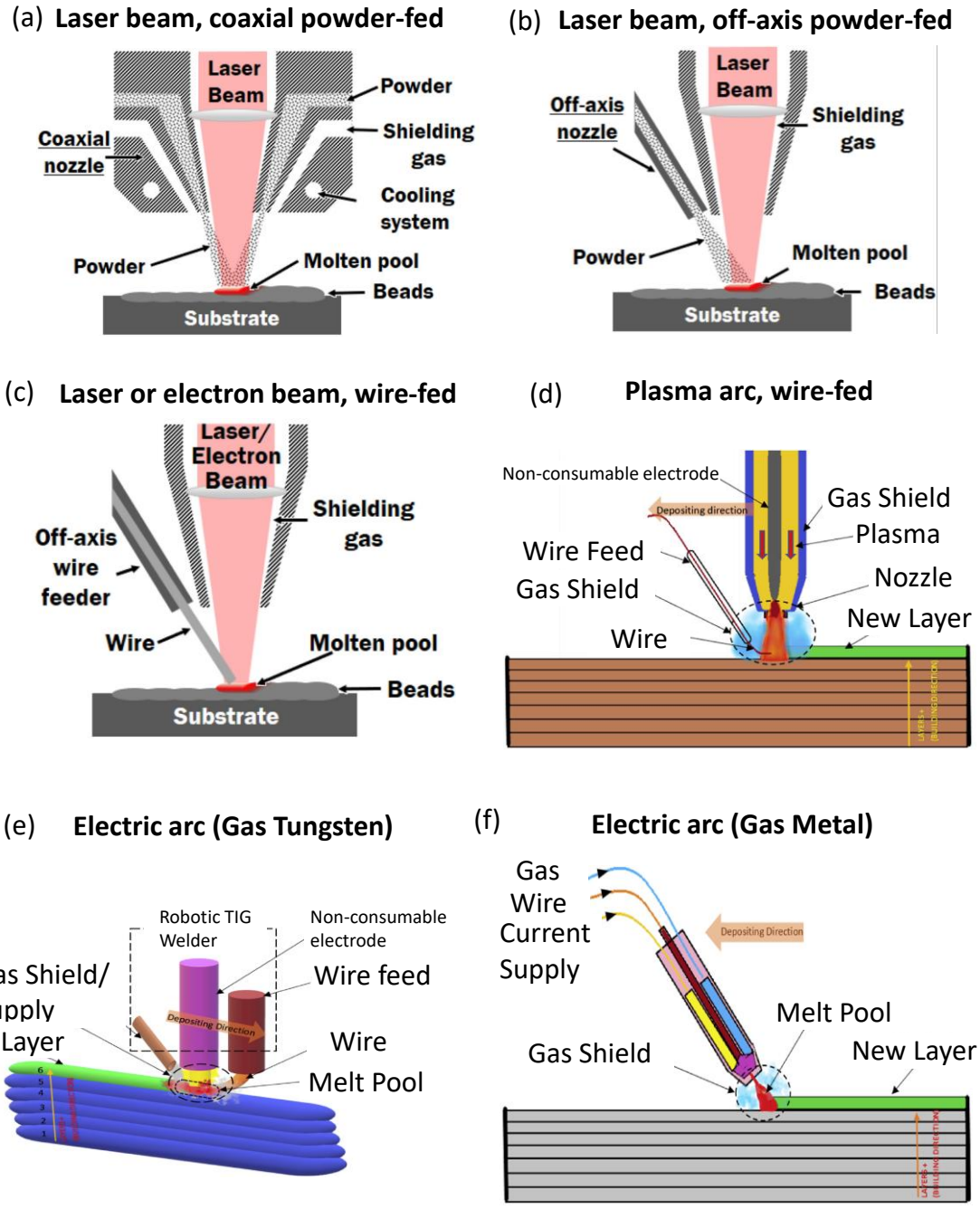

Figure 2.6 Illustrations of different DED technologies. (a, b, c) are taken from Ref [110]. (d, e, f) are taken from Ref [116] with modified labels. (Molten pool and melt pool mean the same thing.)

2.2.1. Factors influencing printed part defects

Directed energy deposition requires that the right amount of material is deposited in the right place consistently, otherwise, there is a high chance of flaws and defects. The defects include undesirable porosity, cracks, deviation from the part geometry, and undesirable microstructures.

The DED process has many factors that influence part defects. Like L-PBF these can be classified into four major categories: feedstock material, build preparation, process influences, and equipment influences. While AM is often referred to as a layer-by-layer process, it is also a track-by-track or bead-by-bead process for a given layer because the moving energy source melts material with a finite width. The term bead, track, and melt pool are used to describe the process at this level throughout this section. Factors that influence the process at the melt pool and track level propagate to influence the part.

2.2.1.1. Feedstock material

Directed energy deposition uses feedstock in powder and wire form. The use of other feedstocks such as metal chips resulting from machining or cutting processes (e.g., [131]) and combined wire and powder (e.g., [132]) have been demonstrated. Powder sizes for DED typically range from 50 µm to 150 µm, which is larger than L-PBF as a rule of thumb [127]. In DED, the powder is blown rather than spread; however, size and morphology are important characteristics that influence the process. Powder flowability both inside the machine and through the carrier gas used to deliver powder is important. Singh et al. [127] summarize that large particles generally provide better flowability compared to smaller particles that can agglomerate, and larger particles also provide better catchment efficiency (i.e., more of the feedstock material ends up on the part). In contrast, smaller particles may be preferred over larger particles because they result in a more stable melt pool [123]. Particles that are too large can lead to agitated, unstable melt pools [123]. Iams et al. [133] showed that characterizing the powder rheology is important for predicting powder performance rather than relying on general trends. For three powders sieved to an appropriate size range for DED with a modest change in size (15 % to 20 % difference in size), they observed a significant difference in mass flow rates for the same machine feeding setting, and this resulted in the varying geometric quality of printed parts. The powder that had the largest cohesion strength and the highest complete fluidization velocity yielded the lowest mass flow rate [133]. This was the largest particle size in the group of three powders; there were also small differences in morphology and internal porosity among the three powders in the study. With wire feedstock, cracks and scratches in the wire and variations in the wire diameter can lead to porosity in the part [16].

The feedstock quality is also determined by the presence of existing defects and surface contamination. Powders may contain limited amounts of gas-entrapped porosity introduced during the atomization process [16, 134]. These can survive melting and remain in the built material. Although, it is just as likely these gas pores escape to and exit the molten metal surface [134]. For powder and wire feedstock, hydrocarbons and water contamination on the feedstock can result in gaseous byproducts forming and remaining in the part [113, 135]. Zhao et al. [135] showed that drying Al-alloy powders to remove moisture combined with handling procedures to mitigate moisture pickup after drying reduced bands of small pores at melt pool boundaries. Jafari et al. [113] document wire contamination as a source of porosity in a review of wire-feed DED processes. Storage, handling, and reuse factors for powders in L-PBF (see Sec. 2.1.1.1) also apply to DED feedstocks.

Directed energy deposition, particularly with powder feedstocks, allows for printing chemical composition gradients and/or location-specific chemical compositions. However, the accuracy of the chemical composition is still a significant challenge [124]. Powders can be premixed or mixed at the point of material delivery. Feenstra et al. [124] note that the most accurate functionally graded materials have been achieved with pre-mixed powders. Chen et al. [136] reviewed the use of elemental powder mixtures (i.e., pre-mixed powders) in L-DED citing two studies that report a 4 % deviation in designed chemistry [137] and a 5 % to 10 % deviation in designed chemistry [138]. One cause of chemistry errors is powder segregation during the delivery process. The size, shape, and density determine the speeds of individual particles. Li et al. [139] showed that overcoming powder segregation in blends of elemental powders requires that the size is optimized to account for the differences in speeds of different size/density of particles. In addition to feeding issues that lead to variation in chemistry for compositionally graded or multi-material builds, there can be changes in chemistry from the feedstock to the part due to the vaporization of more volatile alloying elements. Mukherjee et al. [140] gave examples of mass loss of Al in titanium alloy (Ti-6Al-4V), Mn in stainless steels, and Cr in nickel alloy 625 (IN625), which are predicted using the Langmuir equation. Finally, not all alloys are easily printable. Mukherjee et al. [140] defined the printability of an alloy based on its ability to avoid defects (porosity, thermal distortion, cracking, etc.) and provided several dimensionless numbers that can be used to rank alloys in this regard. Such analyses can help in foreseeing potential issues when choosing a feedstock material.

2.2.1.2. Build preparation

An overview of build preparation aspects is often covered in design guides (e.g., [122]). Specific factors worth discussing here are part orientation and process planning (i.e., path planning and part slicing). Part orientation and process planning influence surface roughness, geometric quality, and build time [113, 141, 142]. These factors influence the process by determining the characteristics of the scan paths for depositing material.

The slicing aspect (breaking down the 3D model into layers) of DED is more flexible and complex than L-PBF because the deposition of material on the part is not constrained to a specific plane. As noted in Sec. 2.2, some 5 (or more) axis DED systems allow for support-free printing [113]. Process planning is a critical step to avoid collisions between the printing head and part and to ensure process quality. **Figure 2.7** shows a simple example of different build orientations and building strategies based on build platform orientation (α) or energy source rotations (γ). For the three angled columns, the layers are sliced and printed differently resulting in potential differences in the final part despite having the same prescribed geometry. Slicing strategies include unidirectional and multi-directional slicing [113], and within unidirectional slicing there are several options: uniform slicing, adaptive slicing, region-based adaptive slicing, and feature-based inclined slicing [113]. Xu et al. [143] devote a review article to slicing for DED with a summary of advantages and disadvantages. Advanced slicing methods offer improved surface roughness, elimination of support structures, improved geometric accuracy, and reduction in the staircase effect; however, these can come with the disadvantages of complexity, manual inspection of build files, and a lack of universality for different geometries [143].

Part orientation affects the final properties because the microstructure and properties of DED parts can be anisotropic [144, 145]. Anisotropy is not necessarily a part defect; however, the presence of defects may be a cause of mechanical anisotropy. In cases where defects are primarily present at melt pool boundaries and/or layer boundaries, weaker ultimate tensile strength perpendicular to the layers may result [144]. Kersten et al. [146] investigated part orientation effects on the mechanical properties of DED-produced material bonded to wrought substrate material (half of each inside the gage section). They also found anisotropy in the ultimate tensile strength and elongation with the lowest values when the layer interface was perpendicular to the loading axis [146].

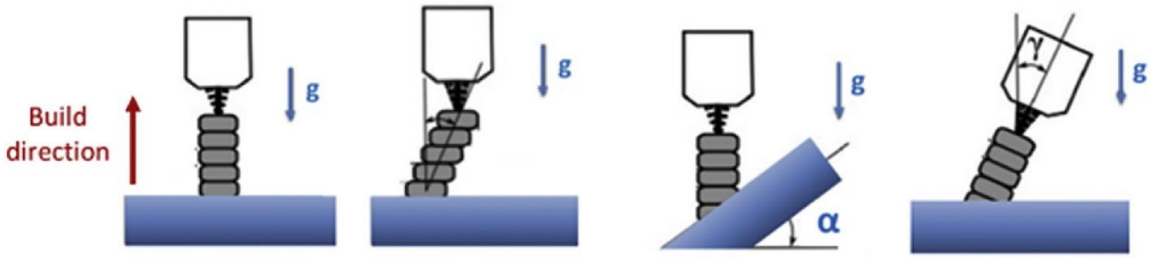

Figure 2.7 Examples of different build orientations and building strategies taken from Ref. [113]. ('g' indicates the direction of gravity)

2.2.1.3. Process influences

After picking the feedstock material, ***user-programmed parameters*** for DED relate to the thermal energy source, feeding of material, scan speed, and scan path or strategy [110]. These categories are common with L-PBF except for the feeding of the material. The energy source, feeding of the material, and scan path and speed are often optimized for each feedstock material to achieve fully dense parts with high build rates for a variety of part geometries. Parameter reduction is helpful for discussing general trends. Directed energy deposition has two parameters that are commonly used for process development. These are the linear heat input (heat source power divided by the speed of the relative motion between the deposition head and fabricated part) and the material feed rate [110]. The material feed rate can be in units of mass per time [147], mass per unit length [110], or volume per unit length [113]. These two parameters (linear heat and feed rate) can be combined into an energy density term with units of Joules per unit mm or per unit cubic mm [148]. There are other formulations of the process variables that include the laser beam diameter (e.g., [147, 149, 150]); however, linear heat and feed rate as defined above are sufficient for explaining general relationships between process parameters and defects.

Dass and Moridi [147] illustrate a process map of linear heat input versus material feed rate for powder feed L-DED in **Figure 2.8**, where colored regions represent process windows. The general idea in this L-DED process map holds true for other DED methods. Low linear heat input and/or excessive material feeding cause insufficient melting and lack-of-fusion porosity. Excessive material feeding and/or large particles of powder feedstock can attenuate a laser energy source [151] causing a lower linear heat delivered to the fusion zone. The lack-of-fusion can occur between layers or between laser scan tracks within a single layer. For layer-to-layer remelting, a certain amount of re-melting is required such that the melt pool penetrates the previous layer.

The ratio of the remelted depth to bead height plus remelted depth is referred to as the dilution ratio. A review by Dass and Moridi [147] summarizes that a minimum dilution of 10 % to 30 % is typical to ensure good metallurgical bonding between layers. Within a layer, lack-of-fusion porosity occurs due to a lack of remelting between tracks. The track-to-track spacing (also called hatch spacing) is typically a constant (e.g., an overlap of 25 % of the bead width for L-DED [110]), and if the melt pool width gets smaller during the process, this can lead to regions that remain unfilled by the next layer. The hatch spacing is not captured in the process map provided in **Figure 2.8**.

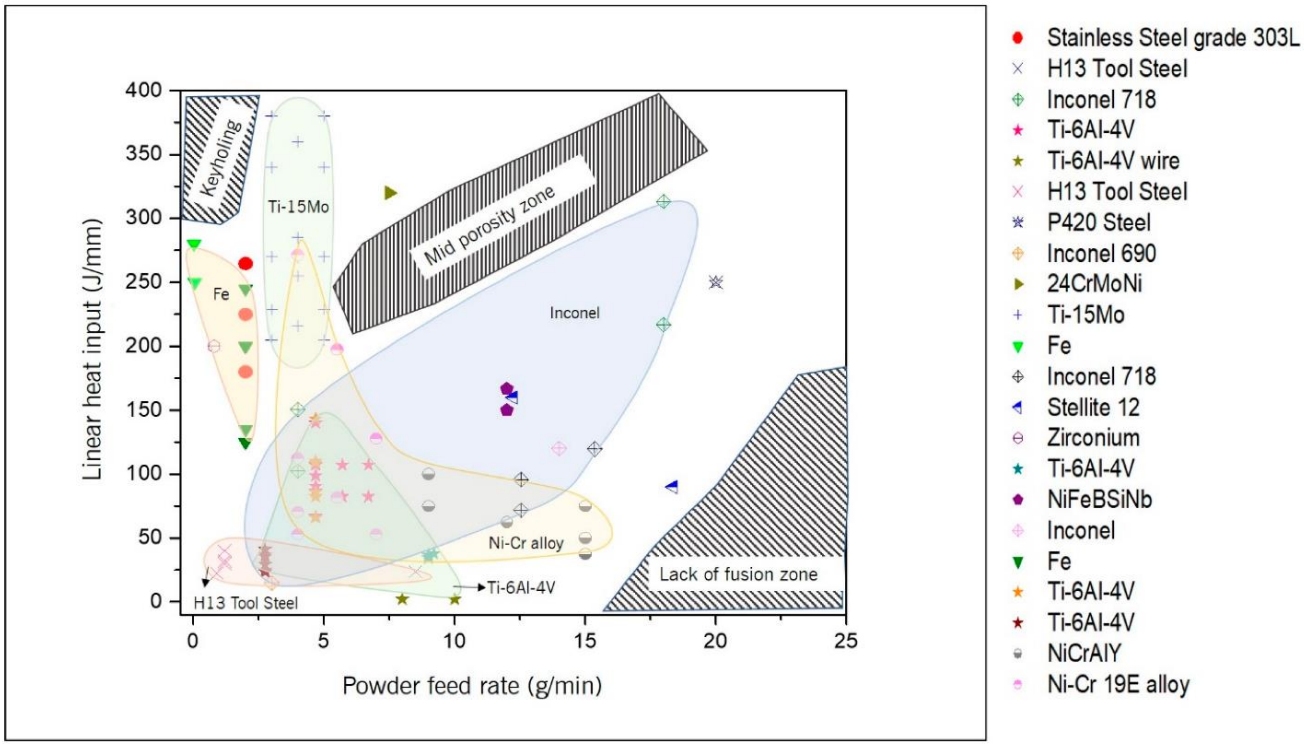

Figure 2.8 Process map for powder feed L-DED [147].

Excessive linear heat can lead to an increase in gas-entrapped porosity from an unstable, turbulent melt pool. The turbulent nature of the molten pool can entrap gas from the environment. This is often termed metallurgical and/or keyhole porosity, which is also present in L-PBF. Keyholing refers to the shape of the melt pool where the depth increases significantly. Excessive linear heat can also lead to an increase in ejected molten metal, which is seen by more metal splashing and adhering to the deposition head (e.g., [152]). The "Mid porosity zone" in **Figure 2.8** is a combination of the keyhole and lack-of-fusion porosity [147]. This occurs when some of the feeding material sees excessive linear heat while the rest is shielded and receives insufficient linear heat input.

Linear heat input and material feeding are also important parameters because uncontrolled changes to the melt pool size will lead to geometry defects. Excessive linear heat increases the melt pool size, which can lead to mushrooming, overbuilding, and general waviness [115, 123]. The incorrect feed rate for wire feedstocks is characterized as dripping when the wire feed rate

is too low and stubbing when the wire feed rate is too high, and both lead to poor bead quality [110]. Liu et al. [153] cataloged examples of many common geometrical defects for powder feed L-DED, which are often mitigated by energy source and material feeding parameters. Directed energy deposition is mostly a near-net shape process; machining is required to produce usable parts due to the large layer thickness causing large surface waviness [110]. Even when post-machining is part of the production process, geometric defects during printing can make it so that post-machining cannot achieve the desired geometry.

Unlike L-PBF, the layer thickness is less of a user input since it is a function of the linear heat input and material feed rate. The layer thickness determines the step distance of the deposition head in-between layers to maintain a consistent stand-off distance of the deposition head from the part. The stand-off distance is also referred to as the working distance and nozzle-to-part distance. This is critical for consistent beads and accurate geometry [110]. Cumulative layer height errors can lead to errors in the standoff distance. Powder feed L-DED has a unique property of passive stability where the layer height and stand-off distance self-correct within a specific process window due to the nature of the powder stream and laser attenuation [154]. For GMA-DED, an incorrect stand-off distance can result in poor shield gas coverage or collision of the head with the part [155]. The material feed rate to the part, particularly for powder streams, can also change with stand-off distance [123].

Users also have some selection of the scan path or scan strategies used to fill in specific layer [113, 144]. The scan strategy can have a significant influence on the part quality. Comparative studies can be found between scan strategies (e.g., [156, 157]), which illustrate tradeoffs between surface roughness, residual stress, geometrical accuracy, etc. **Figure 2.9** shows a visual example of the influence of the hatch spacing and scan strategy on the geometry for a simple cube. For WAAM processes, Jafari et al. [113] note that complicated intersections in scan strategies can lead to overbuilding at intersections and many arc-extinguishing areas can increase the chance of defects. During L-DED, the start and end of scan tracks can also have a characteristic nodule or hump [123]. Changing the scan strategy is often used to reduce residual stress [16, 144, 158].

Intrinsic process characteristics are not directly controlled by the user, although users have some ability to influence them. These characteristics include residual stress, heat buildup, spatter, plume, heterogenous and spatially varying microstructures, and solidification cracking. Residual stress is inherent to AM processes. Just like L-PBF, residual stress that leads to part warping is a serious issue for all DED methods. Reviews on residual stress in metal additive manufacturing can be found in Refs. [85, 159]. As mentioned previously, deposition strategies have a significant influence on residual stress for DED [110]. In some cases, parameters require a tradeoff between issues. For example, increasing the interpass dwell time (time between beads) to reduce heat buildup may increase residual stress [115].

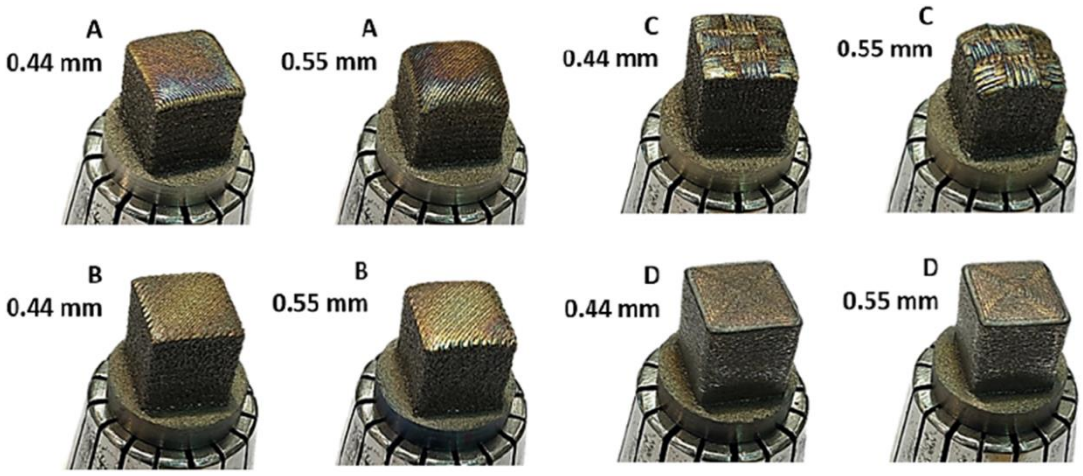

Figure 2.9 A simple cube geometry printed using powder-fed L-DED with different hatch spacing (0.44 mm and 0.55 mm) and different scan strategies: A – linear, B – zigzag, C – checkerboard, and D – contour [156].

Heat buildup in the part with successive layers is a common issue for DED. Material printed close to the substrate has a short path for heat dissipation through the substrate. As the material is built upward, the path increases, and heat dissipation is reduced causing heat buildup. A hotter part causes the process window to shift, and the defects (porosity and geometry) associated with excessive linear heat input will arise. Basically, the temperature buildup in the part causes the melt pool size to grow and move toward unstable processing [113]. Heat build can also occur locally when the scan path causes the heat source to scan near a location that has not cooled down. The issue of heat buildup can be overcome by reducing the linear heat input, adding interlayer/interpass dwells, using alternative scan strategies, and/or build plate heating or cooling so that a consistent melt pool is maintained with successive layers [110, 115, 160].

As mentioned for L-PBF, the formation of large spatter (molten metal that is ejected from the melt pool) is also an issue for DED. Large spatter that lands on the part can cause a scenario of insufficient melting. If the large, solidified spatter is not fully melted by the next pass, it may lead to a lack-of-fusion porosity [16]. In addition to spatter, the plume (evaporated metal that condenses into suspended nanoparticles) can also lead to defects [161]. If enough plume, sometimes also called fume, is generated and in between the energy sources and part, it can reduce the energy delivered to the melt pool. This is well documented in laser welding [162, 163].

Like L-PBF, DED processes can create components with heterogenous and spatially varying microstructures. This includes variations in grain morphology, crystallographic texture, chemistry, and phases. Microstructure defects in this case are unintended and unacceptable variations in microstructure leading to unacceptable performance. Post-process heat treatments can be used to create a more homogenous microstructure and reduce porosity to address this issue [144, 145]. Post-process heat treatments and a comprehensive review of process-microstructure relationships for DED are outside the scope of this review. The process-microstructure-property relationships for DED are a good starting point for determining potential microstructural defects and their sensitivity to process parameters.

Briefly, the ratio of the temperature gradient at solid-to-liquid interface (G) to the solidification rate (R) and their product (cooling rate) are used to predict different microstructure morphologies [144, 145, 147]. Microstructure variation is also linked to the melt pool shape variation [145]. The crystallographic texture is controlled through a competitive growth process during solidification. Competitive growth is achieved for crystal orientation easy-growth directions aligned with the maximum heat flow direction [145]. These aspects of the thermal history may vary spatially within a part, and this can lead to variation in the microstructure. Distinct microstructure regions with different hardness values have been reported for various alloys in L-DED as reviewed by Shamsaei et al. [144]. Wang et al. [164] showed how the microstructure varied along the height of the build for GTA-DED of IN625. Yeoh et al. [165] found that the grain size, primary dendric arm spacing, Nb concentration, and texture varied with build height and component size for simple cuboid IN718 parts built with L-DED.

The high cooling rate in AM in L-PBF and DED can lead to solidification cracking in certain alloys. There are two different types of cracking: liquation (occurs on the edge of welds in the partially melted zone) vs. solidification cracking (occurs in the middle of welds, also known as the fusion zone) [16, 166-168]. Solidification cracking occurs due to large thermal strains during cooling, specifically during the final stages of solidification [166]. Liquation cracking occurs in partially melted zones due to the high stresses and the presence of a liquid phase at grain boundaries [166]. The temperature versus the fraction of solid curves can be used to predict susceptibility to liquation and solidification cracking based on the alloy composition. [166]. Delamination is sometimes discussed as a macroscopic cracking because entire layers crack; however, this is also inherently a lack-of-fusion issue where the bonding between layers is insufficient to resist the buildup of residual stresses [16]. Strategies to reduce solidification cracking include ultrasonic vibration applied during DED [169], alloy modification [170], introducing nanoparticles in the feedstock [171], increasing substrate temperature [172], controlling the printing sequence for multi-materials [124, 173], and changing the energy source and scan path parameters [174]. In a similar vein to solidification cracking, shrinkage porosity, a term used for metal casting [175], is also reported in the literature for metals-based AM [176, 177]. Shrinkage porosity in metal casting is caused by variable rates of solidification in the melt pool and poor molten metal flow [16]. The shrinkage that occurs during solidification then causes irregular internal pores. It is difficult to distinguish between the different types of porosity (shrinkage, lack of fusion, metallurgical, and keyholing) based on their shape and size without additional corroborating evidence to decipher which mechanism caused the porosity [16].

2.2.1.4. Equipment influence

There is a sizable variation in equipment design and performance in DED machines. Here we focus on equipment influences that span multiple DED technologies. Clearly, each DED method (feedstock and energy source) comes with specific pros and cons that are briefly discussed in the introduction and covered in Refs [110, 121, 122]. The common equipment influences are feedstock delivery, shielding gas or environment, and positioning equipment.

The feeding style and location are typically fixed for a given DED machine. The variation of feeding location between machines is a unique variable of DED that influences geometric accuracy. Off-

axis feeding (see **Fig. 2.6**) of powder and wire can lead to anisotropic deposition resulting in varying bead quality and geometric accuracy with scan direction [110, 115, 123]. For example, off-axis wire feeding with arc energy sources leads to differences in the bead geometry at the start and end of tracks [115]. For a fixed feeding location, the feeding material switches from the front of the melt pool to the rear of the melt pool when the scan direction changes. The deposition head or part needs to rotate in order to maintain the same feeding location with respect to the melt pool traverse direction [110]. The feed angle is also a factor in controlling the bead quality [110]. Co-axial feeding (see **Figure 2.6**) reduces this complexity. Co-axial configurations exist for powder and wire feed L-DED and GMA-DED while EB-DED, GTA-DED, and PA-DED are primarily off-axis feeding configurations [110]. A review of powder delivery methods for DED can be found in Ref. [127], and a review of nozzle types for powder feedstocks in DED can be found in Ref. [178].

Inert atmospheres are required to reduce the reaction of the liquid and hot solid metal with the atmosphere and avoid unwanted changes in chemistry. The gas mixture and method for creating an inert environment have an influence on the process. Studies have found that equipment improvements can be made to reduce oxygen pickup. Ding et al. [114] found that adding secondary shield gas reduced oxygen pickup of the part for Arc-DED. Nalam et al. [179] found that additional shield gas was required to reduce oxygen pickup when using an elevated substrate pre-heat temperature. Both studies note that the typical shield gas approach for welding does not work well for some DED processes because the standoff distance is higher during DED, and this causes the shield gas to entrain the surrounding non-inert atmosphere. Silwal et al. [180] studied the effect of altering the cover gas on Arc-DED by using different mixtures of argon, carbon dioxide, and helium. The change in thermo-physical properties of the gas changed the arc length and heat transfer resulting in a change in the melt pool cross-sectional geometry [180]. For arc melting, the shielding gas flow also affects the arc stability, and thus the melt pool stability [113]. In addition to shielding gas, some DED systems have inert chambers that contain the entire build volume. Aversa et al. [181] compared these two options (inert chamber vs. shielding gas only) for L-DED of 316L stainless steel, and the shielding gas only option was slightly less effective because parts printed with this approach had an increase in oxygen content.

Lastly, DED systems can have CNC and/or robotic arms for deposition head and part motion. The geometric accuracy of parts is tied to the accuracy of motion systems. CNC machines are typically more accurate than robotic arm systems [160, 182, 183]. CNC machines are also typically stiffer than robotic arms, and robotic arms suffer from slowing down at sharp corners [160]. However, robotic arms are maneuverable and capable of working in parallel on large-build volume systems [160].

2.2.2. Process signatures, anomalies, and in-process flaws

This sub-section briefly introduces the connection of process signatures, anomalies, and in-process flaws for DED technology. The measurement technology and methods to accomplish this is covered in Section 3. The flaws can be grouped into four categories: porosity, cracking, geometry, and microstructure as summarized above. Directed energy deposition is more likely to require process control and feedback than L-PBF because building with constant parameters

tends to lead to defects due to the heat buildup issue and because the path planning *a priori* is more challenging [144]. Hence, there are many successful demonstrations of process control using process signatures to improve part quality. Based on factors that influence the printing parts, monitoring aspects of the feedstock, melt pool, and layer and part geometry are essential to ensure a consistent process.

2.2.2.1. Feedstock delivery

As previously discussed, uncontrolled changes in the feedstock delivery lead to an inconsistent process and poor part quality. Powder feedstock monitoring includes the flow of powder in supply lines as well as the powder flow from the nozzle to the melt pool. Acoustic emission (Sec. 3.3.1.4) and optoelectronic sensors have been demonstrated for monitoring consistent powder delivery in supply lines [184]. Vision and infrared imaging methods have been used to monitor powder delivery to the melt pool, which includes the powder velocity and temperature [184]. The use of electrical resistance between the wire feedstock and melt pool to control the wire feed rate has been successfully shown to improve the consistency of the material deposition [184].

2.2.2.2. Melt pool

The two-dimensional (2D) top-view melt pool geometry can be observed through visible and infrared imaging [184]. The temperature can also be measured with the same detectors as well as point detectors (e.g., pyrometers) [184]. A change in the process can lead to changes in the melt pool geometry and/or temperature and degradation in the part quality: geometry, porosity, and/or microstructure [184]. Monitoring the plume (melting byproducts) using spectroscopy has also been shown to successfully detect changes in the process that lead to degradation in the final part chemistry [184]. The topic of melt pool monitoring and process anomalies is covered in Sec. 3.1.3 (DED Melt pool characteristics).

2.2.2.3. Fused layer and part geometry

Monitoring the height of deposited layers and the displacement of the substrate and part is critical for ensuring geometric quality. Unlike powder bed fusion, some of the processes and part are visible from the side during DED. Visual methods and/or displacement sensors can be used to monitor the quality of the part [184]. Visual methods are covered in Sec. 3.2.3 (Potentially observable anomalies and defects in L-DED using machine vision). Acoustic emission has also been demonstrated to indicate when porosity, cracking, or geometric flaws occur [184], which is covered in Sec. 3.3.1.4 (Acoustic emission).

Table 3 lists common process signatures and process flaw correlations. In most cases, the process signature is related to multiple process flaws. The table lists both methods (e.g., acoustic emission) and features (e.g., melt pool temperature and shape) as process signatures. When a feature is listed, it is because there are multiple methods to measure that feature (e.g., infrared camera, optical camera, pyrometer, etc.). Table 3 was generated from several reviews. First, Ahn

[110], Dass and Moridi [147], and Tang et al. [184] provide references to specific studies with process signatures and defects across different DED technologies in easily digested tables. Reviews by Ruetzel and Nassar [185], Everton et al. [186], and Tapia and Elwany [187] cover in-process monitoring for metals AM that includes DED. Tang et al. [184] is the most specific review focused on process monitoring for DED. Readers are referred to Table 4 in Tang et al. [184], and Table 12 in Ahn [110], for references that support **Table 3**.

Table 3 Process signatures and related process flaws. Readers are referred to Table 4 in [184] and Table 12 in [110] for references that support the summary in Table 3.

Process signatures	Related in-process flaw(s)
Melt pool temperature and shape	Porosity, geometry, microstructure
Layer geometry (including deposition height)	Geometry
Feedstock temperature and feed rate	Porosity, geometry
Acoustic emission	Porosity, geometry, cracking
Part temperature	Porosity, geometry, microstructure
Substrate/part deflection	Geometry
Optical emission spectroscopy (plume)	Microstructure
Electrical resistance of molten pool and wire (GMA-DED only)	Porosity, geometry

3. In-process monitoring and in-process NDE methods

Similar to ASTM E3353-22, this section focuses on those in-process monitoring systems that are most widely deployed on industrial AM machines, and primarily provided as accessory options by the original equipment manufacturers (OEMs). While these systems may be described as 'in-process NDE', the instruments and applications differ greatly from 'traditional' NDE inspection methods such as ultrasonics or acoustic emission, eddy current probing, active thermography, radiography, etc. While there are research and development (R&D) efforts to introduce some of these 'traditional' NDE methods within the AM process, for the most part these systems are not sold as commercial products dedicated and integrated within industrial AM machines. Nevertheless, familiar readers may note that certain machine vision applications discussed in Section 3.2 (e.g. standard imaging or surface roughness techniques) and other applications discussed in Section 3.3. (e.g., ultrasonics or acoustic emission), are more clear examples of integration of 'traditional' NDE techniques to in-process monitoring of AM.

Ultimately, there is no 'one-size-fits-all' system or application of in-process monitoring for AM that can comprehensively observe or predict all AM part qualities. Furthermore, these systems, even the commercial products provided by machine OEMs, require a fundamental understanding of the measurement process chain: from the dynamics and signatures of the observed object or phenomenon (e.g., melt pool), to the transformation of those signatures, through the process monitoring instrumentation, to measurement data, to the processing and analysis of that data to derive or extract meaningful features that can be correlated to part qualities of interest.

3.1. Melt pool monitoring

Melt pool monitoring (MPM) is an example of a prevalent set of AM in-process monitoring technologies with little similarity to traditional NDE techniques. ASTM E3353-22 defines MPM as "the continuous measurement of process signatures associated with perturbations, anomalies, or trends stemming from the laser (or another heat source) induced molten metal pool." MPM, generally and as defined in this document, acquires melt pool signatures stemming from radiant thermal emission from relatively high surface temperatures in and around the vicinity of the melt pool. It differs from machine vision approaches described in Sec. 3.2, which use external illumination sources[1], and observe relatively static objects (e.g., a fully solidified layer). MPM systems have become widely available by original equipment manufacturers (OEMs) or third parties as accessory products on most commercial L-PBF and L-DED machines [188]. The hardware and instrumentation (see **Figure 3.1**), data processing, and derived melt pool features or anomalies are largely similar between L-PBF and L-DED systems (e.g., Sections 3.1.2 and 3.1.3). On the other hand, while most L-PBF machines utilize similar laser and optics configurations and powder layer spreading mechanisms, DED machines have a greater diversity in precursor material types (e.g., powder or wire), heating source types (e.g., laser or electric arc), or geometric configurations (e.g., robotic arm or gantry-based), all of which alter the design requirements for in-process monitoring systems for DED. Large variation of these configurations leads to diverse variations of MPM for L-DED. Larger scale of spatial, temporal, and temperatures of L-DED melt pool signatures, compared to those of L-PBF, relaxes some design constraints on MPM systems. Therefore, the application of MPM in L-DED machines tends to be more developed than for L-PBF. These reduced spatial and temporal constraints have also enabled closed-loop feedback control in L-DED, including commercial systems [194, 229–231]. In this subsection, MPM is discussed first in the context and perspective of L-PBF systems, followed by the discussion of different characteristics for DED.

A key advantage of MPM, and the likely reason for the significant R&D efforts and commercialization of MPM, is that the measured signals, images, and data, are known to be physically related to melt pool temperatures, which relate to key phenomena affecting part quality such as microstructure evolution and formation of residual stress. Other dynamic melt pool phenomena, such as spatter, plume, size/shape fluctuations, etc. are thought (or anticipated) to physically relate to in-process flaw formation mechanisms, such as a keyhole or lack-of-fusion pore formation. These relationships between melt pool signatures and part qualities are discussed further in Sec. 3.1.2. A key disadvantage, or the main challenge with MPM inhibiting broader adoption, is that while these physical relationships are known to exist, they are also extremely complex. Therefore, accurately distinguishing (and predicting) flaw formation from MPM measurements is inhibited by the convolution of multiple influencing physical sources and misinterpretation of measurement results. A common refrain among MPM researchers and users: *"we have all this data, now what do we do with it?"*. This principle technological gap, also emphasized by the ASTM Center of Excellence (CoE) report on AM "In-situ Technology Readiness" [277], is not unique to MPM, but shared among the other in-process NDE and monitoring

[1] Note that there are many examples in research literature using strong illumination sources to capture high speed imaging of melt pools (refer to online version of [216] for example). While valuable researching melt pool dynamics, this technique is not broadly utilized for industrial part production or incorporated by OEMs into commercial AM machines.

modalities, as are the other gaps outlined in Sec. 7 of this report. However, MPM methods can incur unique data interpretation and processing challenges, stemming from the wide array of potentially observable physical phenomena as described in Sec. 3.1.2.1 for LPBF and Sec. 3.1.3.1 for DED.

In summary, MPM is generally still under continuous advancement, improvement, and development, including commercial MPM systems. Therefore, they are generally underutilized in production environments. Consequently, such systems have yet to be used broadly and effectively in AM part or process qualification.

3.1.1. Monitoring modalities

MPM systems come in a variety of 'modalities,' or groups of similar characteristics related to the melt pool phenomena they measure, the design or implementation of the instruments, or the physical configurations. The MPM modalities are similarly employed on both L-PBF and L-DED machines.

The following describes several MPM modalities:

Co-axial vs. staring configuration: The most common categorization of MPM systems is related to the physical configuration of the instrumentation as it is positioned within the AM system. ASTM E3353-22 calls these 'co-axial' (on-axis or inline) or 'staring' (off-axis or offline). **Figure 3.1** shows the schematics of different MPM configurations on L-PBF or L-DED machines. Note that while configurations for L-PBF machines are nominally similar, the variety of L-DED types and motion axis configurations (e.g., in Fig. 2.6) are not completely depicted in this figure. Staring configuration MPM systems are the simplest: the sensor or camera is in a fixed position with respect to the AM machine and build platform, as shown in **Figure 3.1 a**. These can be mounted inside or outside the AM machine environment chamber, but they are typically affixed outside using a protective window to isolate the sensor optics and electronics from the dirty build chamber. Debris buildup on these windows can occur and can attenuate the amount of light received by the instruments, affecting any calibration or subsequent data analyses. However, staring-configuration instruments are typically placed far enough away from the melt pool processing zone that the inert gas flow system limits contamination, and cleaning is only necessary between AM builds, or less frequently. For e-beam systems which operate in a vacuum, contamination stemming from vaporized (and then re-condensed) metallic buildup requires the use of mechanical shutter or rolling protective film [247] over any optics-based monitoring system.

Many applications of thermographic imaging in research utilize a staring configuration. Optical tomography (OT) is another approach using a staring configuration thermal imager that is provided on several commercial L-PBF machines. The unique aspect of OT is that individual thermal image frames are digitally 'superimposed' together, such that the resulting thermal emission data from multiple melt pools or scan vectors combine to form an image of the layer-wise geometry of each part, but with thermal features such as local hot spots or spatter. By varying camera settings such as exposure time, or the algorithm used to compute the image-to-image superpositioning, the geometry of the parts in each layer are apparent (i.e., between

regions where the melt pool passed through or did not). Most important for in-process monitoring, different process signatures such as overheating or melt pool spatter may be emphasized in the resulting static images. The superpositioning algorithms generally apply on a per-pixel basis, that is, some calculation performed on the signal vs. time (or temperature vs. time) at a specific pixel location. Each pixel may experience a number of heating and cooling cycles stemming from the melt pool passing over or nearby the stationary pixel location. Image superpositioning algorithms can vary [258], but commonly utilize calculated features such as maximum observed signal, or time above a user-defined signal threshold (i.e., 'time over threshold' or 'time over temperature' (TOT) [225]). Several examples of OT and observed melt pool signatures are provided in Sec. 3.1.2.

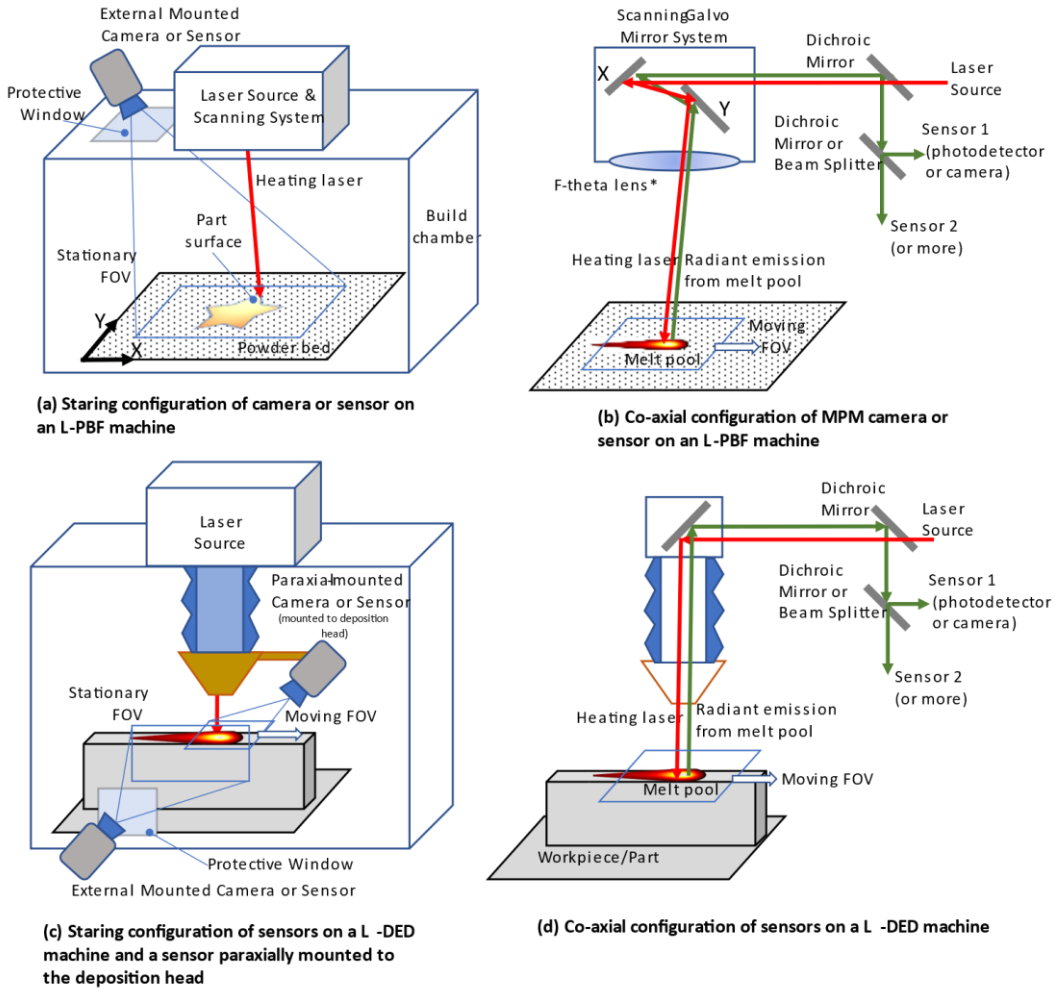

Figure 3.1 Schematics of different MPM configurations on L-PBF or L-DED machines.

Co-axial MPM utilizes a bit more complex optical design, in which the sensor or camera shares the same optical path as the heating laser, **Figure 3.1 b.** In this way, the field of view of the sensor moves with the melt pool, such that the melt pool appears to remain stationary to the sensor despite moving at high speeds around the build area. The primary optical component to enable this is a dichroic mirror or 'beam splitter' placed in the laser path, which selectively transmits and reflects different light wavelengths. The laser (typically ≈1070 nm wavelength) transmits through

this splitter and through the steering optics (e.g., galvanometer mirrors for L-PBF, or through the deposition head, which is moved by machine axes of motion for L-DED). The radiant emission from the hot melt pool transmits back in the opposite direction than the laser propagation and is 'split off' the beam splitter so that it impinges on the co-axial MPM detector. Multiple beam splitters may be used to employ multiple MPM detectors [189–191].

Commercial process monitoring of powder-blown DED systems typically employ co-axial MPM (e.g., [192], and **Figure 3.1 d),** but many experimental systems utilize staring configuration cameras due to simpler setup, and line-of-sight access to the side surfaces of parts which are otherwise inaccessible in L-PBF (e.g., [193]). However, some DED systems (often wire-fed) might use a camera or detector affixed to the deposition head. Similar to co-axial MPM, sensors mounted to the deposition head retain the hot molten pool within the sensor field of view, despite not sharing the same optical path as the laser [194]. This is sometimes called paraxial mounting [195], as shown in **Figure 3.1 c.** The relative strengths and weaknesses of co-axially configured cameras or sensors (including paraxial DED sensors) vs. staring configuration sensors are described in **Table 4**.

Table 4 Comparison of general strengths and weaknesses pertaining to co-axial vs. staring configuration melt pool monitoring systems. Note that these modalities may be combined with others in this section (e.g., single-point detector vs. imager).

Modality	Strengths	Weaknesses
Staring Configuration	• Point-and-shoot (with proper windows and/or AM environment shielding) • Part shape/geometry is directly observable with imagers and measurable with spatial calibration. • Simpler optical integration with AM machine.	• Spatial range vs. resolution tradeoff (limited by size of imager sensor and magnification of optics). • Field of view and line-of-sight are fixed. • Single point detectors require simultaneous acquisition of laser positions data to align/register/coordinate. • Signal or images may depend on relative orientation of melt pool direction and detector line of sight. • Susceptible to dirty environment and contamination of optics.
Co-axial Configuration	• Spatial range can span entire build area (where the laser goes, the MPM goes). • Spatial resolution can be very fine. • Enables single-point detectors to access entire build area. • Multiple detectors (imagers and/or single point) can be co-axially aligned.	• Complex hardware integration with AM machine optics. • Requires simultaneous acquisition of laser position(s) to register with locations in the part. • Data processing requires more complex algorithms. • Susceptible to dirty environment and contamination of optics.

Single-point detector vs. imager: Single-point detectors (e.g., photodetectors and pyrometers) integrate the spatially varying radiant emission of a target surface into a single value (sensor signal) over time. Melt pools generated in a metal AM process are a result of highly dynamic phenomena involving the melting of feedstock and rapid cooling of molten metal by the fast-

moving heat source, sometimes even boiling some constituents of the metal alloys in the process, creating recoil pressure, molten and unmelted particle spatters, and vaporous/nanoparticulate plumes. The total radiated emission of the melt pool (i.e., the summation or integration of all radiating sources in and surrounding the melt pool) which might be indicated by an MPM system is a very complex function of these dynamic phenomena. As such, it is practically impossible to isolate these individual phenomena from a single MPM measurement apparatus. Application of single-point detectors or pyrometers in fixed or staring configurations is relatively uncommon, except for a few examples [196, 197]. This is likely due to the fact that only a limited stationary, typically small, area (i.e., the sensor field of view) is measured, analogous to measurement with thermocouples. However, one L-PBF machine may utilize multiple single-point photodetectors fixed to the build chamber that acquire radiant emission from the entire build area, as shown in **Figure 3.2 a**. This requires the simultaneous acquisition of the laser position to register the acquired signal to the associated location within the part, similar to co-axial configurations. **Figure 3.2 b** shows the detector signal magnitude, represented by the color bar, mapped to the XY positions of the laser spot, over one layer consisting of 32 cubic parts. This effectively aggregates the measured melt pool signatures into a visualized representation of the 32 cubic parts and their geometry within this example layer. High or low signal magnitudes, shown in **Figure 3.2 b,** indicate relatively high or low melt pool radiant emissions (corresponding to temperatures) due to a change in applied laser power. The thin blue lines corresponding to zero signal magnitude show the scan path of the laser while traversing between parts. This mapping to the XY laser path is an example of 'data registration', which is essential to interpret the results of the fixed position, staring-configuration photodetectors.

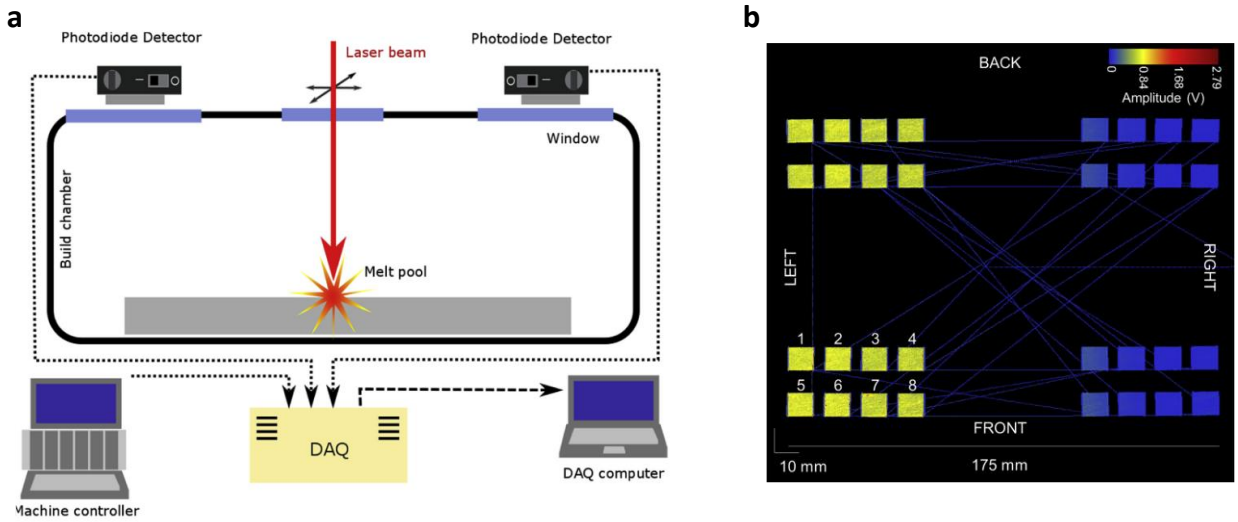

Figure 3.2 (a) Example schematic of two staring configuration, single point detectors sensitive to the entire build region (example from 3D Systems [198]). (b) Acquisition of photodetector signals, shown as voltage amplitude, are synchronized with the XY positions of the laser scan path.

Imager-based MPM systems observe radiant emission over an area (field of view) and can provide additional spatial information related to the melt pool. Certain process signatures, such as melt

pool size or shape, hot spatter [199, 200], or incandescing plume [201], may be distinguishable using imager-based MPM systems. Such signatures may be indicative of process anomalies such as thermal heterogeneity, overheating or undermelting, etc. However, for commercial single-point or imager-based MPM systems, isolating or differentiating individual melt pool phenomena from the acquired images is generally not attempted outside of research. **Table 5** provides a comparison of single-point detector and imager-based systems.

Table 5 Comparison of general strengths and weaknesses pertaining to single-point vs. imager-based melt pool monitoring systems.

Modality	Strengths	Weaknesses
Single point detector	• Inexpensive. Many options. • Extremely high potential acquisition rate (>MHz). • Relatively wide dynamic range • Optical system design is relatively simple (i.e., spatial aberrations don't matter)	• All radiating melt pool signatures integrated into one signal (i.e., individual phenomena are indistinguishable)
Imager	• Spatial and temporal information available. • Easier to identify process anomalies (directly observable through visual inspection)	• More complex data analyses • Relatively lower acquisition rates • Relatively lower dynamic range • Optical system design is critical to avoid aberrations (e.g., chromatic, spherical, etc.)

Wavelength dependence: The performance of an optical MPM system and the interpretation of the measurement results are highly dependent on which wavelength(s) are measured. From a hardware perspective, wavelength choice poses multiple competing advantages and disadvantages pertaining to the sensitivity, resolution, cost, complexity of design, and interpretability of the measurement results [202]. Very generally, shorter wavelengths (such as visible spectrum or near-infrared) are less expensive and easy to integrate and can operate at much higher sampling rates, but they are relegated to measuring very high-temperature sources (e.g., those which incandesce, or approximately > 1000 °C). Longer wavelengths (mid-infrared to long-wave infrared), have fewer commercial options, have generally slower sampling rates, can widely vary in cost or complexity to integrate into an AM system, but are able to measure lower temperatures (e.g., < 1000 °C). **Table 6** provides a comparison between short and long-wavelength imaging systems.

Other researched MPM systems: Some more unique and potentially promising melt pool monitoring systems are demonstrated in research, though are not yet widely implemented in commercial products. Certain in-process measurement systems, such as acoustic emission (AE), acquired via contact AE transducer [203, 204], airborne AE or microphone [205–207], or fiber-Bragg [208] might be considered 'melt pool monitoring' as they continuously measure the process and can be affected by melt pool signatures. A number of researchers have investigated spectroscopic measurements (multiple discrete wavelengths) of melt pool emission, primarily to identify elemental emission lines [194, 209, 210]. Some research has been demonstrated that monitors the *reflected* laser energy from the melt pool, which is shown to be sensitive to keyhole formation [211–213].

Table 6 Comparison of general strengths and weaknesses pertaining to selected wavelength range for melt pool monitoring systems. Note that the relative strengths and weaknesses highly depend on the type of sensor or camera. A more comprehensive comparison is available in [202].

Modality	Strengths	Weaknesses
Shorter wavelength (visible or near-infrared)	• Less expensive sensors; wider range of options. • Less expensive optics (i.e., cheaper materials). • Generally higher available acquisition rates.	• Potentially sensitive to heating laser wavelength. • Measurable temperature range is narrower. • Cannot measure low temperatures (< 500 °C, or below incandescence).
Longer wavelengths (mid-infrared or longer)	• Measurable temperature range is wider. • Can measure lower temperatures, potentially down to ambient providing more information about cooling/solidification rates.	• Generally lower acquisition rates available. • More expensive optics, fewer choices, and more critical design. • Potentially sensitive to ambient reflections or other error-inducing effects.

3.1.2. L-PBF melt pool characteristics

Part defects, such as pores, voids, or cracks, are formed during the fabrication process via multiple dynamic, interacting physical mechanisms. The physical links that connect an identified anomaly from in-process monitoring, the formation of an in-process flaw, and whether or not an identified in-process flaw results in a defect in the final part are exceedingly complex. Therefore, it shouldn't be expected that one process monitoring instrument whose data are analyzed/processed one way would be able to observe the formation of multiple types of in-process flaws. Identifying these causal relationships, while good practice to support instrumentation design or data analyses, is ultimately plagued by complexity due to the interaction of multiple influencing factors. Nevertheless, the melt pool is the physical feature, core to the fabrication quality, and provides the most measurable information regarding that fabrication quality. As such, the melt pool is the most often-targeted area for in-process monitoring for quality control.

Researchers are familiar with the multitude of complex physical mechanisms at the scale of laser-induced melt pools through multiscale computational simulations [214] or direct observation through high-speed X-ray [215] or visible-light imaging [216]. As such, the spatial, temporal, and temperature range characteristics of melt pools are known well enough that resolution criteria can be defined for melt pool monitoring instruments:

- ***Spatial:*** Although, depending on the material, the length of them can be as long as 1 mm or more, L-PBF melt pools are generally on the same size scale as the laser spot size (10's of µm). The size and shape (length, width, depth) will dynamically fluctuate depending on the applied instantaneous laser parameters (power, speed, spot size), or effects from residual heat buildup, or conductive losses affected by local part geometry and/or scan strategy [59, 217].

- ***Temporal:*** Temporal fluctuations of size and shape of L-PBF melt pools are primarily driven by the modulation frequency of the laser, which is determined from the laser parameters (e.g., scan speed) and scan pattern. The 'hatching' pattern common in L-PBF, and common laser parameters, result in laser modulation frequencies on the order of 100's of Hz. This hatch-type scanning pattern may also elicit strong periodicity in any MPM measurements. Many higher-frequency phenomena, such as spatter/ejecta formation or fluctuations in the melt pool, are generally more chaotic or less periodic and can occur at rates greater than 200 kHz. Commercial MPM sampling rates typically vary between 10 kHz to 200 kHz. Caprio et al. provide in-depth detail on melt pool oscillatory behavior and range of frequencies [218].
- ***Temperature or radiant intensity***: Surface temperatures of L-PBF melt pools range from the vaporization point of the metal (possibly higher), down to the metal solidification temperature are observed within distances of 10's of µm to 100's of µm. Temperature changes, from metal solidification temperature down to near ambient temperature, occur within millimeters outside the melt pool boundary. Optical sensors such as cameras or photodetectors used MPM, indicate signal values related to the radiant emission, which increases exponentially with temperature. Therefore, while temperatures may range from that of ambient to greater than 3000 °C, resulting sensor signals may range many orders of magnitude.

Grasso et al. [188] provide organized tables of reviewed literature that list each work's L-PBF MPM modalities, and their spatial, temporal, or temperature resolutions, and the targeted melt pool signatures.

3.1.2.1. Potentially observable L-PBF process anomalies from MPM

Review articles by Grasso and Colosimo [219], and an updated review by Grasso et al. [188], provide extensive collection and organization of L-PBF in-process measurement systems including MPM, the melt pool signatures each study attempted to capture or observe, and the part characteristic that the signatures are related to. The following provides a general summary of the types of melt pool signatures captured by MPM:

General thermal heterogeneity or thermal anomalies:

- **Overheating or 'hot spots'**: This is exemplified by a larger, hotter melt pool, which increases the measured signal from MPM detectors. The temperature field around the melt pool increases in magnitude and size as well.
  - *Sources*: Residual heat buildup due to local part geometry [59] and scan strategy [217]; improperly applied local laser parameters; local contaminant (e.g., via spatter particles, debris, etc.)
  - *Effects on fabrication or part quality*: Increased local porosity (e.g., 'hot spots' in OT and MPM data versus pore clusters seen in XCT, outlined in **Figure 3.3**) due to keyholing or misshapen melt pools; excessive surface roughness particularly on overhang or downskin regions [220, 221]; and locally varied microstructure.

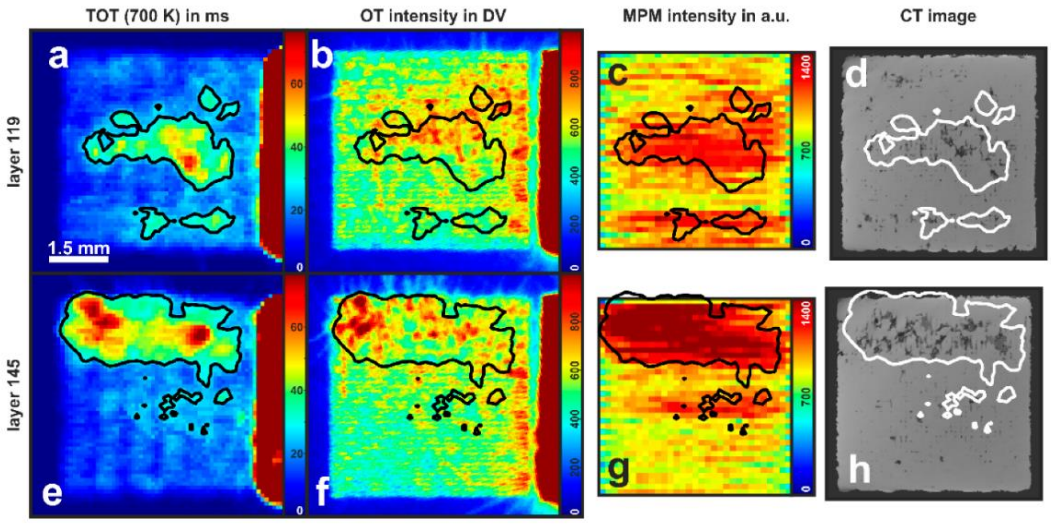

Figure 3.3 Examples of thermal heterogeneity observed on two different layers by various MPM instruments and methods of processing data. (a & e) TOT calculated using 'superpositioning' of data (see OT methods in Sec. 3.1.1) from a staring-configuration thermographic camera. (b & f) OT of emitted light 'intensity', expressed digital values (DV), via staring configuration, near-infrared camera (c & g) emitted light intensity by a commercial MPM system using co-axial photodetectors (d & h) post-fabrication XCT indicating local porosity in corresponding layers [225].

- **Undermelting or 'cold spots'**: This is exemplified by a smaller, cooler melt pool, which decreases the measured signal from MPM detectors. The temperature field around the melt pool decreases in magnitude and size as well.
  - *Sources*: Laser beam obstruction by plume condensate [87, 222], which occurs when the vaporized metal cools above the melt pool into increasingly larger condensate particles (approximately 100's nm), enough to scatter the laser energy; a gap, hole, or waviness in the underlying metal surface may increase the local powder layer thickness [223], which reduces the effective energy density; improper laser parameters or applied energy density [198, 224].
  - *Effects on fabrication or part quality:* Increased local porosity, primarily from horizontal (within layer) lack of fusion porosity, affecting bulk part density [198]. Variation in local part microstructure.
- **Hot spatter (ejecta):** Some commercial MPM systems enable the visualization (and potential quantification) of hot spatter particles emanating from the melt pool region. For example, **Figure 3.4** shows an OT camera output, where general spatter magnitude and direction can be observed. The relationships between anomalous (excessive or muted) levels of spatter and defects are complex and still being researched; however, spatter is targeted by commercial MPM systems as an effective process signature. For a review of various literature that employs in-process monitoring to detect or quantify spatter, see Li et al. [226].
  - *Sources*: Spatter is a naturally occurring part of the L-PBF process. Anomalous spatter may be induced when the melt pool interacts with a preexisting large defect (see 'Defect induced spatter' in [62]). Excessive spatter from one part on

the build platform may redeposit onto another part on the same build platform, causing thermal heterogeneity (**Figure 3.4** and [72]), or interfere with recoating blade (**figure 3.5**). Excessive spatter may indicate locally deep powder layer (i.e., a hole or gap) [227].

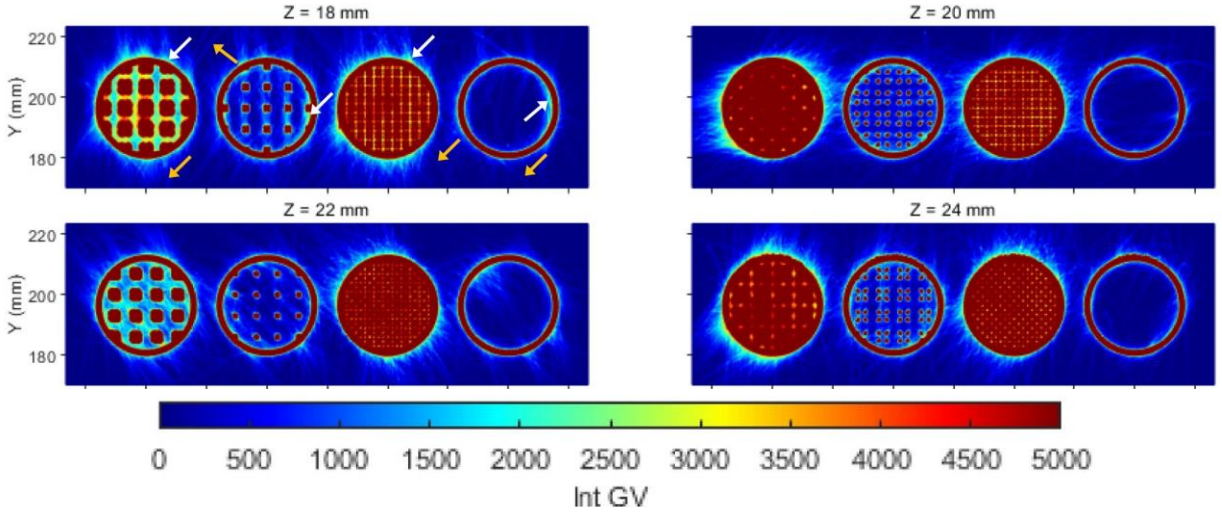

Figure 3.4 Example of optical tomography (OT) system (staring configuration camera which superimposes multiple video frames), with settings to observe hot spatter and plume [70]. These appear as 'halos' around the perimeter of each part, showing the general intensity (i.e., magnitude and frequency) and the direction in which hot spatters occurred.

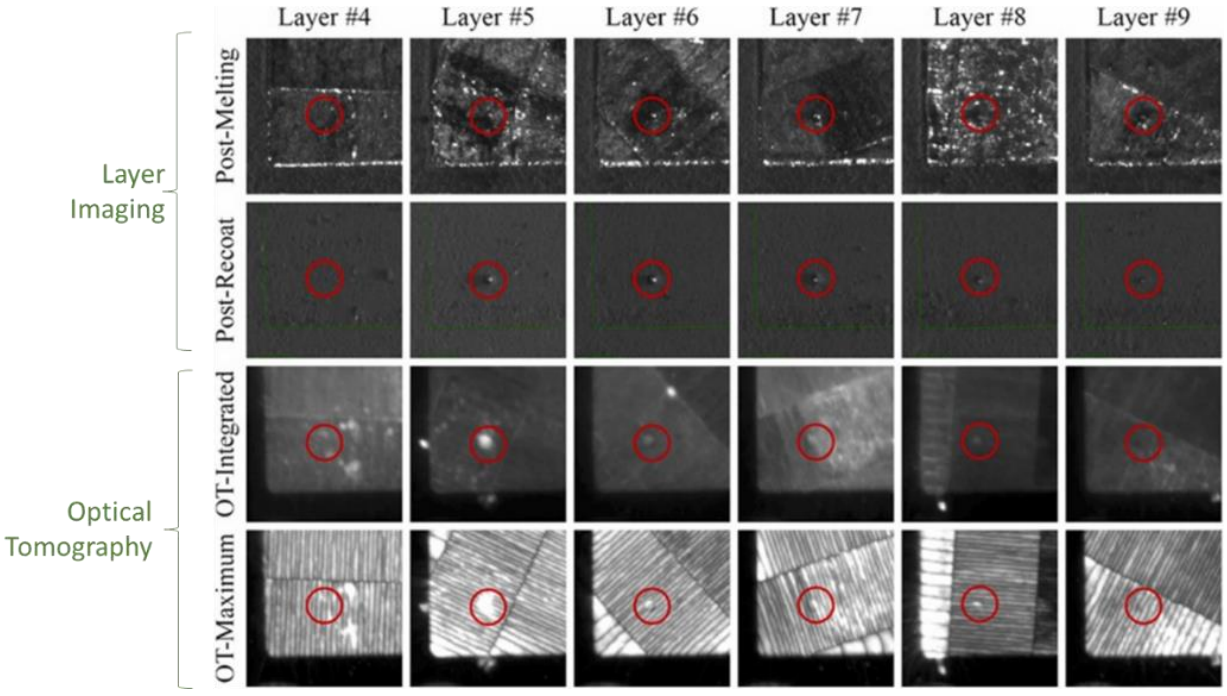

figure 3.5 Example relating features observed in two in-process measurement techniques to infer physical causality (from [71]). A large spatter particle was successively re-scanned over multiple layers, resulting in indicated thermal heterogeneity in the MPM measurement (optical tomography).

- *Effects on fabrication or part quality*: The effect of anomalous spatter on fabrication quality depends on the source of the anomalous spatter, but ultimately results in reduced part density or higher porosity (e.g., **Figure 3.6** from [228]).

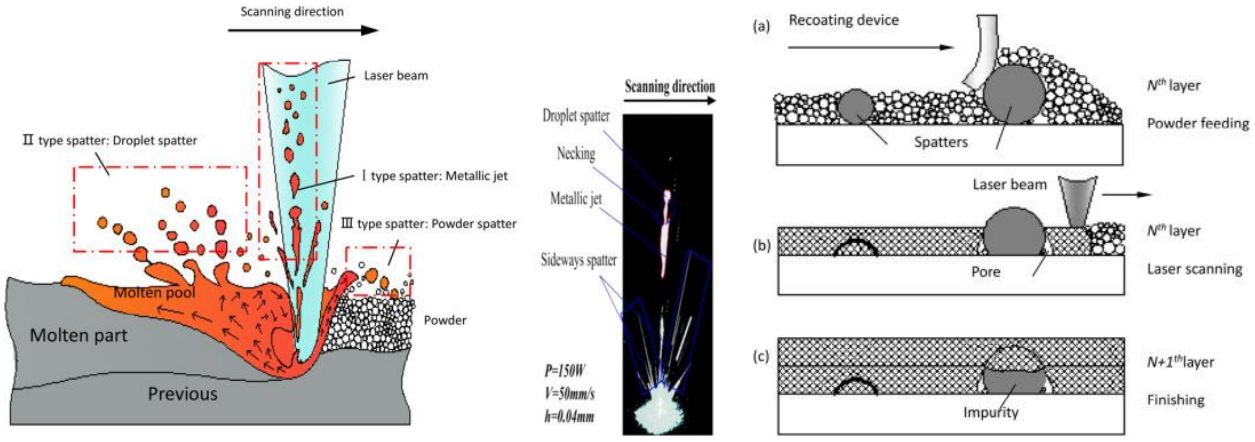

(a) (b) (c)

Figure 3.6 (a) Schematic of various types of spatter formation mechanisms in an L-PBF melt pool; (b) Staring configuration melt pool monitoring camera image with segmented spatter features; (c) Schematic of hypothesized mechanism for one type of spatter-induced defect formation mechanisms [228].

3.1.2.2. Conclusions on L-PBF MPM

L-PBF melt pool monitoring is a set of technologies that acquire radiant thermal emission from the laser-induced melt pool, which is known to have physical relationship to melt pool signatures of interest such as size/shape, temperature, and temporal dynamics. MPM systems can be categorized based on different modalities: physical configuration (staring vs. co-axial), availability sensor spatial information (single point detector vs. image-based), filtered light wavelength(s), etc., all of which have varying strengths and weaknesses described in Sec. 3.1.1.

How the acquired MPM data is processed is just as important as the physical instrumentation. Generally, laser parameters (power, spot size, speed) should be known or acquired in addition to any MPM sensor data for two reasons: 1) Melt pool signatures will vary with applied laser parameters, therefore are essential to know to separate anomalies from predictable behavior. 2) Synchronously acquiring actual laser spot positions along the scan path with MPM systems is essential to map any measurement to the physical position within the part, particularly for co-axial MPM or single-point MPM configurations (See Sec. 3.1.1 and **Figure 3.1**). Staring configuration imaging systems have less stringent necessity for simultaneous acquisition of laser parameters and scan path since the melt pool path and position may be directly observed in the video stream. However, the specific algorithms used to convert a video stream to static images (e.g., optical tomography examples in **Figure 3.3, Figure** 3.4, and **figure** 3.5), or map to physical attributes such as temperature, will have significant effect on what process signatures are observable.

Applications of MPM systems for L-PBF have, as of yet, generally been unsuccessful in accurately observing and/or predicting highly localized process flaw formation such as individual pores or voids. More often, relative trends are analyzed over larger spatial areas from the melt pool monitoring data (e.g., **Figure 3.3**). Additionally, since MPM systems observe only the surface during fabrication, lower layers may be remelted, causing any defects or anomalies detected by the MPM system to no longer exist in the final part. This can and does lead to large false positive rates and remains an un-solved challenge.

3.1.3. DED melt pool characteristics

In the powder-blown L-DED process, the delivery of powder and energy occurs simultaneously at a given location on the substrate. The melt pool forms on the substrate, and subsequently consolidated layers. **Figure 3.7** shows a schematic of this process from Piscopo et al., where the powder is blown into the melt pool where it quickly melts and the deposited track is formed [232]. As mentioned by Piscopo et al. [232], the melt pool characteristics can be dependent on several parameters, such as laser power, laser characteristics (wavelength, mode), laser spot size, carrier gas flow (temperature, pressure, velocity), powder material properties (size and size distribution, shape, thermal properties), nozzle configuration, and process characteristics (hatching distance, scanning speed, scanning strategy).

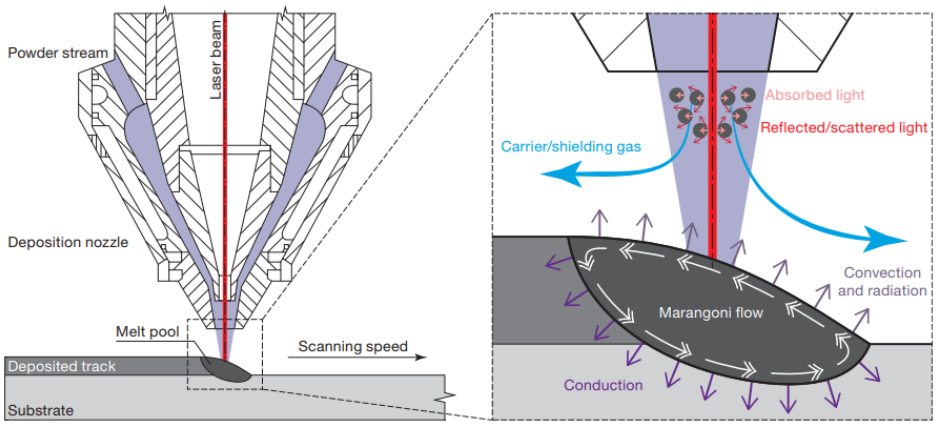

Figure 3.7 Schematic of the powder-blown L-DED process [232]

The melt pool dynamics in DED are still an active topic of research [233]. In the melt pool, a very large temperature gradient causes high surface tension and free convective and Marangoni flows. The deposited layers on the substrate are affected by the Marangoni flow in the melt pool. The Marangoni flow occurs when the melt on the surface flows from regions with lower surface tension to those with higher surface tension. The Marangoni flow can carry the entered powder particles in the melt pool toward the melt pool boundaries or its center depending on the flow direction [234]. Due to high temperature, thermal radiation of the molten material is also emitted. Heat conduction through the substrate and the convection generated by the shielding gas occurs during the melt pool generation. Solidification from the melt pool occurs primarily due to conduction into the substrate [233].

The melt pool convection current is important for mix homogeneity in the process of alloying, but it can also lead to increased porosity [233]. A greater amount of porosity is observed where fluid velocity inside the melt pool is faster. The porosity also increases with higher powder feed rate, shield gas flow, and laser power [233]. Spatter generation happens when a portion of the melt gains enough momentum to leave the melt pool, which is usually associated with overheating of the melt pool resulting in vaporization [234].

The energy density applied in DED processes is typically much greater than in L-PBF, which results in:

1) The spatial scales of L-DED melt pool signatures are larger (i.e., larger melt pools), and temporal scales are longer (i.e., lower frequencies) compared to L-PBF. Caprio et. al. provide a thorough review and comparison of L-PBF and L-DED melt pool signature temporal frequencies observed by researchers [218].
2) The temperature or radiant emission scales are similar to L-PBF (i.e., from ambient to boiling of metals). However, the much higher energy densities may induce superheating or plasma formation [222, 235, 236].

Furthermore, the shape or aspect ratio of DED melt pools tends to be more circular rather than elongated, due to the relatively low scan speed compared to L-PBF (e.g., **Figure 3.7**).

3.1.3.1. Potentially observable DED process anomalies from MPM

Common L-DED flaws were discussed in Sec. 2.2.1, including 1) porosity stemming from systematic or locally incorrect processing parameters, 2) geometric defects or warping stemming from a) residual stress or b) weld bead height variation, 3) cracking from a) macro stress-induced delamination or b) micro-scale solidification cracking, and microstructural defects. Similar to L-PBF MPM, much of the research on L-DED MPM observes anomalous melt pool signatures, such as changes in size, shape, or temperature, from which they infer, correlate, and/or predict the occurrence of one or more of these flaws, rather than direct observation of the flaw formation.

One of the more commonly cited flaws is the variation in track height, which is commonly monitored using a laser triangulation profilometer [237]. While this arguably may be considered MPM, track height monitoring is discussed in Sec. 3.2 on machine vision applications. The following is a brief synthesis of the reviews by Tang et al. [184] and Wang et al. [230], and the summary of signature and in-process flaw relationships in Sec. 2.2.2 **Table 2** for those signatures observable by MPM:

- **Melt pool temperature:** Measured via cameras or single-point detectors in co-axial, staring, or paraxial configurations. Additionally, dual-wavelength cameras or pyrometers are generally more commonly cited for use on DED systems, as are paraxially-mounted configurations (see Figure 3.1). Similar to L-PBF MPM, measurements of L-DED melt pool temperature signatures are most often correlated to part qualities or flaws without a direct physical/causal relationship elucidated.
    - *Physical sources of variation*: Off-nominal processing parameters, including power, scan speed, material feed rate, or variations in distance from the part surface to the deposition head (e.g., dilution).

- *Effect on fabrication or part quality:* porosity (e.g., [238]), part geometry or dimensional accuracy (e.g., [239]), microstructure (e.g., [240])

- **Melt pool geometry:** Like L-PBF, melt pool size in L-DED is intrinsically tied to the temperature field in and around the melt pool. While calibrating for temperature is unnecessary for determining melt pool size, size metrics are commonly acquired in conjunction with melt pool temperature monitoring. Geometry metrics can include width, length, height, outline, or area of the melt pool [184], extracted from imaging sensors via similar image processing algorithms to L-PBF MPM.
  - Physical sources of variation and effect on fabrication or part qualities are similar to melt pool temperature signatures.
  - *Effect on fabrication or part quality:* Effect on fabrication or part quality: porosity, especially lack of fusion (e.g., [147]), surface roughness (e.g., [239]), part distortion or geometric inaccuracy due to material buildup or insufficient material delivery (e.g., [110]).

- **Plume signatures (spectroscopy):** The most common objective of spectroscopic MPM in L-DED is to identify and measure the intensity of alloying elements that have disassociated in the highest temperature (e.g., plasma) regions of the plume, and emit radiation at fixed and narrow wavelength bands or 'lines'. These elemental lines are most commonly referenced from a NIST database [241].
  - *Physical sources of variation:* Anomalous variation in feedstock material composition; anomalies in melt pool; and plume size/temperature stemming from process parameter variations; anomalous interaction shielding gasses; etc.
  - *Effect on fabrication or part quality:* Most commonly cited is microstructural anomalies, which are highly dependent on the specific alloy being processed (e.g., Cr in H13 tool steel [242], Cr and Fe in Metco 42C stainless steel [243], or Ni and Cr in a nickel superalloy [244]), although correlations to melt pool characteristics such as size/shape [243], or structural flaws such as porosity (e.g., [210, 245]) are common.

3.1.3.2. Conclusions on L-DED MPM

Although the MPM system modalities are relatively similar between L-PBF and L-DED systems, due to the differences in melt pool size, scale, and dynamics, measurement parameters such as spatial resolution, sampling rate, etc. generally are much more stringent for L-PBF. MPM systems can be categorized based on different modalities: physical configuration (staring vs. co-axial), availability sensor spatial information (single point detector vs. image-based), filtered light wavelength(s), etc., all of which have varying strengths and weaknesses described in Sec. 3.1.1. The discussion and conclusions about MPM systems and their use in L-PBF machines presented in Sec. 3.1.2.2 are also applicable to L-DED machines.

While some challenges are relaxed in the MPM of L-DED compared to L-PBF, L-DED adds unique challenges. Feedstock delivery (powder or wire) can often obstruct the MPM sensor's view of the melt pool or present itself within the field-of-view of the sensors (e.g., **Figure 3.8**). Another

challenge is that sensors mounted paraxially to the deposition head (e.g., **Figure 3.1 d**) must rotate with the change in motion direction of the deposition head, or they risk the deposition head blocking the sensor's view of the melt pool. This has been alleviated by using multiple sensors configured around the deposition head [194].

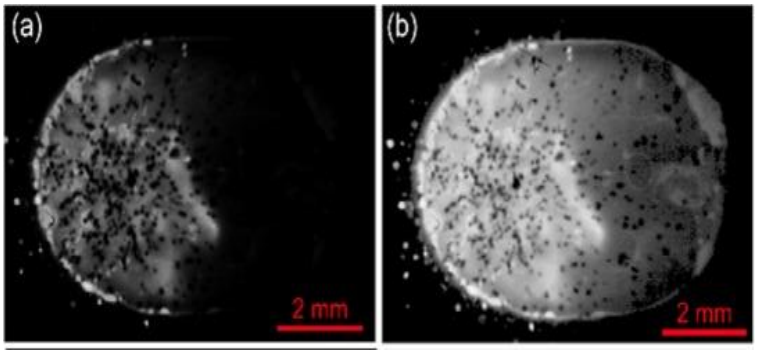

Figure 3.8 Example co-axial melt pool imaging system on powder-blown L-DED system. Small dark spots stem from relatively cool powder particles. (a) original image (b) gamma-corrected (i.e., grayscale values shifted) [231].

In-process monitoring review papers specific to L-DED include Reutzel and Nassar [185], Tang et al. [184], and Wang et al. [230], who provide summary tables of various monitored process signatures in L-DED (see also 3.1.3.1).

3.2. Machine vision (optical) methods

AM process reliability is challenging due to the inherent variability among even the same model of the AM machines. Machine vision (MV) approaches have the potential to identify and, in some cases, mitigate issues in real-time [188]. Additionally, the wide range of capabilities, speed, and low cost of these systems compared to thermal imaging systems make MV a promising technology for in-situ NDE. For the purposes of this document, MV will be defined as a method, process, or system that uses sensing techniques in the visible portion of the light spectrum as input to a decision process. This differs from computer vision, where the goal is to optimize meaningful output(s) for the operator to use for a decision [253]. Both systems can use optical measurement data but differ in how the data are used and analyzed after collection. Thus, while many of the technologies described can be used for both methods, the focus will be on the sensing techniques and how they are used in a MV system.

Moreover, the process of analyzing the data for the decision process in MV systems can range from simple thresholds (e.g., a "go" or "no go" decision from a single-value threshold) to highly complex machine learning (ML) and artificial intelligence (AI) algorithms. Thus, the potential algorithms that could be used in MV are too vast to adequately detail here; however, review articles describing these methods in detail exist in the literature. McCann et al. provided a review of in situ sensing techniques and their application in ML in Sec. 4.3 of the work [254]. Sahar et al. reviewed ML for anomaly detection in L-PBF [255]. Sarkon et al. reviewed the application of ML, including in-situ anomaly detection in Sec. 2.3 of the work, covering aspects of design, manufacturing, and property prediction and control for L-PBF and L-DED [256].

3.2.1. Machine vision modalities

Staring vs. coaxial: For machine vision systems, staring and co-axial configurations are the same as described in Sec. 3.1.1 and **Figure 3.1**. MV systems can also be mounted directly to the recoater mechanism in L-PBF systems. This setup is similar to a paraxial system described for L-DED in Sec. 3.1.1 and is used to capture information about the powder bed, spread consistency or quality, and solidified material geometry in situ [248]. An example of this type of system is shown in **Figure 3.9**, where Berez and Saldaña mounted a commercial laser line profiler, for measuring height variations along the line (based on triangulation), to a commercial LPBF system [248].

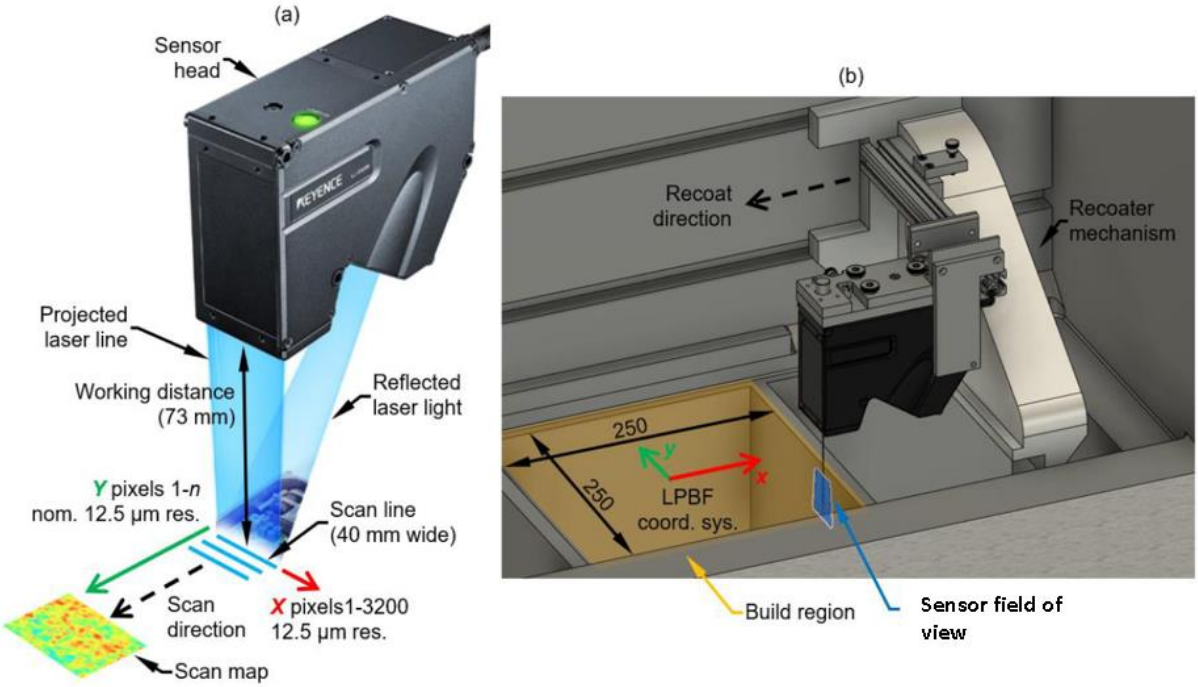

Figure 3.9(a) Instrument schematic and description (figure adapted from Keyence Corporation). (b) Instrument as implemented in an EOS M280 LPBF system. All dimensions shown are in mm [248].

In both L-PBF and L-DED, co-axial systems often use the radiated light from the melt pool (i.e., light emitted from the metal due to the increased temperature) as opposed to reflected light as the setup is most often used to monitor the melt pool. Additionally, the speed of the L-PBF process necessitates frame rates that would require significant additional lighting to use reflected light [73]. Additional light can be from an off-axis or co-axial light source, and a schematic of the latter is shown in **Figure 3.10**.

Wavelength and Light Source: Most MV applications rely on charge-coupled devices (CCD) or complementary metal-oxide-semiconductor (CMOS) cameras to acquire data and capture light in the visible portion of the spectrum (i.e., wavelengths of 380 nm to 700 nm). The captured light can be either emitted from the object (e.g., thermal radiation) or reflected by a target surface illuminated from an external light source. This section will only include systems that use reflected light rather than emitted light. MV systems that utilize emitted light primarily for MPM are discussed in detail in Sec. 3.1 and will not be included in this section.

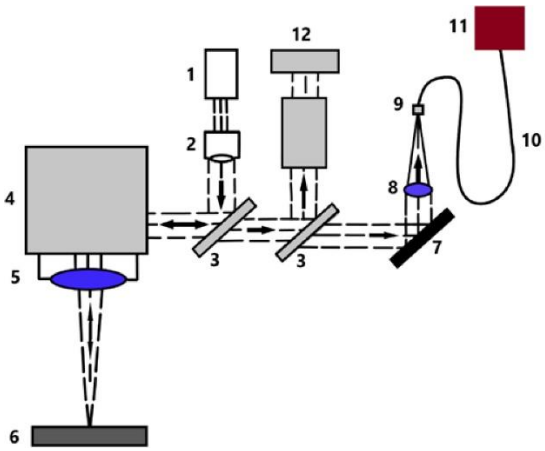

Figure 3.10"Coaxial System with additional lighting. (1) fiber laser, (2) beam expander, (3) laser beam/thermal signal separating mirror, (4) scanner head, (5) F-theta lens, (6) powder bed, (7) mirror, (8) pyrometer lens, (9) fiber tip, (10) optical fiber, (11) pyrometer, and (12) CCD camera" [257].

2D Methods vs 2.5D and 3D Methods: MV systems can also be grouped by the type of data they capture, such as 2D optical image data, surface height data, or 3D position data. 2D image data are obtained from visible cameras (e.g., CCD, CMOS) and the range of potential cameras and optics allows these systems to be set up with a field-of-view that can capture the entire build platform [96] or zoom in close enough to better understand the physics of the process [73]. Visible cameras are frequently used for investigating the geometry and temperature information of the molten pool. In L-DED, they are also used to determine the deposition height [110, 246]. In the case of wire-fed L-DED, a CMOS camera has also been used for monitoring the interaction between the wire tip and the molten pool during the deposition process [110, 270]. Visible cameras are also used in combination with IR cameras or pyrometers or both [110]. Grasso et al. provide a review of all in-process monitoring methods, including imaging in the visible range [188]. While not specifically for machine vision, the work provides a good reference for the capabilities of visible-range imaging systems used in PBF.

Surface measurements typically consist of one-dimensional (1D) height measurements in a 2D plane as a function of 'nominal' location. For example, this may be an array of height values where the X- and Y-spacing of points is derived from the fixed spacing of pixels of the microscope's sensor and the magnification during measurement. Furthermore, there can be only one height value for each position in the array (e.g., no two data points can have the same (x,y) coordinates). 3D methods consist of a measurement along all three orthogonal directions and are not constrained to the 2D plane (e.g., there can be multiple data points with the same (x,y) coordinates). Thus, surface height measurements of this type are often referred to as a two-and-a-half-dimensional (2.5D) method to differentiate it from 3D methods. 2.5D and 3D data can be obtained from many instruments, though commonly used in situ are optical coherence tomography (OCT) and structured light (SL) systems [188].

An OCT system has three components, shown in **Figure 3.11**: an illumination source, an interferometer setup (usually Michelson interferometer), and a spectrometer to detect the interference [273, 260]. The OCT device calculates the difference between a stationary reference and the measurement object with high spatial resolution. Samples with a high aspect ratio can

also be measured because the axial and lateral resolution of the OCT is not coupled. Thus, the OCT system can detect shape deviations from normal, which would affect the quality of the workpiece [273].

Optical coherence tomography is often used in the near-infrared range, but the technology also works in the visible portion of the spectrum. DePond et al. showed that spectral-domain OCT (SD-OCT) can be used to identify surface topography, spatter, and part dimensions [260]. That system was used co-axially with the process laser, though it can also be set up separately from the process optics.

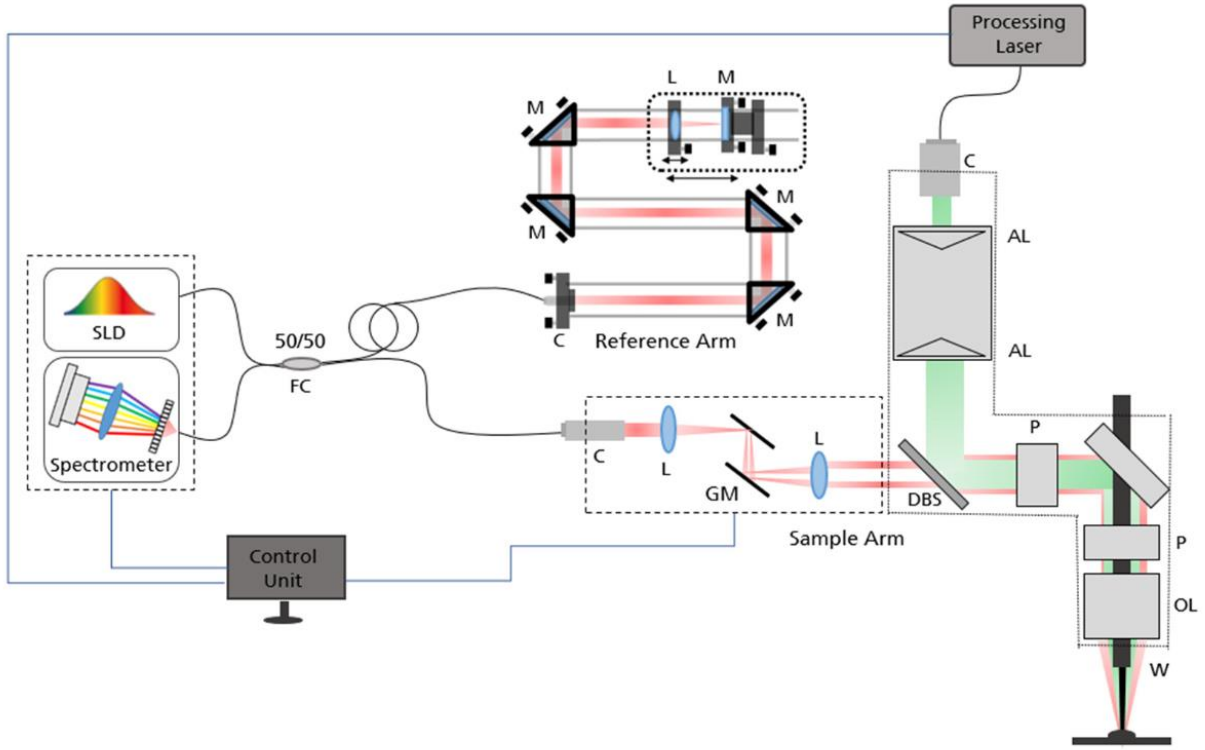

Figure 3.11"Schematic representation of the [L-DED] system. It includes the coaxial processing head, the wire feeding system, and the integrated SD-OCT measuring system. (FC: Fiber coupler, DBS: Dichroic beam splitter, C: Collimator, OL: Objective Lens, M: Mirror, GM: Galvo mirrors, AL: Axicon Lens, P: Prism, W: Wire)" [273].

Structured light scanning (e.g., fringe projection) is a commonly used high-speed and low-cost system for capturing height data or 3D geometry data in situ from the powder bed for L-PBF and solidified layers for both L-PBF and L-DED. The SL scanning system is made up of three components: a projector, a camera, and a control system. The projector projects a fringe pattern on a surface to be measured, while the camera captures fringe patterns [272]. A schematic of the system is shown in **Figure 3.12** from [261].

The structured light is often a sinusoidal variation in the intensity of the light. Deformations to the structure of the reflected light detected by the camera can then be used to reconstruct the 3D shape of the topography. The capabilities of the system will be dependent on the choice of a

projector, camera, and period of the detected sinusoidal variation of the structured light [261]. **Figure 3.13** shows an example of SL scanning of a fused layer by L-PBF process.

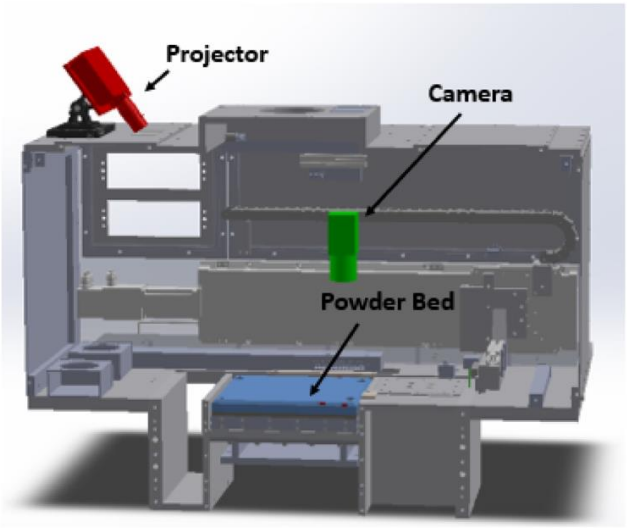

Figure 3.12 Example setup of a fringe projection system. [261]

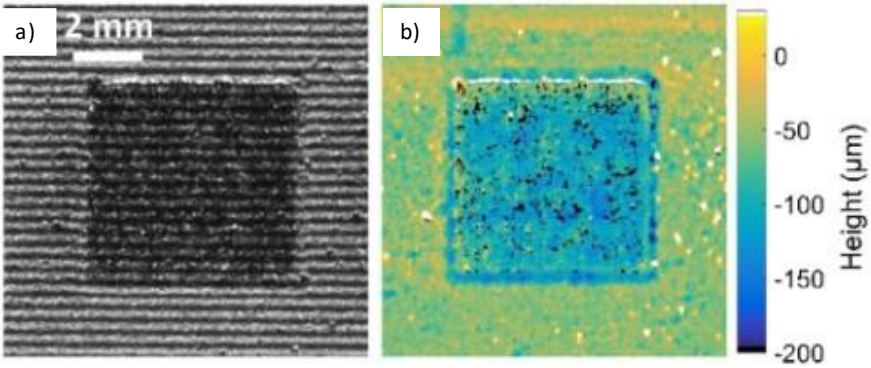

Figure 3.13"(a) Photograph of deformed fringe pattern on the fused powder surface on the 18th layer and (b) the corresponding fringe projection measurement of the surface topography. Black and white points in (b) are data drop-outs caused by shadowing and camera saturation respectively" [261].

Structured light and SD-OCT are height measurement systems that are used to determine the surface topography and dimensional accuracy of the fused region in situ. Other technologies for height and dimensional measurement exist and are well described in Leach et al. [262] and ISO 25718-602 through ISO 25178-607, which describe the working principles of the non-contact chromatic confocal probe, phase shifting interferometric microscopy, coherence scanning interferometry, point autofocus probe, focus variation, and confocal microscopy instruments, respectively. While these technologies provide high spatial (i.e., x and y) and height (i.e., z) resolutions, it comes at the cost of long measurement times when compared to fringe projection and SD-OCT. As such, these technologies are more often used ex situ to identify and characterize process signatures in the solidified material, such as weld ripples, chevron patterns, etc. for research purposes (e.g., [256, 262, 263]).

3.2.2. Potentially observable anomalies and defects in L-PBF using machine vision

Grasso et al. [188, 219] also provide an excellent resource for identifying and categorizing the types of defects (e.g., porosity, geometric inaccuracies, etc.), as well as the monitoring systems that have been used to capture the various signatures. Grasso et al. [188] categorize the in-process sensing and measurement methods into five levels based on their spatial-temporal characteristics. From that review, off-axis imaging of powder bed and printed slice data can provide spatial resolution below 10 µm/pixel, though it is more often in the tens to hundreds of micrometers per pixel, and co-axial systems are consistently below 20 µm/pixel spatial resolution [188].

Scime et al. [96] used the built-in layer-wise imaging of a commercial system to identify various anomalies observed on the surface of the powder bed. Examples of the various anomalies are shown in **Figure 3.14**. These anomalies are caused by undesired vertical motion of the recoater blade (i.e., recoater hopping, **Figure 3.14 a**), damaged recoater blade (i.e., recoater streaking, **Figure 3.14 b**), debris resulting from the fusion process landed on the powder bed (**Fig. 3.14c**), warpage of the fused part, curling out of the powder layer (i.e., super-elevation, **Figure 3.14 d**), lack of fusion on the part surface (i.e., fusion failure, **Figure 3.14 e**), and incomplete coverage of powder layer on the build platform (i.e., incomplete spreading, **Figure 3.14 f**) [96]. An example of the identification of these anomalies in the layer-wise images is shown in **Figure 3.15**.

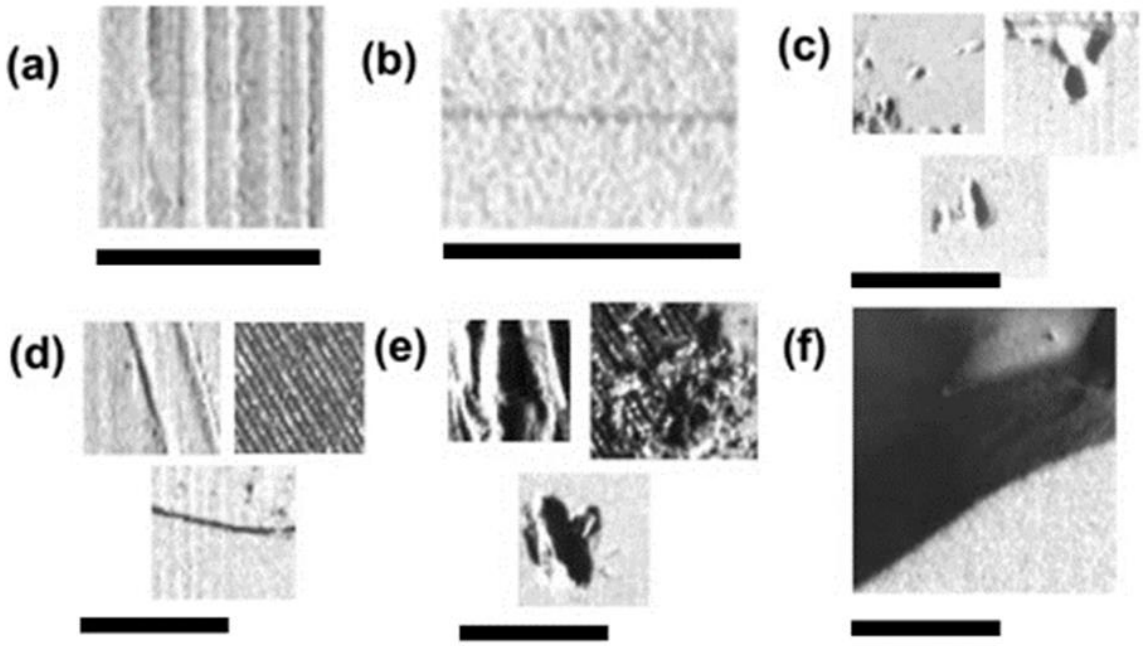

Figure 3.14 Examples of the different powder bed anomaly classes provided in [96]: (a) Recoater hopping, (b) Recoater streaking, (c) Debris, (d), Super-elevation, (e) Fusion failure, and (f) Incomplete spreading. Note that the relative sizes between the anomalies have been preserved. Scale bars (i.e., black bars below each example) are all 25 mm.

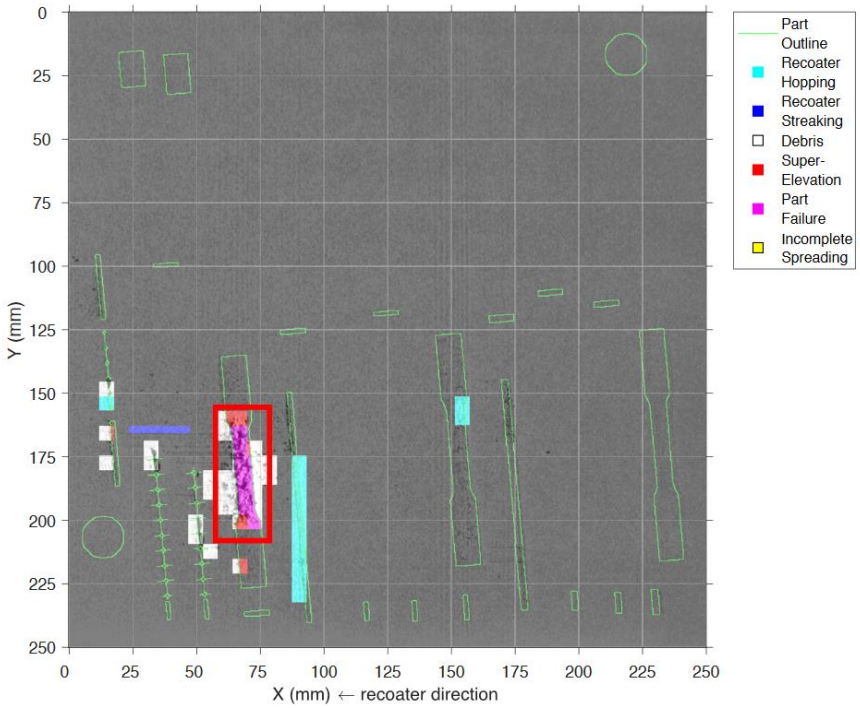

Figure 3.15 "Examples of detected anomalies in the printed layer. The green lines show the CAD outline of the parts at that layer" [96].

Pagani et al. used layer-wise imaging to identify the fused material contour for comparison to the intended geometry [252]. An example of this comparison is shown in **Figure 3.16.** The authors were also able to combine this with statistical process control charts (i.e., a one-sided control chart) to automatically detect and flag potential anomalies. The control limit for flagging potential anomalies is based on extreme value statistics (i.e., fitting the nominal deviations with a Gumbel distribution to determine the maximum likelihood a part will exceed the limit), where the threshold is determined based on a moving window of nominal deviations for a given part [252].

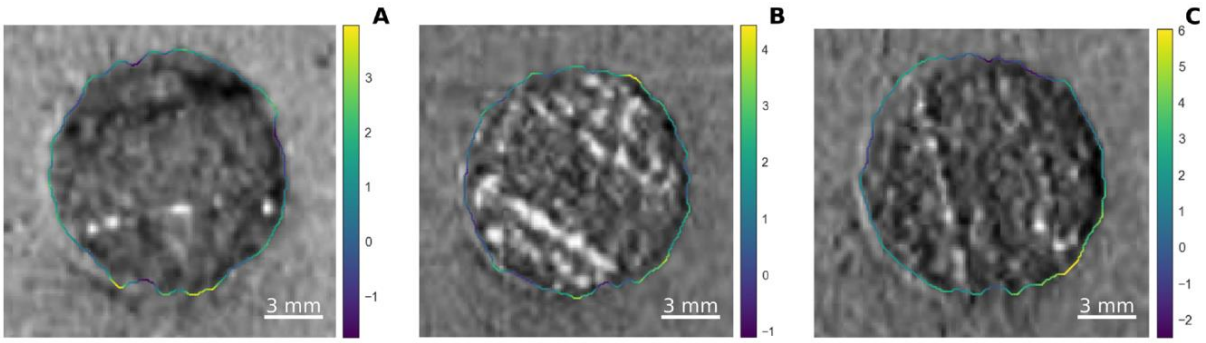

Figure 3.16 Example of segmentation of three circular slices of cylindrical specimens in one layer; the color map of the reconstructed contour indicates the local deviation – in pixels – from the nominal contour. [252].

2.5D and 3D data can be used to identify the powder spreading. Berez and Saldaña [248] were able to identify differences due to the recoater blade material, shown in **Figure 3.17.** Depond et

al. [260] used an SD-OCT system to identify surface quality and spatter in situ, as shown in **Figure 3.18.**

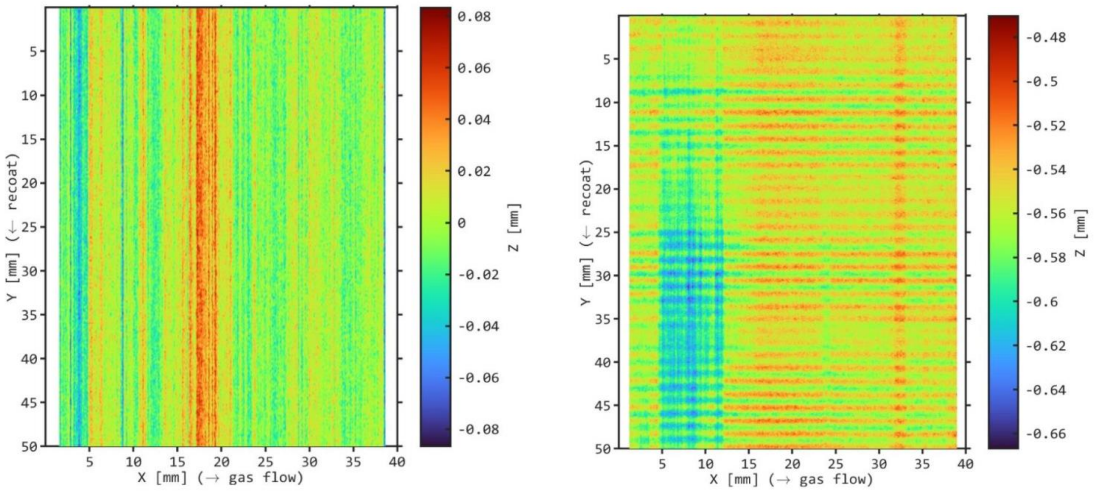

Figure 3.17 2.5D data from the spread powder layer using a brush (left) and blade (right) style recoater (Adapted from [248]).

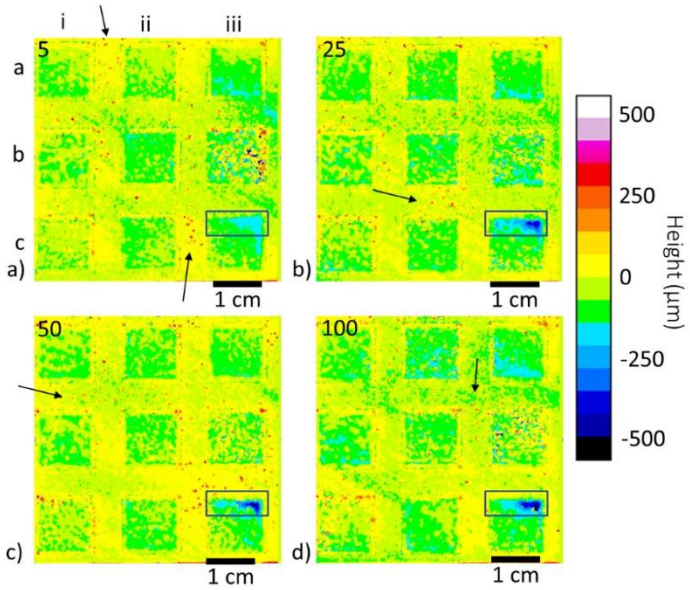

Figure 3.18 "OCT scan of nine L-PBF printed cubes recorded in each layer during a 100 layer build a) - d) clockwise from top right, the images represent layers 5, 25, 50, and 100 respectively, arrows indicate regions of spatter." (Adapted from [260]).

Zhang et al. [261] used their SL system to monitor the fusion of material at different laser power settings, shown in **Figure 3.19**, and the qualitative relationship between the fused material topography and the next layer of spread powder is shown in **Figure 3.20.**

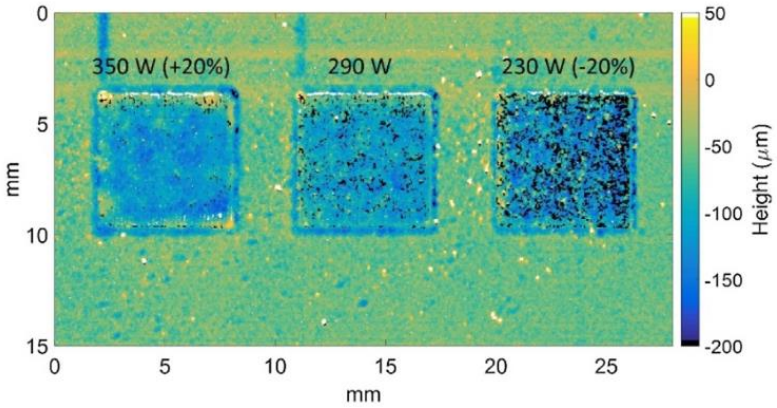

Figure 3.19 Image of powder bed surface height map taken after laser fusion at the 18th layer. Adapted from Zhang et al. [261].

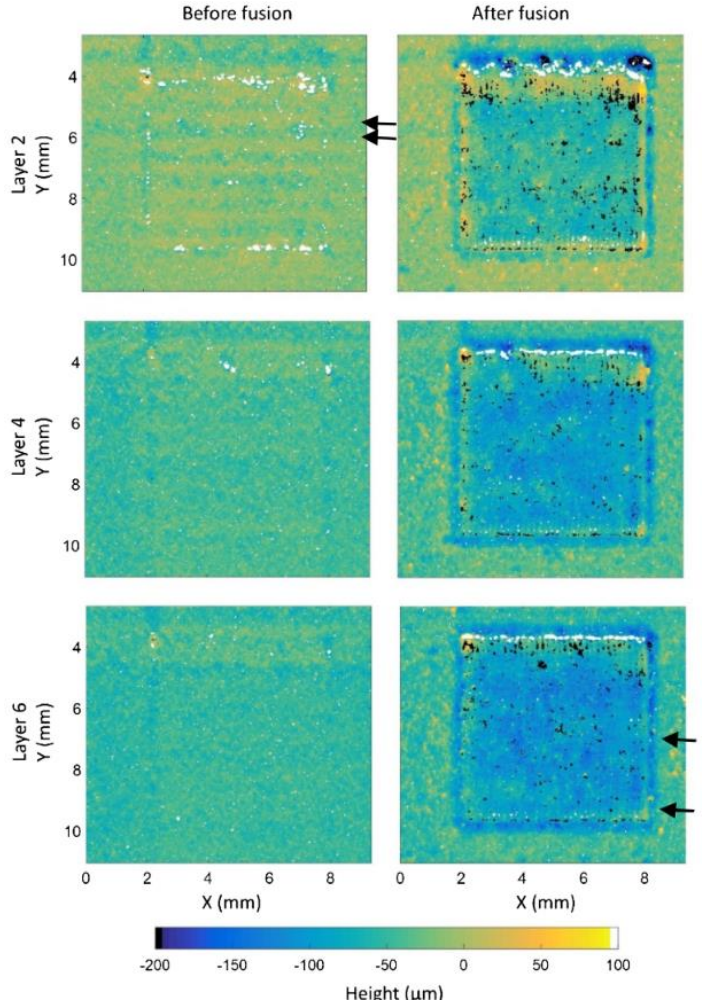

Figure 3.20 "Height maps of powder bed before and after laser fusion measured on every other layer" [261].

Many recent review articles cover defects, anomalies, and in-situ monitoring techniques for metal L-PBF. A comprehensive review is from Mostafei et al. [265], which aims to describe the research communities' understanding of the formation mechanisms, their effect on performance

(e.g., fatigue, fracture, distortion, etc.), detection methods for both research and production environments, and mitigation strategies found in the literature across multiple materials and machine manufacturers. In-process monitoring and MV are discussed in the work, but the breadth of knowledge conveyed in the paper prevents much depth into either topic [265]. For that depth, many review articles focused on in-process monitoring techniques exist [256, 262, 263].

3.2.3. Potentially observable anomalies and defects in L-DED using machine vision

In an L-DED system, fast cooling rates and high thermal gradients are usually present. These can lead to several anomalies and defects, such as non-uniform residual stresses, distortions, porosity, and cracking [259]. Defects such as high surface roughness can occur due to low heat input, large powder particles, high laser scanning speeds, etc. [259]. The melt pool is also generally unstable due to Marangoni effects, powder, shielding gas, etc. Therefore, only focusing on the melt pool for defect detection has some limitations [249]. Barua et al. used a commercial single lens reflex (SLR) camera and proposed a method to model a cooling curve for a desirable process for use as a reference in detecting defects, such as cracks and porosity [249]. Meriaudeau et al. used CCD cameras for determining surface temperature for estimating the mass flow rate of powder and monitoring the height and width of the deposited track [269]. Tabrizipour and Toyserkani [271] used three CCD cameras and interference filters for determining deposition height in real time. A system based on optical triangulation [275] can be used in DED for metal deposition height monitoring [237]. Zhang et al. used a SL system for in-situ monitoring of L-DED's layer-wise information (e.g., layer profile and roughness) with a resolution of 10 µm over a field of view of 12 mm by 12 mm [272]. Stehmar et al. used OCT for multi-directional process monitoring in the case of wire-based laser metal deposition [273]. The OCT system was able to observe variations in track geometry for future in-process mitigation and closed-loop control strategies. It could resolve individual weld beads, the occurrence of waviness, and shape deviations [273].

3.2.4. Applications for process and part qualification

Applications for process and part qualification using machine vision are still mostly limited to research environments. To develop MV for qualification purposes, Liu et al. presented a novel method for using light scattering techniques and machine learning to identify defective parts [276]. In this system, a laser illuminates the build surface and uses the scattering pattern as input to a convolutional autoencoder. Their work provided a fast, non-contact method for identifying defective parts, which is promising for use in production systems. Experiments, however, have yet to be performed in situ. AbouelNour and Gupta [257] provided a review of in-process monitoring systems with a focus on sub-surface and internal defects in AM. To help ensure process stability, the authors discuss the use of in-process monitoring methods to create closed-loop processes for defect correction. In that work, they review 2D optical imaging with little discussion of 2.5D or 3D methods. On the other hand, they discuss the application of ML and AI to in-situ monitoring for developing in-process defect correction. They also discuss the combination of in-process monitoring data and ex-situ validation by X-ray computed tomography

(XCT) to assess the quality of in-process monitoring techniques [257]. Both of these are valuable steps toward using MV for qualification.

While commercially available in-process MV systems for AM exist, application of these systems in production is also hindered by the lack of strong process-structure-property-performance (PSPP) connections. Data-driven in-process inspection has been considered for part qualification through capture and analysis of the melt pool geometry and temperature, residual stresses, and various defects. It has also been hypothesized that a data-driven in-situ process and microstructure-property correlation can be used for predicting product performance to report real-time defects and predict failures in printed products [280]. A comprehensive review of research developing these links to performance, including mechanical (e.g., tensile, fatigue) and corrosion behavior is provided by Mostafaei et al. [265]. That work also identifies many of the challenges to the wider adoption of in-process sensing techniques in the industry, which include the calibration of sensors and management of large quantities of data. The latter is also discussed extensively in the work by Gronle et al. [268].

3.3. Other in-process NDE methods tailored to AM

The techniques described in this section are relatively new implementation to AM in-process NDE and they are rapidly advancing. They have many possible variations and we have only seen limited applications of them so far. These are fast changing techniques, and there are still areas for improvements, and it is too early to generalize their strengths and weaknesses.

3.3.1. Ultrasonic/acoustic methods

Ultrasonic and acoustic-based inspection methods are common nondestructive testing (NDT) methods for various engineering applications. Ultrasound is sound with a higher frequency (e.g., > 20 kHz) than what humans can hear. Pulse-echo mode and pitch-catch mode are the basic detection modes. In the pulse-echo mode, the transducer both sends and receives ultrasound signals. In the pitch-catch mode, one transducer sends ultrasonic waves, and another transducer receives the signal over a distance or from another surface. The time-of-flight for the sound wave to penetrate one surface and echo off of another surface determines the distance between surfaces.

An A-scan of ultrasound, produced by a single sensor, represents individual sound pulses sent through the material tested, resulting in a plot of ultrasonic echo amplitude as a function of time. A B-scan of ultrasound represents 2D cross-sectional views of material measured at different positions. A C-scan of ultrasound represents 3D cross-sectional views plotted over an area. Ultrasonic methods have also been explored for AM in-process inspection. Unlike other methods described in earlier sections, the ultrasonic methods can simultaneously provide information about the current build layer and below.

Ultrasonic methods, however, have some limitations. For example, parts with a rough surface, irregular shape, or small, thin, and/or non-homogenous features are challenging to inspect. Ultrasonic waves may also be affected by temperature. A review of relevant research activities is provided in this section. Various transducer types (e.g., contact piezoelectric transducer, non-

contact laser-based source, and detector, or a contact transducer without the need for coupling agent), excitation/detection frequencies (e.g., nanosecond to femtosecond pulse width), and techniques (e.g., pulse-echo, pitch-catch, phased array, and total focusing method) were implemented in these studies. The feasibility of detecting flaws and measuring material properties/microstructure are described, and practical limitations are also discussed. Many techniques demonstrated in-process inspection feasibilities through off-line demonstrations at this point, and the TRL is rather low.

3.3.1.1. Contact ultrasonics for in-process NDE

Contact ultrasonic methods were used to demonstrate online inspection of AM processes [281, 282]. Contact transducers (10 MHz) with grease coupling were installed underneath the L-PBF build plate. This type of setup needs to withstand environmental conditions such as an inert gas atmosphere and elevated temperature (80 °C). The ultrasonic signals showed indications of higher porosity resulting from lower laser power applied to some AM layers during the build (**Figure 3.21**). The collection of recorded A-scans is plotted against the build time in the left image, which is referred to as B-scan by the authors in this paper [282]. The diagonal lines are related to reflection from the build surface whose height from the build plate is changing over time, and the horizontal lines are related to reflection from the porous layers. Information regarding the size of the flaw was not available. The residual heat seemed to affect the material ultrasonic velocity, which may need to be corrected. This type of configuration, however, is not sensitive to complex features that may not be directly connected to the build plate (e.g., overhanging structures). Therefore, applicability is limited to prismatic structures. Space below the build plate may not be readily accessible in some commercial systems. The needs of a coupling agent and direct transducer contact may hinder the AM build process. The TRL is about 5-7 for this type of approach, but applications are limited.

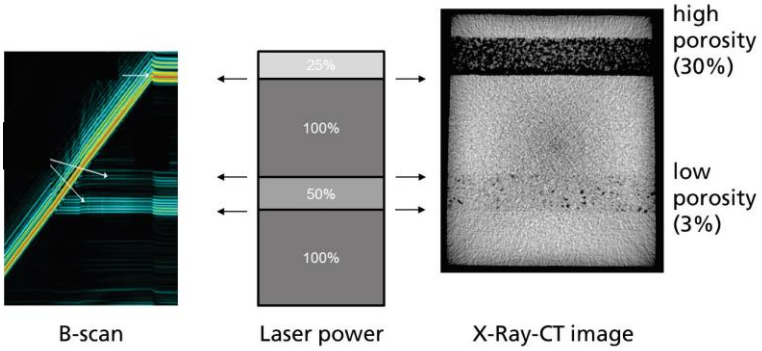

Figure 3.21 A direct comparison of the monitored B-scan with the CT-image shows an excellent correlation of the ultrasonic features with the specimen's microstructural appearance. [282].

3.3.1.2. Laser ultrasonics for in-process NDE

Laser ultrasonics (LU) is a promising in-process NDE tool for AM processes as the ultrasonic waves can be generated and measured without direct contact of transducers to part surfaces. A detailed overview of LU methods and their applications are provided in [283]. LU has the benefits of

dealing with variations of surface temperature, roughness, and when direct access to part surface is limited. One of the disadvantages of LU is the lower sensitivity compared to contact transducers. It is possible to increase the laser power to improve the sensitivity, but laser melting or laser ablation can occur depending on the laser pulse width. There are also safety hazards associated with high-power lasers, which must be considered in some NDT practices. Researchers are also investigating the use of existing lasers and optics of the AM system for laser ultrasonics to reduce the cost of having additional laser sources and associated optics. Surface roughness generally reduces reflected signals on the detector, which is one of the challenges associated with the inspection of AM parts or processes.

An LU setup requires components for ultrasound generation and ultrasound sensing. A pulse laser can be used to generate ultrasound and the same pulse laser or another continuously running laser source can be used for ultrasound sensing. Laser pulses cause localized heating on part surfaces, which generates thermoelastic stresses and strain to produce ultrasonic waves. Various types of elastic waves and amplitudes can be generated including bulk waves, surface waves, and guided waves. Ultrasonic sensing can be accomplished based on different methods such as two-beam homodyne, two-beam heterodyne, time delay, Fabry-Perot, dynamic holographic, multibeam, fiber interferometry, optical beam deflection, and knife edge detection. Laser interferometry using the Doppler effect, a type of the two-beam heterodyne method, is often used due to its high sensitivity and stability. An example setup of a heterodyne interferometer with an acousto-optical modulator (e.g., Bragg cell) is provided in [284] as shown in **Figure 3.22**. The Bragg cell introduces a carrier frequency (f_C) either in the reference or measurement beam. The photodetector (PD) receives frequency f_C if the sample is not in motion, and $f_C + f_D$ if the object is moving towards the interferometer, and $f_C - f_D$ if the object is moving away from the interferometer. f_D is the doppler frequency ($f_D = 2 \cdot v / \lambda$), and the moving object velocity (v) can be estimated from the known frequency (λ).

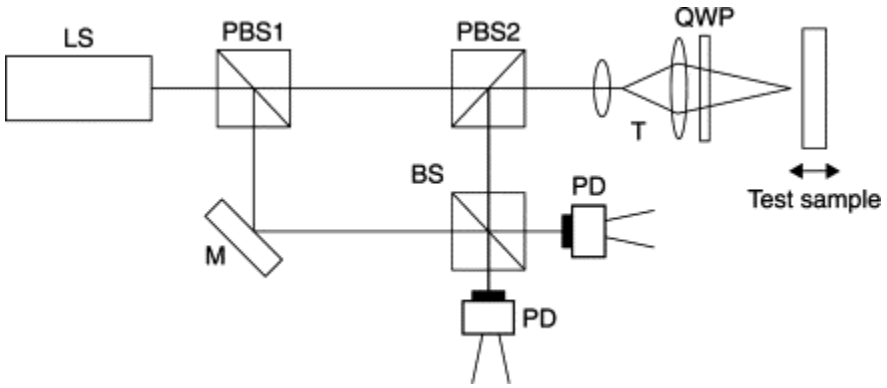

Figure 3.22 Heterodyne interferometer with an acousto-optical modulator, the Bragg cell (BC) [284]. LS denotes a laser source, PBS denotes a polarizing beam splitter, QWP denotes a quarter-wave plate, and M denotes a mirror.

There are various inspection methods demonstrated using LU-based principles. The following list provides some of the reported methods applied for or have the potential for in-process NDE of AM processes.

• **Time of flight (B-Scan):** An off-line LU study was conducted by Everton et al. [285]. They seeded designed flaws in a zone of 10 mm x 3 mm x 0.2 mm within a Ti-6Al-4V part (20 mm x 10 mm x 10 mm block) through an L-PBF process by changing processing parameters (scan speed and hatch spacing), and they illustrated the time of flight method to detect them. The result was compared to XCT scans (38 µm/voxel), but actual flaw sizes were not measured. Two separate lasers were used for the LU setup. A pulsed laser (Nd:YAG laser, 1064 nm wavelength, 200 mJ energy, 10 ns pulse, 20 Hz frequency) was used to generate ultrasonic waves, and a continuous laser (Yb-fiber laser 10 W, 1550 nm ± 10 nm wavelength) was used to detect the signals with an interferometer. The B-scans provided some indications of the presence of flaws, but they were unable to fully locate or quantify the flaws.

Millon et al. have similarly demonstrated an off-line LU setup for detecting electro-discharge machining (EDM) notches with an intention of extending to in-process NDE [250]. The EDM notches were introduced on both forged and AM-produced blocks with size of 0.3 mm width by 0.5 mm depth to 0.05 mm width x 0.1 mm depth. The B-scans showed the indications of the smallest notches (0.05 mm width x 0.1 mm depth). The amplitude of the reflected Rayleigh wave varied with the fabrication process (forging vs. AM) partially due to the difference in the microstructure. The study focused on surface-breaking notches, which may be healed during the build process of the following AM layers. TRL for in-process NDE is estimated to be 2-4.

• **Phased array:** Laser-induced phased array (LIPA) was also demonstrated off-line on a part for possible in-process NDE applications [286]. Instead of using optical delays or multiple laser sources, they used full matrix capture (FMC) and total focusing methods (TFM) to post-process and synthesize the array. One of the advantages of this type of approach is that images with spatial information can be generated. The test was carried out on a simple cuboidal part with through holes of different sizes still attached to the build plate. The laser was focused from the smoother build plate side to demonstrate the feasibility. A hole as small as 0.2 mm diameter was detected using a shear wave of 3 MHz. One-dimensional LIPA of 129 elements was synthesized in this study, which can be extended to a 2D LIPA array that will enable 3D volumetric inspection. An Nd:YAG laser with the wavelength of 1065 nm, a repetition rate of 5 kHz, and a pulse energy of 0.1 mJ was used as the generation laser. The laser was focused down to a 5 mm x 0.2 mm region while a laser vibrometer was used to measure the out-of-plane displacement using a continuous laser with 633 nm wavelength with power less than 1 mW focused down to a 0.04 mm spot. The detection laser moved along the part for FMC detection and the TFM was used to synthesize the captured data. The work was carried out from the bottom of the build plate, and it can be applied to in-process monitoring of relatively small parts of simple geometry without overhanging features. For a larger part with more complex geometries, the inspection should also be carried out from the build layer side. The high-temperature thermal gradient and rough surfaces would need to be considered. TRL of 2-4 is estimated.

• **Spatially resolved acoustic spectroscopy (SRAS):** SRAS is another LU-based technique, which can measure grain orientation similar to the electron backscatter diffraction (EBSD) technique [287, 288]. SRAS uses surface acoustic waves (SAWs, mostly Rayleigh wave) to

probe the material to a depth of 10's or 100's µm, which provides information about the microstructure and flaws at the surface and near the surface. The change in SAW velocity provides an indication of microstructure change and a signal dropout indicates possible flaws. Two separate lasers are used; one laser generates SAW on the sample surface, and the other laser detects perturbation caused by the SAW. The SAW velocity ($v = f \cdot \lambda$) was measured based on excitation frequency (f) and wavelength (λ) corresponding to grating fringe spacing. It uses a pulsed laser combined with an optical mask in the beam path to generate a fringe pattern with spacing λ on the sample. A continuous laser combined with a knife edge detector (KED) was used to detect the signals.

- Smith et al. [289] demonstrated an off-line inspection of an AM part using SRAS. Example results are presented in **Figure 3.23** where optical images (**Figure 3.23 a and b**), scanning electron microscope (SEM) image (**Figure 3.23 c**), acoustic velocity maps (**Figure 3.23 d and e**), and XCT (**Figure 3.23 f**) are compared. The bottom of the part was polished to improve the specular reflection of the SAW. They intend to move toward in-process inspection, but there are some challenges such as integration of instruments in the AM system, overcoming the effects of surface roughness, and ensuring fast inspection time. There is a potential opportunity to integrate SRAS setup into the existing laser optics used for laser-based AM processes. Surface roughness of less than 100 nm Ra is suggested to ensure specular reflection, but L-PBF roughness is in the order of 10's of µm to 100's of µm Ra. Optically rough surface detectors are still available to accommodate surface roughness. Surface roughness also affects surface acoustic wave generation and propagation. For rough surfaces, the waves can be attenuated and may not fully propagate to the detection point. For frequency of 10s to 150 MHz typically implemented in SRAS, the required propagation distance is typically only about 200 µm and therefore the signal attenuation hasn't been a problem in this research. Hirsch et al. discussed the trade-off between speed and resolution, and the needs to further improve SRAS technique [290]. While SRAS has been demonstrated for some time, application to AM in-process NDE is relatively new. TRL of 3-5 is estimated.

- **Pico/femtosecond LU:** Laser ultrasonics measurements with pico/femtosecond laser pulses are gaining attention for AM in-process NDE [291]. Femtosecond lasers can generate much higher frequencies that are sensitive to smaller flaws in principle. For example, Liu et al. [292] demonstrated the capability to detect porosity through femtosecond laser ultrasonics insensitive to the thermal effect. A pump-probe setup was used with a single laser source, which was split through a beam splitter. A delay stage was used to produce time delay variation between the pump and probe pulses, and probe pulse reflection at multiple time points can be measured. In order to improve measurement efficiency and signal quality, the pump pulses were modulated using an acousto-optic modulator with a reference sine wave. This essentially allows longer time interval to accommodate the pump pulse heat dissipation and individual pump pulse input can be assumed to be linear and time-invariant without the effect of pump pulse heating. A lock-in amplifier extracts the measured reflection component at the modulation frequency.

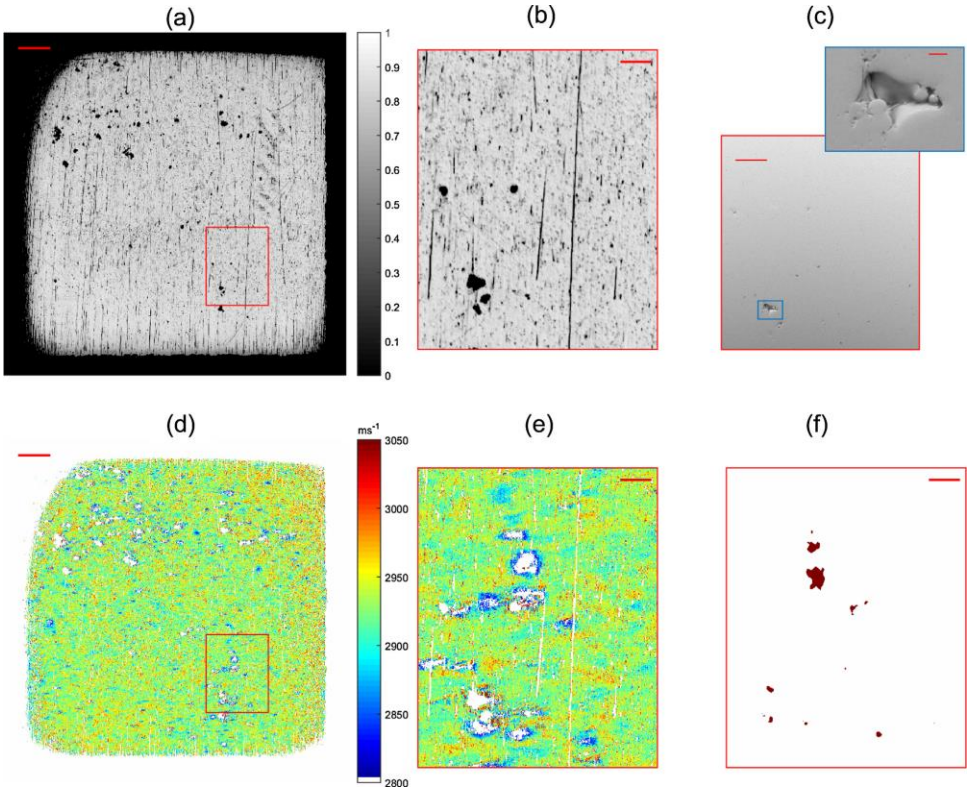

Figure 3.23 Images for the 190 W AM test sample (a) Optical image (scale bar 1 mm) (b) Optical zoom (scale bar 250 µm), (c) SEM micrograph of the corresponding area (scale bar 250 µm) and inset zoom of the large pore (scale bar 25 µm), (d) Acoustic velocity map (scale bar 1 mm), (e) zoom of acoustic data (scale bar 250 µm), (f) XCT subsurface (with no surface) data of zoomed region up to an approximate depth of 60 µm (scale bar 250 µm) [289]

Femtosecond laser ultrasonic measurements were also demonstrated for the estimation of elastic modulus and Poisson ratio for the L-DED process [293]. Laser polishing was implemented to reduce surface roughness to improve signals for laser ultrasonic measurements. The peaks of the longitudinal wave and Rayleigh wave were improved after the laser polishing. The laser polishing process, however, was implemented by the L-DED nozzle itself, which increased the total AM build time. In addition to the detection of flaws and measurement of microstructure, the femtosecond laser was also used to reduce porosity through accelerated and turbulent Marangoni flow, ultrasonic waves, and shock waves into the melt pool [294]. In-situ grain refinement was also demonstrated [295]. Most measurements are made off-line away from the AM system to demonstrate feasibility. **Figure 3.24** shows a potential implementation concept of incorporating the femtosecond laser next to the printing L-DED nozzle.

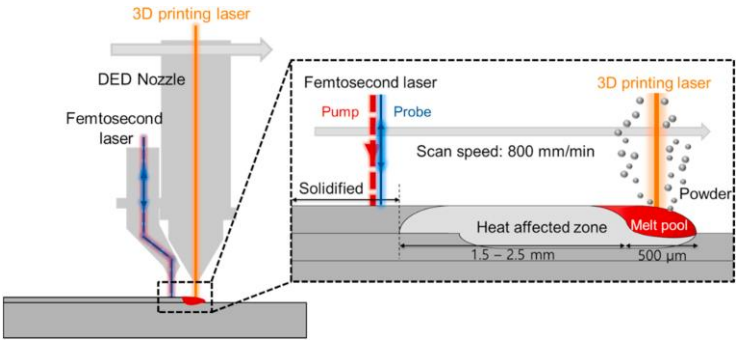

Figure 3.24 Schematic of the developed transient thermoreflectance (TTR) measurement system incorporated with a L-DED printing nozzle [292].

3.3.1.3. Roller-based transducers

The use of a roller-based transducer was also demonstrated for the in-process NDE of the wire arc-based DED process [296, 297]. The approach overcomes the limitation of conventional contact transducers. Silicone rubber is used for the roller probe tire, which conforms to undulating and curvy part surfaces without the need for a coupling agent. The tire material is expected to be thick enough to withstand high temperature (350 °C) but not too thick to reduce signal attenuation. Water is filled between the tire and the transducer, and a phased array ultrasonic transducer was used as the transducer. A Force-Torque sensor was used to allow real-time adjustment of the inspection robot kinematics. The roller transducer is shown in **Figure 3.25**. In addition, a robotic arm was demonstrated for both metal deposition and for the automatic operation of the roller transducer as shown in **Figure 3.26**. In another paper [297], they used one robot for metal deposition and another robot for inspection. A calibration block with curved surfaces and embedded flaws was used for demonstration of the capability. Flat bottom holes (1 mm diameter) placed at different depths (6 mm, 9 mm, and 12 mm) were successfully detected. Additional research is needed to reduce inspection time for in-process NDE application and to test on more complex part geometry. TRL is estimated to be 2-4 for this technique.

Figure 3.25 Computer-aided design and physical assembly of the phased array ultrasonic transducer (PAUT) roller probe: (1) silicone tire, (2) 5 MHz, 64-element linear PAUT and (3) PAUT carrier [296].

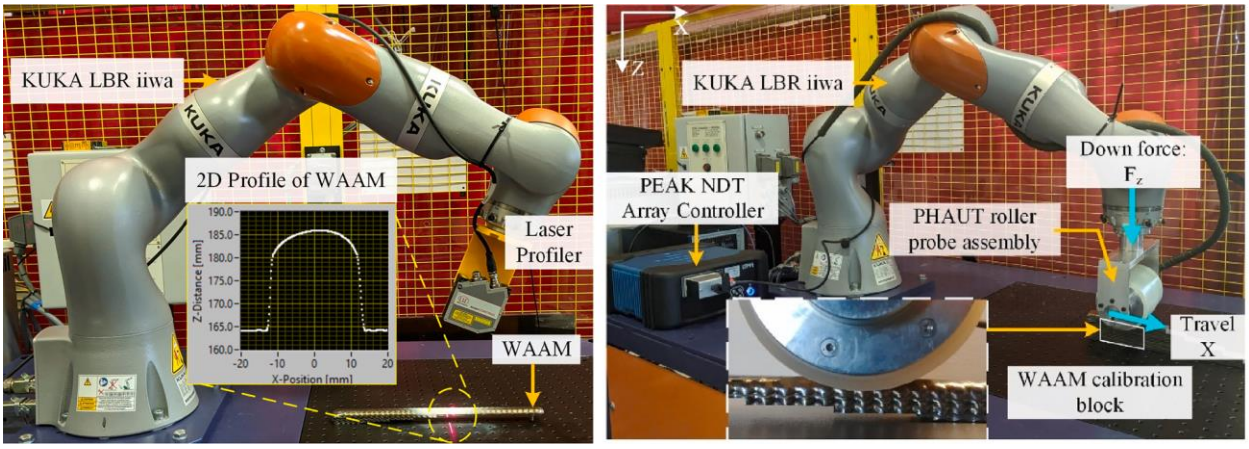

Figure 3.26 (a) Quantification of wire arc additive manufacturing (WAAM) lateral curvature using a 2D laser profiler and (b) experimental setup illustrating PAUT roller probe, array controller, Ti-6Al-4V WAAM calibration block with 1 mm flat-bottom hole (FBH) and industrial robot with built-in force-torque control capability [296].

3.3.1.4. Acoustic emission

Acoustic emission (AE) is gaining attention for AM in-process NDE due to its ability to retrofit and lower cost. **Figure 3.27** shows an example implantation of AE on different types of AM systems. The material delivery rate and variability (if any) in L-DED can be monitored in-process by acoustic emission sensors [251]. A device was developed to mount an AE sensor and also allow metal powders to flow, and AE signals were correlated to the actual powder flow rate. Eschner et al. correlated AE signals to part density through an artificial neural network (ANN) [298]. Part density was varied by changing laser power, scan speed, and hatching distance in 5 mm cubes, and part complexities were also further varied at three levels in the cubes. A total of 54 cubes were prepared (3 levels of laser power, 3 levels of scan speed, 2 levels of hatching distance, and 3 levels of design complexity). Reference density measurements were made using the Archimedes method after the build. Structure-born AE signals were collected by a contact acoustic sensor on the bottom of the build platform, which is mounted with a bolt with a coupling agent at the interface. The AE signals were analyzed in the frequency domain with the help of ANN. The density range was separated into 3 classes (class 1: > 99 %, class 2: 99 % - 94.3 %, and class 3: < 94.3 %), and F1 scores up to 88 % were found for classifying the density class. F1 score is the harmonic mean of precision and recall, and it can be also represented by true positives (TP), false positives (FP), and false negatives (FN) as shown in the equation below:

$$\left(F1 = \frac{2}{recall^{-1}+precision^{-1}} = \frac{2TP}{2TP+FP+FN}\right) \qquad (1)$$

The performance generally reduced as the design complexity increased. Porosity was induced by changing AM process parameters, but the AE signature of real flaw formation may be different.

Hauser et al. investigated the feasibility of AE for a wire arc-based DED process and a laser-based DED process [299]. The source of the AE signal for the wire arc-based DED process is the plasma expansion of the arc. The size of the arc was found to be correlated with AE signals and process anomaly. The nozzle-to-work distance variation also caused the change in AE signals. When geometrical fluctuations in the part exist, the nozzle-to-work distance changes, which resulted in

a change in the AE signal. The source of AE signal for the laser-based DED process is the interaction between the laser beam and powder. At a higher powder flow rate and higher laser power, the mean AE signal intensity increased. AE signals were captured when powder particles melted from solid to liquid and when the liquid resolidified. Interaction between molten particles also caused a change in AE signals, and this can be an indication of an unstable process. An AE technique for in-process NDE has been implemented to detect changes in global parameters (e.g., density), but with limited location-specific information. TRL is estimated to be 2-4 for in-process NDE using AE.

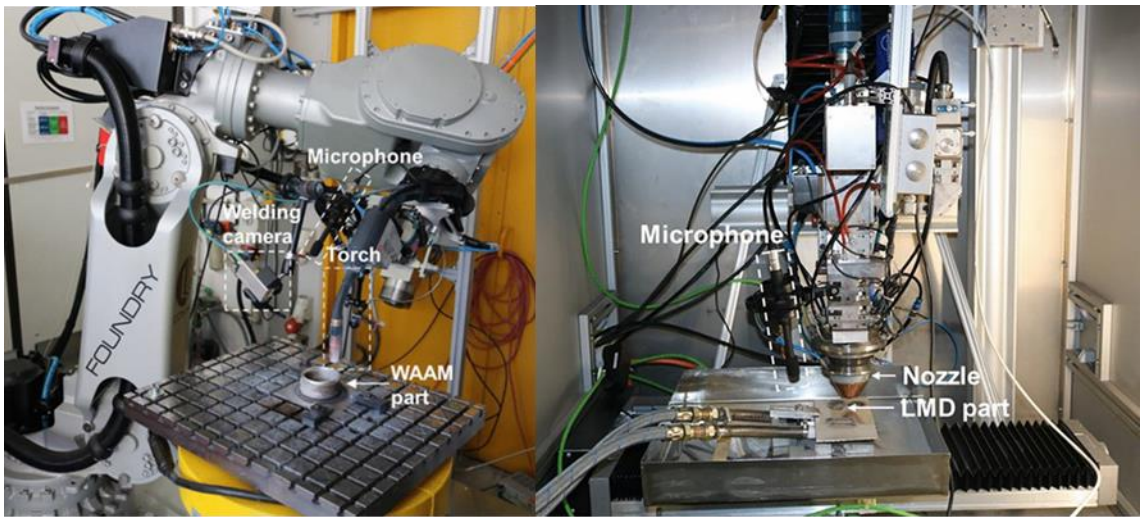

Figure 3.27 Acoustic emission system retrofitted on a robot-based WAAM cell (a) and L-DED process cell (b) [299]

3.3.2. Eddy current

Eddy current testing (ECT) is another widely used non-contact electromagnetic inspection technique. As magnetism is used, the technique can only be applied to conductive materials which include aluminum, stainless steel, copper, titanium, brass, nickel superalloys, and carbon steel. The induced EC in the material is highest at the surface and exponentially reduced as the penetration is increased. Therefore, ECT is sensitive to surface or subsurface defects that are close to the surface. The penetration depth is controlled based on excitation frequency. While some post-process inspection has been demonstrated for the ECT of the AM part, limited works have been demonstrated for in-process NDE.

Todorov et al. demonstrated the use of ECT for in-process NDE by integrating an ECT system in a research L-PBF system [300]. Lack-of-fusion pores with widths of 0.09 mm, 0.18 mm, 0.27 mm, 0.45 mm, and 0.9 mm were designed, and the larger four pore sizes showed indications in the ECT magnitude and all five showed indications in the ECT phase. Cuboidal voids filled with powders were also designed (5 mm × 5 mm × 0.4 mm). The feature first showed an indication when the depth was about 0.08 mm. The signal magnitude and phase increased as the depth increased. C-scan images provided indications on the designed pore position and size.

Spurek et al. integrated an ECT system into a commercial L-PBF system for in-process NDE [301]. Parts made with relative densities between 99.0 % and 99.7 % were manufactured by varying laser scan speeds. The ECT setup was incorporated on the recoater arm as shown in **Figure 3.28**. The excitation frequency was controlled such that the penetration depth is more than the remelting region. Approximately 74 % of the penetration depth is estimated to be in the post-process condition without the effects of subsequent remelting after the ECT measurements. The relationship between lift-off distance and a characteristic parameter involving the angular frequency of excitation current, magnetic permeability of the part, the electrical conductivity of the part, the mean radius of the coil, and the frequency of the excitation current was found, which provided information on the effect of variation of electrical conductivity and lift-off (i.e., the distance between ECT sensor and part surface). The effective solidified layer thickness was also measured based on the variation of lift-off, which was also accounted for when measuring relative density from post-process XCT data at a particular layer. The study does not provide information on flaw sizing, and applicability to more complex part geometry was not demonstrated. TRL is estimated to be 2-4 for in-process NDE using ECT.

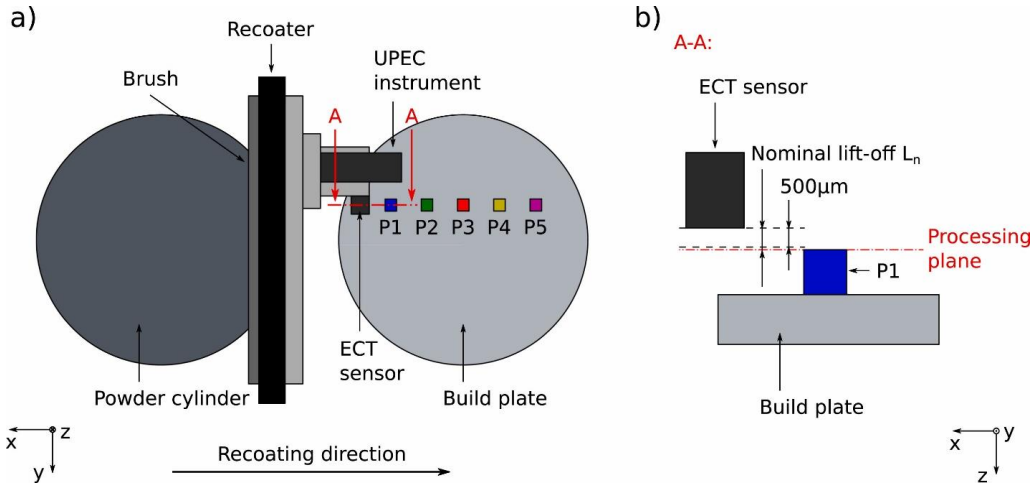

Figure 3.28 (a) Integration of the ECT system into the L-PBF build chamber, (b) Working distance between ECT sensor and part surface [301].

4. Review of codes, standards, and draft standards related to AM in-process monitoring and in-process NDE

While there is not yet a centralized or unified standards development effort specific to AM in-process monitoring or in-process NDE, various related development efforts are occurring and being initiated among several standards development organizations (SDOs), and different subcommittees within those SDOs. Multiple SDOs have developed various general frameworks for AM machine, process, or part quality control, and within these are sparse but existing mention of in-process measurements or monitoring (e.g., Sec. 4.4). However, it is anticipated that the primary source of new AM in-process monitoring standards will be developed in ASTM Committee F42 on Additive Manufacturing Technologies, which has a co-publishing agreement

with ISO Technical Committee 261 (TC261) on Additive Manufacturing. Due to the many unique traits of AM processes, many SDOs are developing standards, often through their own unique perspectives based on the industries they primarily serve. For instance, AWS is addressing AM by leveraging their experience with welding standards and ASME is developing standards under the contexts of codes and product definitions. In respect to standards relevant to in-situ NDE, while several SDOs address them peripherally, the ASTM F42/ ISO TC 261 and ASTM Committee E07 on Nondestructive Testing have developed standards that explicitly address the subject.

As of 2023, the only published standard specific to AM in-process monitoring is the Standard Guide ASTM E3353-22 from ASTM subcommittee E07.10 on Specialized NDT Methods. As discussed in that standard, because many of AM in-process monitoring technologies remain at low TRLs, it is likely that specifications, practices, or test method standards may not exist for some years, whereas guidelines or terminology standards are already being developed.

The following list of standards and standards under development are selected because they are directly or tangentially related to in-process monitoring or in-process NDE of metals additive manufacturing. Some additional standards are also provided that may not directly discuss in-process monitoring and in-process NDE but they are either critical references or discuss certain aspects pertaining to AM in-process monitoring. Foremost, the in-process monitoring standards refer to (and expand upon) terminologies related to AM part defects or flaws (e.g., ASTM E3166 or ISO/ASTM 52948 or ISO/TR 52906), or standard NDT terms (e.g., from ASTM E1316).

4.1. Standards directly related to AM in-process monitoring and in-process NDE

a. **ASTM E3353-22** ***Standard Guide for In-Process Monitoring Using Optical and Thermal Methods for Laser Powder Bed Fusion***

   This standard guide, published in 2022 on L-PBF in-process monitoring, is formatted similarly to E3166 for post-fabrication inspection. The technologies this guide reviews include melt pool monitoring, layer imaging, and a brief discussion of machine condition monitoring (e.g., refer to Sec. 3 of this report).

b. **ASTM F3490-21** ***Standard Practice for Additive Manufacturing — General Principles — Overview of Data Pedigree***

   This standard provides guidance on some descriptive attributes and metadata that should be collected and retained alongside in-process monitoring data.

c. **ASTM F3605-23** ***Standard Guide for Additive Manufacturing of Metals—Data—File Structure for In-Process Monitoring of Powder Bed Fusion (PBF)***

   This standard provides guidance on defining or creating in-process monitoring data file structures and provides examples of different in-process monitoring datasets processed, aligned with one another (registered), and visualized into 3D representation via open-source visualization software (e.g., ParaView).

4.2. Standards in development, directly related to AM in-process monitoring and in-process NDE

a. **ASTM WK82605** ***New Specification for Additive Manufacturing – General Principles -- Metal Laser Beam Powder Bed Fusion Machines for Spaceflight Applications***

This work item (from ASTM Subcommittee F42.07 on Applications) aims to detail requirements for laser beam powder bed fusion machines for metallic spaceflight parts, factory and site acceptance tests, and the in-process monitoring sensors. It dictates minimum monitoring capability for L-PBF machines.

b. **ISO/ASTM CD TR 52958** ***Additive Manufacturing of Metals-Powder bed fusion - In-Situ coaxial photodiode monitoring for lack of fusion flaw detection in PBF-LB***

This Committee draft (CD) technical report (TR) focuses on co-axial photodetectors. It describes experimental procedures and flaw detection algorithms (including AI/ML) to identify the location of flaws created during L-PBF process. It also outlines ideas for building seeded defects and reducing the dimensionality of process monitoring data. This draft is primarily based on a technical paper by Taherkhani et al. [302].

c. **ASTM WK73978**: ***New Specification for Additive Manufacturing-General Principles-Registration of Process-Monitoring and Quality-Control Data***

This draft standard describes terms, concepts, and practical methods related to the alignment, or registration, of process monitoring data with either other in-process data, build design data (e.g., part geometry), or post-fabrication inspection data. The standard will be designated ISO/ASTM 52953 when approved and published.

4.3. Standards that are likely key references for AM in-process monitoring standards

a. **ISO/ASTM 52900:2021** ***Additive Manufacturing – General Principles – Fundamentals and vocabulary***

This standard establishes and defines terms used in AM technology. The terms are classified into specific fields of application.

b. ISO 17295:2023 Additive manufacturing — General principles - Part positioning, coordinates and orientation

This document provides specifications for the coordinate systems for positioning and orientation of parts within AM machines. It is intended to be consistent with the principles of ISO 841 (describing coordinate systems for metal cutting machine tools) and to clarify the specific adaptation of those principles for AM.

b. **ASTM ISO/ASTM 52921-13(2019)** ***Standard Terminology for Additive Manufacturing—Coordinate Systems and Test Methodologies***

This standard is used as a normative reference in many ISO/ASTM additive manufacturing standards, providing definitions of AM machine and part coordinate systems and standardized orientations of those coordinate systems.

c. **ASTM E1316-22a** - ***Standard Terminology for Nondestructive Examinations***

This standard provides extensive terminology for general NDT concepts, and some terminologies for specific NDT technologies that may be applicable to AM in-process NDT (e.g., acoustic emission, ultrasonic testing, infrared testing, visual testing). It is heavily referred to in ASTM E3353, particularly regarding non-AM specific NDT terminologies such as indication, imperfection, flaw, defect, etc.

d. **ASTM E3166-20** - ***Standard Guide for Nondestructive Examination of Metal Additively Manufactured Aerospace Parts After Build [329]***

This standard provides an overview and guidelines to various AM post-fabrication NDT techniques. ASTM E3353 on in-process monitoring is modeled after this standard, and refers heavily to terms or concepts regarding AM-specific post-fabrication defects or flaws such as lack-of-fusion, porosity (keyhole), voids, etc.

e. **ISO/ASTM DIS 52948:2023** – ***Additive Manufacturing of Metals – Non-Destructive Testing and Evaluation – Imperfections Classification in PBF Parts***

This draft international standard (DIS) provides categorization and terminology, either new or referencing ISO/ASTM 52900, of AM flaws or defects. This standard will be published after E3353, but it is anticipated to be a primary reference for future versions of E3353.

4.4. Standards describing AM machine or process controls and qualification procedures, which mention in-process monitoring

a. **NASA-STD-6030 (2021)** ***Additive Manufacturing for Spaceflight Systems*** **[324] and NASA- STD-6033 (2021)** ***Additive Manufacturing Requirements for Equipment and Facility Control***

NASA-STD-6030 defines the minimum set of requirements for additive manufactured (AM) parts used for NASA crewed spaceflight systems, whereas NASA-STD-6033 implements the requirements for control of additive manufacturing (AM) equipment, facilities, and personnel, which are to be documented in an Equipment and Facility Control Plan (EFCP). NASA-STD-6030 mentions that in-process monitoring may inform 'restart procedures' (but no details), and STD-6033 has Clause 4.6.2 on In-Situ Monitoring, which is mostly a placeholder.

b. **SAE AMS 7003** ***Laser Powder Bed Fusion Process***

This standard, issued in 2018, specifies various process controls for "repeatable production of aerospace parts by laser powder bed fusion (L-PBF)." Clause 3.4 of this

standard on statistical process control (SPC) refers to ASTM E2587 and E2281 for practices to follow. Critical L-PBF control variables, including those related to machine condition monitoring are outlined in Appendix A (e.g., build platform preheat temperature, shielding gas flow rate, residual oxygen, etc.).

c. **NADCAP AC7110/14** REV. B: ***Audit Criteria for Welding for Laser and Electron Beam Metallic Powder Bed Additive Manufacturing***

This audit criteria, issued in 2020, provides an extensive checklist for NADCAP accreditation of laser and electron beam PBF operations from input materials control to final part evaluation. There are references to machine condition monitoring (e.g., monitoring chamber temperature and humidity, in Clause 5 Equipment), procedures and associated documentation to ensure consistent and repeatable AM builds (Clause 6 Procedure Control), post-fabrication part inspection procedures and documentation (Clause 9 Inspection and Acceptance Criteria), and AM machine maintenance and calibration (Clause 10 Periodic Maintenance and Calibration), which may eventually affect or utilize in-process NDE or monitoring.

d. **AWS D20.1/D20.1M:2019** ***Specification for Fabrication of Metal Components using Additive Manufacturing***

Clause 5.1.7 of this standard, In-Process Monitoring, states that process monitoring that do not alter or control machine variables are not required to be documented. These variables are listed in Table 5.2 of the standard and include items from the material inputs to laser processing parameters to post-build heat treatment. For in-process monitoring that does alter qualification variables (described in Table 5.2 of the standard), required aspects of documentation are listed, and these systems are considered 'major equipment subcomponents,' and require requalification of the machine. Furthermore, changes to machine condition monitoring variables (e.g., chamber temperature, residual oxygen) trigger requalification of the machine and AM procedure.

e. **ASME PTB-13-2021** ***Criteria for Pressure Retaining Metallic Components Using Additive Manufacturing***

Clause 14 of this standard, In-Process Monitoring, states that any in-process monitoring that alters or controls machine operation (e.g., feedback or real-time control) are not permitted in this standard's criteria. Otherwise, data from process monitoring, that is used to track process qualification variables (listed in Table 7-1, including items such as input material specifications, heat source characteristics, deposition characteristics, or post-build thermal treatment) is allowed, although commentary says more research and development is needed.

f. **ISO/ASTM 52941:2020** ***Additive manufacturing — System performance and reliability — Acceptance tests for laser metal powder-bed fusion machines for metallic materials for aerospace application***

This standard provides brief listing and description of L-PBF machine tests and characterizations. In-process monitoring primarily refers to machine condition

monitoring (e.g., laser power, scan speed, residual oxygen, and build platform temperature)

4.5. Standards complimentary, not directly related to AM in-process monitoring

a. **ISO/ASTM TR 52906:2022** ***Additive Manufacturing—Nondestructive Testing—Intentionally Seeding Flaws in Metallic Parts***

'Seeding flaws,' as a general approach, is commonly used by AM in-process monitoring researchers to evaluate the sensitivity or effectiveness of the monitoring systems. While this technical report does not detail methods specialized for in-process monitoring or flaw formation mechanisms, it may still applicable or useful to characterize in-process monitoring systems.

b. **ISO/ASTM 52902:2023** ***Additive manufacturing — Test artifacts — Geometric capability assessment of additive manufacturing systems***

This standard provides the design of various geometric artifacts designed to test the capability of AM machines to fabricate these geometric features. While tailored for post-fabrication inspection of geometric accuracy (e.g., linear positioning accuracy, fine/small feature accuracy) and/or surface finish, these artifact designs, or the concepts and rationale underlying their designs, can likely inspire or directly be used to characterize capabilities of in-process measurement systems.

c. **ISO/ASTM TR 52905:2023** ***Additive manufacturing of metals — Non-destructive testing and evaluation — Defect detection in parts***

This technical report (TR) provides an extensive review of NDE techniques as applicable to AM, including a comprehensive listing (with figures) of post-fabrication part defects, and a review of relevant NDE standards for AM. It also provides the design of a 'seeded defect' test artifact (a star-shaped geometry with varying-sized voids embedded within), then provides multiple descriptions and results of different post-fabrication NDE techniques used to characterize the artifact(s). It also provides a review (Clause 7.2 In-process NDT review) that provides a brief state-of-the-art and categorizes different in-process applications of NDE techniques based on the capability to detect defects vs. difficulty in applying in situ. It also gives several examples of in-process laser-ultrasonic (LU) measurements applied to L-PBF and L-DED parts.

d. **ASTM F3615-23** ***Standard Practice for Additive Manufacturing -- Powder Bed Fusion -- Condition-Defined Maintenance for Optical Systems***

This standard describes in-process measurement and characterization of laser optics degradation using a camera and subsequent image processing.

4.6. Standards in development complimentary, not directly related to AM in-process monitoring

a. **ASTM WK69731** - ***New Guide for Additive Manufacturing -- Non-Destructive Testing (NDT) for Use in Directed Energy Deposition (DED) Additive Manufacturing Processes***

This work item was initiated in 2019 and has undergone one ballot (will be reballoted). It provides a general review of NDT techniques applied to DED processes, including a review of relevant welding standards and emerging NDT techniques.

b. **ASTM WK75329** - ***New Practice for Nondestructive Testing (NDT), Part Quality, and Acceptability Levels of Additively Manufactured Laser Based Powder Bed Fusion Aerospace Components***

This work item, initiated in 2021, aims to provide AM part suppliers and customers NDT-based acceptance criteria for aviation and space hardware. The status of this work item is unknown.

c. **ASTM WK76038** - ***New Test Method for Additive Manufacturing of Metals -- Non-destructive testing and evaluation -- Porosity Measurement with X-ray CT***

This work item, initiated in 2021, aims to provide instructions for using reference calibration artifacts to quantify AM part porosity metrics such as size, distribution, and shape. Upon completion, this standard may form a key reference for evaluating the defect prediction accuracy of in-process NDE or monitoring techniques. The status of this work item is unknown.

4.7. Identified standardization gaps

Due to the relatively low TRLs of AM in-process monitoring, it is generally recognized that some significant research still needs to be done to establish the instrument design, data collection, analysis, and implementation within a production chain, before these may be standardized. As such, few roadmaps or resources exist that specifically identify standardization gaps for in-process monitoring of AM:

- **ANSI Additive Manufacturing Standardization Collaborative (AMSC) Standardization Roadmap for Additive Manufacturing Version 3.0** (https://www.ansi.org/standards-coordination/collaboratives-activities/additive-manufacturing-collaborative)
  - The Standardization Roadmap identifies 'In Process Monitoring" as Gap PC16. The roadmap does not subcategorize PC16 further.
  - Version 3 of the AMSC report was published in July 2023. Chapter 2.2.2.11 on In-Process Monitoring provides a brief update on developed or in-development standards, in addition to general R&D requirements.
- **Strategic Guide: Additive Manufacturing In-Situ Technology Readiness Findings and Path Forward for Applications in Qualification and Certification -** ASTM Center of Excellence (CoE), NASA Marshall Space Flight Center (MSFC), and America Makes (https://amcoe.org/in-situtechnologyreadiness) [277]

- This guide was published in June 2023. It summarizes the responses from over 60 experts specializing in AM in-process monitoring. This workshop, coordinated by ASTM CoE, America Makes, and NASA Marshall Space Flight Center, was held in June 2022, and included several dozen invited experts in AM in-process monitoring. A coordinated information gathering workshop was held that established the TRLs of various aspects of in-process monitoring, and identified gaps that require R&D to further develop the state-of-art. The guide also includes a 'landscape analysis' stemming from an in-depth literature review and results from interviews of twenty-one (21) domain experts conducted in Spring 2020.

5. Classification of in-process NDE data

AM offers unique opportunities for utilizing data to gain insight into the manufacturing process and the fabricated part. Unlike like most other manufacturing processes, including many other advanced manufacturing processes, metal AM processes allow for the complete observation of the material structure. Layer-by-layer, line-by-line, and point-by-point, in process measurements of AM processes provide unprecedented access to the formation of a part's microstructure and geometry. Viewed through a silo, however, the insight gained through these measurements becomes diminished, as the in process NDE represents only a partial piece of a greater whole.

Advanced manufacturing technologies such as AM have led to newfound interests in manufacturing process behaviors, especially the process physics. Many early advances in AM can be partially attributed to better process understanding, and this improved process understanding can be partially attributed to process insights gained by physics-based process modeling. Physics-based models drove new insights into melt pool behaviors, phase transformations, and dendrite growth, aiding in the maturation of AM technologies to a production ready state. These models, however, currently fall short as a means for ensuring homogenous material structure formation throughout the AM process. Instead, physics-based models provide a theoretical foundation for the validation of a successful AM process, a process that can be observed using many of the measurement techniques described in this report.

Correlations between materials, processes, and mechanical properties are often leveraged to establish expected part performance. Such correlations enable many part analyses techniques, such as finite element analysis. These correlations, however, have proven exceedingly difficult to achieve with AM due to the localized formation of material and introduction of heterogeneity. However, where AM lacks in process homogeneity it gains in process observation. Materials-process-property relationships have been increasingly studied and expanded to support advanced manufacturing. Additional considerations include geometry, structure, and performance often with the microstructure serving as a point of intersection (material /process to microstructure, microstructure to performance) [274]. As the study of these correlations has grown in intricacy, as seen with ICME (Integrated Computational Materials Engineering), the roles and usage of data become increasingly important. This section explores the characterization of in-process data and many of the traits that should be considered when leveraging this data to develop correlations between material, process, structure, properties, and performance.

5.1. AM data viewpoints

In-process AM data can be classified from two primary viewpoints: the manufacturing viewpoint and the data science viewpoint. The manufacturing viewpoint focuses on data characteristics associated with the fabrication of the part. Characterization from this viewpoint is vital to achieving insight into the process and formation of the solid part, providing context into what the data represents and understanding how the data can be used in developing correlations. The data science viewpoint focuses on data characteristics associated with the creation and evolution of the data. Characterization from this viewpoint is critical to understanding the fidelity of the data, providing context into how well the data represents the process or part. When leveraging data to achieve insight into a process or a part, both viewpoints must be carefully considered as they dictate the quality of the data, or how well the data can be used to support the intended objective or correlation.

As in-process data is used to provide insight into the process and part, understanding the manufacturing context in which it is measured, captured, stored, and presented is necessary. Without context, data can easily be misrepresented, misinterpreted, and misused. Properly considered, classification allows for context to be provided to the data even when little is known about its sourcing. When data is used to support analytics, such as for the qualification of a part, additional classification through the data science viewpoint can provide insight into the robustness of the data and the methods used to analyze it.

This section focuses on the transformation of data as it matures across a life cycle and the different ways this data may be classified to add further contextualization to its eventual use.

5.1.1. Manufacturing viewpoint

The two most important characteristics of in-process AM data that can be attributed to their manufacturing viewpoint are their spatial and temporal qualities. In-process data is inherently time-differentiated, as each data point is representative of a different point in time. As AM is a 3D fabrication process, in-process data are also inherently space differentiated. These two characteristics, combined with the various available monitoring techniques, create immediate distinctions that are often associated with big data, namely: volume, velocity, variety, and veracity [303,304]. For this reason, the context through classification can be a valuable means of achieving data clarity. These data are also subject to dimensional reduction, that is to say, data can be viewed at a single point in time or data can be viewed across time at a single point in space.

At the highest level from the manufacturing viewpoint, in-process data can be classified into two categories, process data, and part data [305, 306]. These two categories are not mutually exclusive in AM, instead, they uniquely overlap, similar to the process-structure and structure-performance correlations. The Venn diagram in **Figure 5.1** highlights this notion, illustrating that many types of in-process data can be used to draw conclusions about the process and the part. In-process monitoring data can be used to instill confidence in the process (process assurance), while the in-process NDE data focuses on the part (part quality assurance). As AM locally forms material properties, local process signatures during the formation of the part can also be used to

characterize the localized solidification of the part. Here we will discuss two types of data as defined in the report, in-process monitoring data and in-process NDE data.

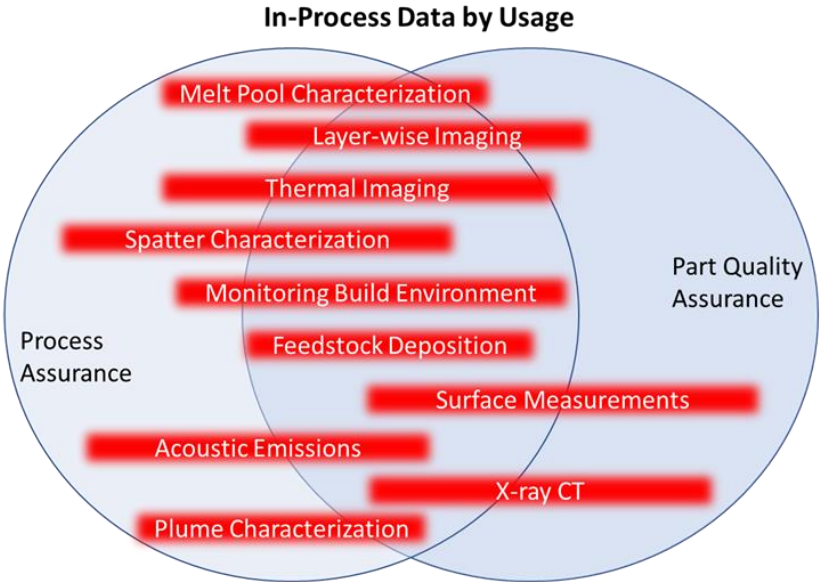

Figure 5.1 In-process data by usage

5.1.1.1. In-process monitoring data

In-process monitoring data refers to the data associated with the process and process physics prior to completed solidification of the material. These data are perhaps the most widely studied and characterized data, as it can be directly correlated with process behavior. Many examples of in-process monitoring behavior are explored throughout this report, including melt pool data (with different types of measurements), materials-related data, temperature data, etc. In-process monitoring data are often classified under several priority objectives: 1) to achieve insight into process behavior for a better understanding of the process; 2) to achieve insight into the process behavior in support of feedback control; 3) to achieve insight into process-material behavior for better-informed parameter selection and derivation of design allowables; or 4) to achieve insight into process-material-part behaviors and develop new correlations or verify against existing correlations. Given the importance of these objectives, the observations can be made that 1) classification of in-process monitoring data are heavily driven by physics and the equipment used to observe the behaviors and 2) classification is heavily driven by the need to correlate these behaviors for analytic purposes (either predictive or evaluative).

Isolating data to the process physics leads to classifications focused on the physical phenomena of the process, including heating, cooling, phase changes, solidification, etc. Much classification has been done in these areas, particularly when related to attaining insight into the physics and their measurements [4] or developing physics-based models and simulations [307, 308]. While the fundamental physics of the AM process is relatively well understood, their translation into real-world applications continues to be a challenge. Consequently, observations of physics are often studied in tandem with material properties and part properties.

Because of the variability that often results from AM processes, material properties in AM are almost always associated with processes and process parameters. Therefore, in-process monitoring data are often classified in a manner to best establish correlations between process properties, material properties (including microstructure), and part properties (i.e., PSPP relationships). Schemas associated with AM databases [309] and classifications associated with design allowables [310] establish explicit structures to facilitate the correlation of process physics with raw material and the final part. While these correlations may not always establish direct classifications of in-process data, they establish a relationship between the process physics, the precursor material, and the final part.

5.1.1.2. In-process NDE data

In investigating the primary factors of data associated with the part, physics still plays an important role but not as directly. Primary in-process NDE considerations are: 1) what the data are representative of (e.g. solidification, microstructure, temperature, acoustic signal); 2) what the data are meant to represent (e.g. porosity, density, cooling rates, flaws); 3) where the data came from (e.g. pyrometer, optical camera, ultrasonic device, simulation); and 4)what granularity the data was sampled at/frequency measured at (e.g. every layer, critical location, 100 Hz, max/min). Each of these factors must be considered when establishing the fidelity of the data against its primary objective. To establish data quality, context from each of these factors must be considered, along with data science considerations, against the objective to which the data will presumably be analyzed.

Classification of in-process NDE data through physical characteristics is an inherent classification of AM processes and how solidified parts are formed. In the context of raw data, classification by physical phenomena refers to the physical aspect of the part that the data are meant to represent. While NDE datasets focus on the solidified part, the multi-physics nature of AM processes inherently requires considerations of a part's underlying formation as well. Therefore, while this classification is primarily in reference to data associated with the solidified part, it may cross into process-related information as well. Regarding the solidified part, data related to physical characteristics may include characteristics such as part density, microstructure, or temperature history. The association/classification at this level is critical to understanding the intended use of the data and how it is meant to represent the part.

Classifying data by the measurement type used provides contextual insight into the origins of the data. This report previously explored many different ways of performing in-process monitoring and in-process NDE, making it clear that different types of measurements, different types of equipment, and different equipment settings can yield drastically different results. In addition, some equipment may often be used to provide "insight" into a phenomenon that the equipment is not necessarily well suited to measure, for instance using a low-resolution staring camera to calculate powder bed density. Classification by measurement/observation type and equipment provides important insight into the boundaries within which the data should be associated, with an understanding that making observations outside of those boundaries may lead to the misinterpretation or misuse of the data.

5.1.2. Data science viewpoint

Data science classification is less about what the data is representative of and more about how mature the data is. The data science viewpoint explores the evolution of data and data provenance as it progresses through what can be considered four different stages of its lifecycle: raw data, pre-processed data, curated data, and analyzed data. These different lifecycle stages offer different perspectives with different opportunities for classification. These classifications can be compounded, meaning that context from classification at one stage will carry over to the next, subsequent stage. The care and detail taken as data evolves through each of the data lifecycle stages will greatly influence the quality of your data, and subsequently, the quality of the "model" or other representation form used to leverage data in decision-making.

5.1.2.1. Classification of raw data

Generally, raw data is associated with the data collection phase. This data is unprocessed, directly from a measurement source without further study or characterization. The classification of raw data can provide important context as the data progresses through different stages. While understanding the manufacturing viewpoint of the data is critical to understanding its value, it is just as important to understand the representation capabilities of the data collected.

As with any data, in-process data can come in many shapes and forms. At the highest level, these many different "types" of data can be generally separated into two categories: "**heavy data"** and **"light data**." Heavy data refers to data types that are expensive to store when accounting for all measured data necessary to represent a specific instance of the collection. For example, consider a melt pool image, collected at time t, that requires the collection and curation of 10 000 image pixels to fully represent a single collected measurement. On the other hand, light data may refer to the ability to fully represent or characterize a measurement with a single number or set of only a few numbers. For instance, consider the temperature of the melt pool at time t. This measurement can be observed with a scaled image of various intensities, which may be considered heavy data, or as a single integer, which may be considered light data. While there is no clear delineation between what constitutes "heavy" data versus "light" data, this is an important classification to understand as it influences how the data is collected, curated, and ultimately analyzed. It is often the case in AM that high sampling rates are desired, meaning that heavy data is often preferred.

Given the variability associated with AM processing, predictive models have been increasingly used to optimize process parameters. Additionally, physics-based models have long been used to provide important insight into process behavior. Whether **simulated data** is driven by physics-based, empirical-based, or hybrid models, it is important to understand that in AM any simulated data is highly unlikely to be representative of the part or process that it is meant to portray. Due to idealizations or assumptions associated with the simulation model, simulated data is subject to inherent simplifications. However, simulated data can provide valuable insight into expected behaviors, particularly when extrapolating or interpolating values that cannot be observed otherwise.

5.1.2.2. Classification of processed data

Pre-processed data involves the transformation of the raw data, often using techniques such as labeling or trimming. When data reaches its pre-processed stage there is often both data loss and information gain through data characterization. The methods used in processing the raw data are important to understand and convey as they can influence the fidelity of the data and introduce bias. Preprocessing of the data may be used to "clean" raw data to remove outliers, interruptions, or generally unrepresentative data, in essence separating the "good raw data" from the "bad raw data." Preprocessing allows for the characterization, labeling, and subsequent classification of data by using data representation/data intent. Improper processing of the raw data may lead to incorrect conclusions drawn during analysis (e.g., mislabeling or loss of key data points). The classification of preprocessed data provides important insight into the quality and scoping of the data. For AM data, classification at the preprocessing level can quickly contextualize and scope the scenarios in which the data is meant to be applied.

One common AM data preprocessing exercise is **reducing the size of the dataset**. This reduction can be achieved in various ways, each having specific implications for how the data should be viewed.

Trimmed data refers to the downsizing of a data sample to place a focus on a specific area of interest. Data trimming is especially common in AM NDE, as the measured area or volume often exceeds that of the part. While trimming the data is an effective way of creating more manageable datasets, the practice is inherently exposed to subjectivity, especially when setting thresholds for determining the data that is "not of interest." Understanding when a dataset is been trimmed, and what considerations were taken, is an important part of accepting a dataset at "face value."

The dimensional reduction of data is just that, removing a dimension for the purpose of creating more manageable datasets. While this practice may scope datasets to their intended use, it may also cast aside data that may be found important for future inquiries.

Downsampled data is becoming an increasingly common practice with edge computing. Here the datasets are not altered, but instead selectively sampled. Surrogate datasets may include those reduced through dimensional reduction or downsampling, but also refer to those that are "summarized" through a simplified representation, such as a curve fitting algorithm.

Data labeling can be an important part of data preprocessing. Data labeling refers to the "characterization" of data and datasets so that they can be more readily identified, classified, and interpreted. Data labeling is perhaps the most common way of classifying AM data and AM datasets. Data labeling is traditionally completed manually but is increasingly relying on machine learning and artificial intelligence [311], allowing for unsupervised learning and thus automated classification [108].

When classifying data within a dataset, data labeling can be used to perform functions such as to identify outliers, to observe common behaviors, to identify patterns, or to identify features [312, 313]. Data labeling essentially provides semantics to what may otherwise be uninterpretable data. How data is labeled will depend on what the data is representative of and what the intent

of the data usage is. For instance, data labeling can be used to identify observed porosity in an XCT image or delamination in a powder bed image.

Data labeling can also use to distinguish datasets [314]. For instance, large uninterrupted data streams may be parsed to scope to particular events. Data labeling provides a means for relating the raw data with different sets of events. Such an approach can also be used to relate multiple sets of data to the same event. In either scenario data labeling provides an important avenue for establishing context through classification.

5.1.2.3. Classification of curated data

The data curation phase leverages the preprocessing of the data and introduces additional characterization. This phase is where metadata becomes increasingly associated with the data, allowing for the grouping and clustering of data to prepare for analysis. Data curation refers to how and where the data is eventually captured, stored, and managed, often through a database. Classification of curated data can provide valuable insight into context or into how the data may be further classified.

Data curation is often achieved through taxonomies that support property inheritance, where the root represents a general class that is increasingly diversified as new attributes are added and the branch is expanded. Unless driven by a larger management software, these top-down classifications are often subjective. Regardless, any diversion along a branch will increasingly contextualize a curated dataset through important relationships that can later be analyzed. For this reason, objectivity during any AM data classification is important, as subjective classifications of AM data can lead to bias.

Where the classification of data generally refers to hierarchal taxonomies, the **clustering of data** generally refers to similarities that may be observed through shared values or characteristics (which can also be achieved through classification). Clustering can be used to make observations about similarities between observed behaviors. Such methods are especially useful to gain insight into correlations between observed process behaviors and observed part characteristics. This phenomenon is important when preparing AM data for analysis because of the variability of the process. As exact repetition of process phenomena is rare, clustering supports the grouping of data within established allowable ranges.

An increasingly common practice in AM is leveraging transfer learning, where **data from "similar" or "related" datasets** is used to complement data in a target dataset. Transfer learning in some ways is comparable to simulated data at the raw data level, as it is not indicative of the actual part or process but instead provides general insight into what might be expected where the target data is not available.

The notion of **registered and/or fused data** is important because it provides not only further insight into to intent of the data but also a valuable data point on which the data can be analyzed. Registration and fusion generally occurs on the spatial and temporal levels and is used to align data from disparate sources to a single thread. Given the multiphysics nature of AM and the multimodal measurements required, data registration and data fusion are increasingly important

concepts [315, 316]. Understanding when and how data has been registered and fused can be a critical aspect of building confidence in the analysis.

5.1.2.4. Classification of analyzed data

Analyzed data is when conclusions are drawn based on how well the data indicated that the part "performed" against its intended objective. Here the data can be considered a "**model**" of the part [311, 317]. Analyzed data refers to the result of the evaluation of data given some evaluation criteria. How the data is analyzed can be largely dependent on the type of data, the data preprocessing, and the data curation. As outlined previously, the resulting datasets are very much susceptible to loss of quality as the data evolves through the different stages. Ultimately the quality of the data is relative to the intent for which it is being adopted, and it is important to understand the data provenance and how it relates to the intent of the data usage when making any decision.

The presentation of the analysis results will be influenced by how the data is analyzed. When using the data to support a decision, models or charts are often involved. For AM in particular, the assumptions and idealizations involved in the development of the model can play a significant role in determining how well they represent their intended target.

The Raw Data section noted that simulated data may be introduced to complement observations at times. Similarly, **physics-based models** are occasionally referenced as a predictive tool. As noted with the simulated data and its progression, the complexity of AM processes does not lend itself well to physics-based models and the data derived from them.

Empirical data and models derived from empirical data (data-driven models) are perhaps the "best" datasets on which decisions can be made, though it is important to consider the transformation across the lifecycle of the data and understand the loss that may have occurred throughout. **Empirical models** often lend themselves well to representing a given, well-constrained AM part or process but are not well-suited for representing generalities. Factors such as machine or location can play a significant role in introducing bias to such data.

Hybrid models are being increasingly used in AM and when properly contextualized may outperform the capabilities of purely empirical models or physics-based models. These models can leverage the generalities of the physics adaptations while also accounting for bias introduced by specific implementations. The usefulness of these models, however, is very much reliant on how well the simulated data was scoped and how well the measured data was incorporated for a given implementation. These models can also play an important role in establishing the quality of the data derived from transfer learning.

Statistical models are perhaps the most common way analyzed data is presented in manufacturing, though such models have proven extremely difficult to adopt in additive manufacturing. Achieving allowable distributions can require prohibitive sampling sizes. For instance, design allowables that are commonly used for process-material-property correlations in traditional manufacturing cannot be directly adopted for additive manufacturing. When statistical models are adopted in AM, the criteria they were developed to must be well

understood before any decision can be made on them, as they are often developed under specific settings that are not widely applicable.

Given the challenges of developing true statistical models, **frequency-based data**, such as histograms, provide distributions in the number of times a certain event was observed or triggered. Such approaches are being increasingly deployed as a way of showing general trends in datasets. These frequency-based presentations can be used to provide general insight into specific scenarios but are not well suited for making predictions on future behaviors. As AM parts and processes are very difficult to accurately predict, depicting trends can provide some insight into expectations, but such trends should not be interpreted as absolute.

5.2. Summary

This section explored different types of NDE data, and different ways this data can be classified. By diverging the discussion into two main viewpoints, namely the manufacturing viewpoint and the data science viewpoint, the section addressed challenges associated with establishing data accuracy and data fidelity. By documenting the transformation of data as it matures across a life cycle, insight was provided into different ways this data may be classified to add further contextualization to its eventual use. The lifecycle approach also provided insight into potential information loss, where transformations in data can lead to a loss in fidelity. Many factors should be taken into consideration when establishing whether or not datasets possess acceptable levels of quality on which decisions can be made.

One consideration not addressed in this section is the role of data formats. With in-process NDE data, these formats are often dictated by the equipment used to take the measurements and are evolving as in-process NDE adoption matures. Many formats are proprietary and not all formats are created equal. Many different data formats can be used when measuring, capturing, and analyzing AM data [318]. The format in which data is represented can have a significant impact on the quality of the data, including associated metadata, resolution, accuracy, and size. The impact of data formats should be considered when accepting or reviewing any AM datasets.

Many of the knowledge gaps explored in Chapter 7 either directly or indirectly relate to data and data usage. In general, the gaps discussed in Chapter 7 are reflective of opportunities to gain greater insight into AM processes and parts, and this insight is often achieved with the support of data. With machine learning and artificial intelligence becoming an increasingly predominant form of analysis, the types of data captured and the ways this data is grouped, managed, and conveyed will significantly influence the utility of AM data in the future.

6. In-process monitoring and NDE for process and part qualification

Although AM processes are being used for manufacturing safety-significant parts in aerospace and medical industries, qualification and certification of those parts create a significant challenge and cost barrier in industrial applications [319, 320]. There are currently no clear methods and procedures about how to achieve necessary and adequate quality control of AM processes and parts. For example, the National Aeronautics and Space Administration (NASA) has produced two documents to address the qualification of L-PBF processes [321] and the fabricated parts [322].

The specification in [321] defines procedural requirements for L-PBF process control, qualification of L-PBF process, equipment, facilities, and personnel training as well as part acceptance including NDE considerations. For AM part qualification and certification, [322] requires an AM control plan, a quality management system based on [323], and the assurance of vendor compliance via the AM control plan. More recently, NASA published another technical standard, [324] which defines the minimum requirements for AM processes used in the design, fabrication, and testing of spaceflight hardware. The Federal Aviation Administration (FAA) relies on the guidance document developed by the Aerospace Industries Association (AIA) for the certification of AM parts [325]. [325] describes five focus areas: i) process development, ii) supply chain qualification, iii) material properties development, iv) part design qualification, and v) quality controls (including process quality controls, build a quality plan, and post-process inspection methods). The guidance published by the Food and Drug Administration (FDA) provides recommendations specific to the design, fabrication, and testing of AM medical devices [326]. A framework for the acceptance of metallic AM parts used in the oil and gas industry is described in [327].

Detailed procedures for process and part qualification are provided in the standard published by AWS [120]. This standard requires that the AM machine and process be qualified prior to actual part manufacturing for critical classes (Classes A and B) of parts. Machine qualification for L-PBF and L-DED includes specifications for the design, number, locations, and orientations of test specimens to be built. On the other hand, a pre-production test build, which uses the same product definition data set for the entire build envelope along with witness specimens, is required for process (procedure) qualification. All destructive and non-destructive inspection and testing requirements on these parts are also specified.

Although in-process NDE methods described in this report are emerging as the critical components for AM process and part qualification, currently, in all existing qualification standards, guidelines, and specifications, post-build inspections and measurements of AM parts are considered essential. The critical characteristics of AM parts to meet their design intent include dimension, form, surface topography of internal and external features, residual stresses, microstructure, and defects as well as part performance characteristics, such as static and dynamic mechanical properties, and corrosion resistance. While most of the part performance characteristics are determined through destructive tests on witness samples representing the AM parts in question, others utilize well-established post-process NDE methods, such as acoustic, ultrasonic, electromagnetic, radiological, and digital imaging [328]. According to [329], the selection of appropriate NDE methods depends on various practical and material considerations, including geometrical complexity of the part, part size, surface roughness, and accessibility of the feature to be inspected, flaw type and sensitivity of NDE for that type, presence of material and density gradients, and residual stress. Standards committees in ISO and ASTM are currently working on developing guidelines about the application of generic ASTM NDE standards for the application of metallic AM parts.

A comprehensive review on qualification and certification for metal AM was recently published, identifying three fundamental components as standards, rules, and regulations [280]. It reviews global standards development activities, including those in the U.S., Europe, and Asia. It also provides the summary of activities for the development of rules and regulations by organizations

providing services such as feasibility evaluation, training and consultancy, quality management system accreditation, testing and audit, and survey. Among such organizations, Underwriter Laboratories (UL) and American Bureau of Shipping (ABS) from the U.S., Det Norske Veritas (DNV) from Norway, Bureau Veritas (BV) from France, and TÜV SÜD from Germany are listed along with their relevant guidelines and specifications for AM qualification. As an outlook for future developments, this paper proposed another framework for digital qualification and certification as shown in **Figure 6.1**. This framework includes currently available data on the left branch and the new tools from the emerging field of data science to enable digital qualification on the right branch. Note that the left side of **Figure 6.1**more closely aligns with the manufacturing viewpoint of the AM data while the right side is more representative of the data science viewpoint (as presented in Section 5). A holistic view, such as the one presented, is needed to contextualize and scope any qualification or certification activity before informed decisions can be made.

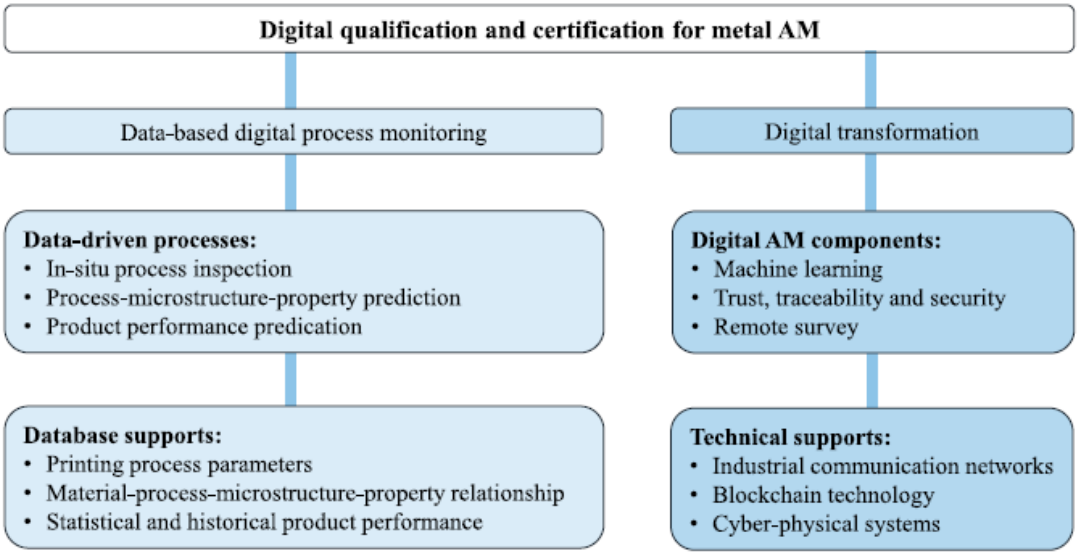

Figure 6.1 Outlook for digital qualification and certification for metal AM [280].

All of the above-mentioned specifications and guidelines require an expensive and time-consuming series of destructive and non-destructive tests on parts and representative witness test specimens to qualify and certify the AM parts. Furthermore, such post-process inspections result in high scrap rates and multiple build iterations when the AM processes are out of control. To reduce the cost of qualification and certification of AM processes and parts, significant research effort within the AM community focuses on utilizing in-process monitoring and in-process NDE methods as complementary tools to detect process anomalies, in-process flaws, and defects in time to correct for those (or stop the build process without further waste), thus, to minimize the need for post-process testing and inspection. This paradigm was first introduced as "*certify as you build*" in 2015 [330]. It was implemented on a L-DED machine integrating a fast-response optical-monitoring system based on optical emission spectroscopy with capabilities of defect (pinholes, porosity, and micro cracks) detection, composition sensing, and material phase transformation sensing.

Further improvement of this paradigm is recently described as the "*born qualified*" grand challenge by Sandia National Laboratories (SNL) [331]. As part of this paradigm, model-assisted qualification utilizing multi-physics modeling supplemented with in-process monitoring and NDE data is being pursued by SNL and others within the AM community [332]. Five key areas were identified to implement this paradigm [331]:

1. Novel real-time AM diagnostic tools to quantify and monitor critical AM process variables for materials control and optimization.
2. Innovative and rapid experimental techniques to calibrate and validate models as well as correlate materials performance to in-process diagnostic measurements.
3. Computational models to relate process conditions to microstructure and ultimately to bulk measurable properties.
4. Approaches to characterize, model, and control variability in AM processes.
5. Intelligent data collection from various and diverse sources to develop science-based heuristics

Utilizing physics-based models is critical to understanding the PSPP relationships associated with the AM processes, materials, and parts. The overall framework of this paradigm integrating multi-scale part and process models and their validation, in-situ process monitoring and diagnostics, and design optimization processes and tools is shown in **Figure 6.2**. Note that "*Properties Alinstante*" in this figure refers to rapid, automated characterization tests instantly conducted after the part is built.

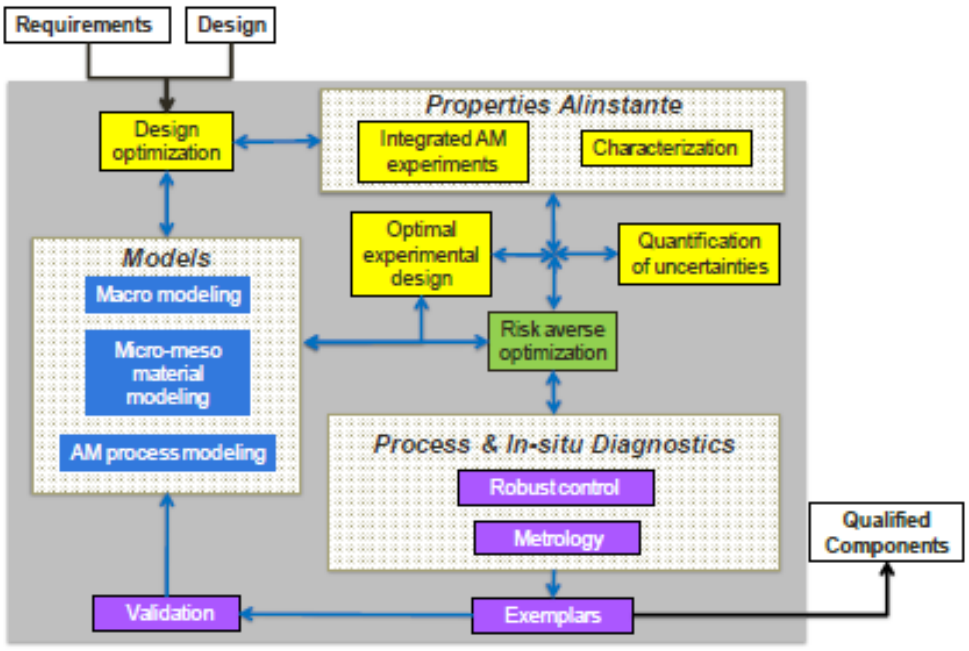

Figure 6.2 Framework for "Born Qualified" paradigm [331].

Recognizing that certification and qualification of processes and/or parts produced through AM presents a significant challenge for the nuclear power industry, a similar approach towards the certification of AM parts utilizing a digital platform integrating various models and data is recently proposed by Oak Ridge National Laboratory [333]. The required characteristics of this approach are listed below:

1. generic (can be applicable to any advanced manufacturing technology, any supported material, and any application which may have a strong safety significance),
2. flexible (can be scaled to large programs with a variety of advanced manufacturing technology derived component applications, or small programs that have only a few, but clearly defined desired applications),
3. complementary to existing industry approaches under development (those being developed by the U.S. Nuclear Regulatory Commission and other industry trade groups),
4. performance-based (allows for operational feedback and building confidence in the digital platform).

It is emphasized that the wealth of in-process data collected during AM processes has the "potential to reduce or eliminate the need for any supplemental testing." A digital thread integrating all digital information associated with the AM process and the part is described in that report. The digital thread helps contextualize the data in regards to the manufacturing viewpoint, however, the extent to which analyses can be performed and observations made is still very much dependent on how the data has been conditioned within the data science viewpoint.

AM process qualification is an integral part of all the current qualification and certification standards and guidelines. However, the lack of specificity in these standards makes it difficult to use process monitoring and in-process NDE for process qualification. The latest developments related to the "born qualified" concept include in-process monitoring and in-process NDE as supporting evidence for part qualification. In this context, **AM process qualification** means gaining objective evidence that the process is able to operate at a certain standard level during sustained operation and the output will meet specified requirements within a known confidence interval. Therefore, we believe in-process monitoring and in-process NDE will be used for AM process qualification as well as for supporting post-process NDE for part qualification, especially when post-process NDE becomes impractical or impossible due to the complexity of printed parts. Process qualification can be achieved by assessing the indications of process anomalies to classify them as false, non-relevant, and relevant to compare them against the accepted process specifications. In-process monitoring and in-process NDE are also used to minimize process anomalies using closed-loop control, based on in-process feedback (either during the layer processing or between layers), to keep the AM process under control to avoid undesired variations resulting in part flaws and defects [334].

AM process qualification requires that critical **process parameters** and **process signatures** must be continuously recorded and analyzed to ensure that predefined part quality attributes (metrics) can be achieved throughout the manufacturing process. As detailed in Sec. 2, critical process

parameters include laser power, laser scan speed, hatch spacing, etc. Process signatures are defined in Sec. 1 as observable physical phenomena associated with the selection of process parameters and other conditions. They include melt pool characteristics as well as powder bed (for L-PBF), powder flow (L-DED), and printed layer characteristics. Quantified or classified analysis of measured or observed signatures identify relevant process anomalies that are tracked and eventually correlated to printed part flaws and defects. To establish such correlations, [335] investigated the sensitivity of various process monitoring methods with respect to their suitability for defect prediction. When causal relationships are obtained, these anomalies, or lack thereof, can be used for process qualification purposes. Furthermore, such information can support reduced levels of post-process NDE leading to a part qualification. However, establishing such causal (even statistical) correlations is a significant challenge, requiring a deep physical understanding of repeated melting and solidification of metal at a high rate layer over layer. In the absence of such deep knowledge, researchers recently started to focus on utilizing artificial intelligence and machine learning tools taking advantage of large datasets acquired during the AM processes [103, 336, 188]. Inspired by the post-process NDE methods, the use of the in-process monitoring flow diagram is shown in **Figure 6.3**. It should be noted that the AM community is still debating this perspective related to in-process monitoring.

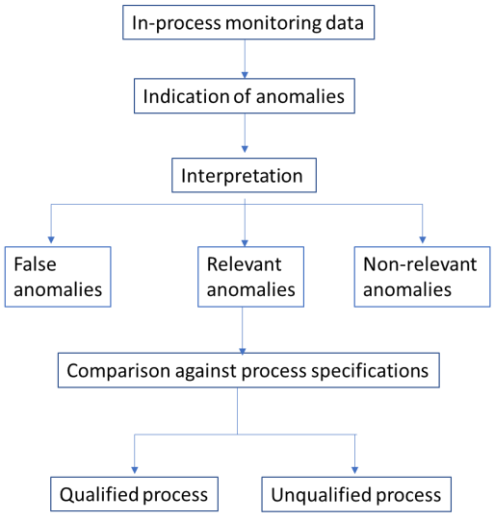

Figure 6.3 Flow chart of in-process monitoring to identify process anomalies and process qualification (adapted from [12]).

To be able to use in-process monitoring and NDE data within the digital qualification paradigm, both metrological and informational traceability are critical. Informational traceability is achieved by applying *"FAIR principles"* to the data (i.e., findability, accessibility, interoperability, and reusability) [337]. According to these principles, in-process data is easily **findable** by both humans and computers. Machine-readable metadata are required for this purpose. Once it is found, the data must be **accessed** with authentication and authorization. Because the data will be used with different analysis tools for qualification and certification purposes, it must be **interoperable** with other applications. Finally, because obtaining in-process data is costly, it must be **reusable** and enabled by well-described metadata so that they can be used for different purposes, such as

statistical analyses, as the needs arise. Common data dictionaries, ontologies, data formats, and databases are enabling tools to implement FAIR principles.

Metrological traceability is defined as the "property of a measurement result whereby the result can be related to a reference through a documented unbroken chain of calibrations, each contributing to the measurement uncertainty" [338]. Metrological traceability is achieved by proper uncertainty quantification of the measurement methods and instruments used for in-process monitoring and in-process NDE. Although such traceability needs are well understood in measurements associated with conventional manufacturing, their importance seems not among the priority areas in the AM community. Therefore, a limited amount of research results related to in-process measurements of AM processes appears in the literature so far. Some examples of existing investigations include measurement uncertainty of surface temperature distributions in L-PBF processes [339] and uncertainty evaluation of pore analysis resulting from post-process XCT measurements [340].

7. Knowledge gap analysis

As highlighted in the recent ASTM CoE report on AM "In-situ Technology Readiness" [277], knowledge and standardization gaps regarding in-process NDE and monitoring span the full range of TRLs from concepts that are still in fundamental research, to readily applied commercial applications. As previously mentioned in Sec. 3, the instrumentation design and integration on AM machines tend to be higher TRLs (5 to 9), whereas the interpretation and application of the *data* from those instruments are still lower TRLs. Of the instrumentation, the CoE report notes that 'optical imaging' (e.g., Sec. 3.2 of this report on machine vision) has the highest TRL of 8, followed by thermal imaging and spectroscopy at TRL 5 to 6 (e.g., Sec. 3.1 of this report on melt pool monitoring), and acoustic methods the lowest at TRL 4 to 5. Numerous additional technology gaps relevant to other aspects of AM, which are exemplified in the broad scope of the ANSI/America Makes standardization roadmap [5]. The gaps listed here solely focus on in-process monitoring and NDE. They are generally applicable to all AM in-process NDE and monitoring technologies and applications, including the more developed commercial systems and those supplied by OEMs on industrial AM machines.

Table 7 highlights what we believe to be the highest priority gaps. Most of these are knowledge gaps that need to be addressed before standardization can take place. This is due to low average TRL for interpretation and application of the data. These gaps are also largely in concurrence with the ASTM CoE report, as to have a great potential impact on in-process NDE if the gaps are overcome. More granular gaps for individual technologies were described in Sec. 3. Readers are also referred the multitude of AM in-process measurement reviews (e.g., [1],[4], [184-188],[195],[219],[254], [257]), for discussion on technology-specific gaps.

Table 7 High priority knowledge gaps

No.	Identified Gap
1. Gaps in fundamental AM process understanding	
1.1	**Clarification of causal relationships between flaw formation mechanisms, and the resultant observable process signatures:**

No.	Identified Gap
	This is identified as the 'key gap' in the ASTM CoE readiness report that hinders the full implementation of in-process NDE for AM qualification. As identified throughout this report, there is a complex mapping between the many potential in-process flaw types, the many methods for in-process NDE, and the varying levels of sensitivity of those NDE methods to those flaws. Understanding and clarifying these relationships has been and will be a continuing and widespread effort in AM research and development. One key barrier is the fact that the physical mechanisms by which in-process flaws form are more numerous and more complex than those flaws studied and observed in fully fabricated AM parts (i.e., via post-build inspection). While post-fabrication flaws are more critical for part function and performance (and qualification and certification), it will be essential for in-process NDE developers and users to accept and understand the nuanced complexities of in-process flaw formation in interpreting in-process NDE results. **Priority:** Medium-High For in-process NDE which requires identification of localized in-process flaw formation and strong correlation to post-fabrication defects, the need to identify these causal relationships is **high**. For in-process monitoring control requirements, such as statistical process control as described in ASTM E3353, identification of 'off-nominal' conditions based on prior monitored AM builds does not necessarily require a strong physics connection, and its priority is **medium**. **Recommendation:** Continued investment in focused R&D. Likely requires research or methods in combination with high-fidelity computational simulations.
1.2	**Guidelines or methods for *determining critical flaw size, density, or concentration* thresholds and their associated size, density, or concentration of associated indication in in-process NDE** Foremost, it is worth mentioning that characterizing thresholds for the criticality of flaws or defects still generally requires further research and development for post-fabrication inspection and will depend on the specifics of individual components and applications. However, post-fabrication or as-built defect thresholds are necessary to define before in-process NDE defect threshold definitions can be defined. Three sub-gaps (1.2.1 to 1.2.3) unique to AM in-process inspection are identified:
1.2.1	***Validation of in-process NDE methods. This is largely due to a lack of sufficient 'ground truth(s)'*. This gap will need to be addressed before the probability of detection (POD) or false-positive issues may be addressed.** **Priority:** High **Recommendation:** Potential methods for establishing or creating these in-process NDE 'ground truths' may be through the development of test artifacts or methods incorporating 'seeded defects' (e.g., ISO/ASTM TR 52906 [278]). "Ground truth" refers to the fact that the defects or artifacts must be independently well characterized with a low measurement uncertainty in order to use for validation. However, this concept requires further development for in-process flaw formation mechanisms and associated in-process NDE.
1.2.2	**Address the issue of *'self-healing' phenomena and the inevitability of false positives* that will occur for in-process NDE results.**

No.	Identified Gap
	A certain degree of remelting is necessary for achieving sufficient physical bonding between layers and welds in order to achieve a high density. The remelting of previous layers and potentially healing existing flaws are inherent in AM processes. In other words, every flaw that is generated and detected may not exist in the final part. It will be necessary to reconcile in-process NDE and post-process NDE. **Priority:** Medium **Recommendation:** Further development of various in-process measurement methods to reduce false positives (e.g., [198]) or modeling/simulation methods that predict and quantify the above-described remelting and self-healing behavior (e.g., [50]). Methods should provide probabilistic/statistical approaches with the assessment of accuracy and uncertainty.
1.2.3	**Define and determine *'probability of detection' (POD),* or other quantitative metrics for characterizing the in-process NDE predictive performance.** This is seldom addressed in in-process NDE research but will be essential to establish the uncertainty in any correlation or predictive models. **Priority:** High **Recommendation:** Address Gap 1.2.1 above on the creation of 'ground truth' test artifacts or standards. Development of best practices and standards for characterizing measurement performance of different in-process NDE techniques (e.g., resolution, range, sensitivity, etc., see Gap 2.3), and methods for evaluating the NDE techniques against the 'ground truth' standards.
2.	**Gaps in instrumentation design and integration for in-process monitoring and in-process NDE**
2.1	**Improved measurement *methods to observe sub-surface in-process flaws*:** The more commonly used commercial in-process monitoring products (e.g., melt pool monitoring, machine vision, etc.) generally do not have the capability to observe subsurface flaws, despite the fact many in-process flaw types are not surface connected. Those methods that are promoted as being capable of observing subsurface defects such as ultrasonics, eddy current, active/flash thermography, tend to be underdeveloped for AM in-process applications [257]. This is also important in the context of 'self-healing' phenomena described in Gap 1.2.2, as the deeper a subsurface flaw is formed, the less likely it will be corrected by subsequent remelting. In other words, accurate identification of subsurface flaws may be less subject to false positives from the self-healing phenomenon. **Priority:** Medium **Recommendation:** It is generally not known or quantified what proportion of in-process flaws are formed subsurface versus surface connected, therefore the prioritization on subsurface flaw detection is to-be-determined. Recommended further R&D on the different NDE techniques capable of internal or subsurface flaw detection that can be applied as in-process techniques (Gap 2.2).
2.2	***Improvements to underdeveloped in-process NDE methods*, or innovation of new methods.**

No.	Identified Gap
	Many in-process measurement techniques have been presented in the research literature but have not been commercialized. Additionally, many of the 'traditional' NDE methods used for the inspection of fully fabricated parts still require further development for implementation as in-process techniques. These include methods such as ultrasonics or acoustic emission (active or passive techniques), active thermography (e.g., flash or pulse-phased thermography), eddy current (single probe or array), or in-process radiography (and/or computed tomography). Challenges hindering these technologies are generally the same as which plague all AM in-process monitoring techniques: 1) the physical complexity of the AM processing, particularly at the heat application and material consolidation region, and 2) the extreme multi-scale nature of AM requiring high-resolution measurements to detect small flaws and anomalies of interest over a large build area. Other challenges specific to each NDE technique typically stem from specific aspects of AM processing and parts. For example, the relatively rough AM surfaces and complex part geometries hinder ultrasonic inspection due to the complex acoustic scattering and reflections. In another example, the optically reflective/specular top surfaces of L-PBF parts hinder flash thermography due to the low absorption of flashed heat sources, and difficulty resolving the relatively low-temperature rise resulting from the flash heat pulses. Novel and innovative techniques will need to be specifically developed for these traditional NDE techniques to overcome challenges fairly unique to in-process AM applications. **Priority:** Medium-High **Recommendation:** Continued R&D implementing NDE techniques within the AM process, including innovation of new techniques.
2.3	**Methods for *calibration or characterization of in-process NDE instruments*** Characterization of critical measurement parameters such as range, resolution, repeatability, etc. are still not generally reported for in-process NDE systems. The characterization methods are currently applied by OEMs or research groups using disparate and internally developed methods. These various methods for calibration or characterization are not technically complex, and therefore suitable for standardized approaches so that the methods and results can be clearly and unambiguously communicated. Two general types of calibration need to be developed: relative and absolute. 'Relative' calibrations may not relate directly to physical values but relate a measurement to a constant or stable reference. For example, a melt pool monitoring detector could be calibrated against a stable light source to characterize its repeatability and reproducibility (R&R). 'Absolute' calibrations relate measurement to a real physical value, assignable with real units, and maybe metrologically traceable to primary standards. In the same melt pool monitoring example, a light source with output calibrated to a specific radiant flux (watts) may be used to calibrate the sensor output (volts or amps). Relative calibrations tend to be easier to develop and may be sufficient for many practical applications such as R&R testing. Absolute calibrations, which can be more complex to develop, can meet the needs for R&R as well as assigning physical units. **Priority:** High **Recommendation:** Continued R&D on the creation of test methods, artifacts, and instrumentation for calibrating in-process monitoring and NDE system. Also see Gap 1.2.1 on creation of 'ground truth' artifacts.
3. Gaps in data processing and management	

No.	Identified Gap
3.1	***Expanded exploration of in-process data processing and feature definitions*, including mechanistic or physics-based features, data fusion from multiple in-process measurement sources, or integration with physics-based or data-driven models:** Many in-process NDE instruments implemented by OEMs have identified one or a handful of data processing techniques that they have found to provide 'optimal' identification of in-process anomalies or flaws. However, these tend not to be particularly complex in the algorithms or steps used to process the data. Exploration of the various methods for processing in-process measurement data is much more diverse in the research literature and incorporates much more complex analysis algorithms and techniques. There is still much to be explored or tested to achieve data features that better (i.e., more accurately) predict the formation or existence of in-process flaws. Similarly, examples in research exist that integrate in-process measurements with physics-based models, which can potentially help account for some of the complex physics and deterministic variability found in AM processes. Data processing transparency and provenance, while technically achievable, is not common practice enough among in-process NDE or monitoring. Transparency is the open provision of the algorithmic steps and/or parameters used in the processing, and data provenance is a recorded history of where the data has been moved, processed, or transformed. These concepts can help accelerate the development and adoption of new data processing methods and may be necessary to accompany the data itself if it is to be used in a qualification or certification data package. **Priority:** Medium **Recommendation:** Continued R&D into in-process monitoring and NDE systems measurement data processing and analysis. OEMs should enable the capability for engineers/users of commercial in-process monitoring and NDE systems to access raw data and develop custom data processing algorithms.
3.2	**In-process and post-process inspection *data alignment and registration*:** Geometric alignment and registration of AM data are essential to identify localized (i.e. voxel-by-voxel) correlations or predictions of part quality from in-process NDE or monitoring. Generally, computational algorithms for 3D model transformation and alignment/registration are well known. However, the practical application to AM part data, including in-process NDE data, has some unique challenges. These include challenges such as the use of freeform part geometries, potentially excessive geometric distortions from residual stresses, and generally poorer surface finishes. These factors inhibit the design, identification, or establishment of reference datums features or fiducials for alignment of the disparate datasets. Guidelines and best approaches are still being developed to define and realize AM machine and part coordinate systems, design and fabrication of reference datums or alignment fiducials, and quantifying the alignment or registration error and effect on the defect or flaw prediction accuracy. Furthermore, AM technologies are pushing the advancement and adoption of digital part/product specifications (e.g., ISO 10303), which may provide localized or feature-based inspection instructions or criteria. For in-process NDE or monitoring data to be implemented, alignment and registration will be critical. **Priority:** Medium **Recommendation:** Standardized techniques for calibrating and describing positioning error resulting from AM system motion mechanisms and their influence on part geometric accuracy; improved part distortion prediction models; and improved standard definitions and methods for realization (i.e., determining in

No.	Identified Gap
	real, physical space) of AM system and part coordinates. Continued R&D to determine best practices for alignment fiducial design in AM parts, choice and realization of part datums.
4.	**Gaps in standards, qualification, and certification framework** All the knowledge gaps above need further R&D before standardization can take place; hence there are too many standards gaps to list. Section 4.7 highlights two reports identifying high priority standards gaps and necessary R&D to develop these standards. The following is a standard that can be developed without any further R&D
4.1	***In-process monitoring and in-process NDE and monitoring terminology*** **and catalog of in-process flaw types:** Perhaps the most valuable yet achievable gap to overcome for AM in-process NDE and monitoring is greater standardization in relevant terminology. Standards exist and are being further developed that catalog and describe the many AM flaws identifiable in fabricated parts (e.g., ISO/ASTM TR 52905 or ASTM E3166-20). However, these tend to lack in several aspects pertinent to in-process NDE or monitoring: Current standards lack in their separation or categorization of different flaw formation mechanisms relevant to in-process NDE or monitoring more so than post-fabrication inspection. For example, while ISO/ASTM TR 52905 or ASTM E3166 uniquely defined 'keyhole porosity' or 'lack-of -fusion' porosity, these commonly cited flaws may be induced via multiple different physical mechanisms, and therefore elicit different process signatures which may be targeted via in-process NDE or monitoring. In other words, in-process flaw terminologies need to be expanded to meet the key 'causal relationship' knowledge gap described above. Current standards may lack providing terminology regarding the installation, use, calibration, characterization, or application of in-process NDE instrumentation. These terminologies can be found in non-AM standards (e.g., those from ASTM E7 or ISO TC 135 on Nondestructive Testing), but the specific relevance or relation to AM in-process NDE, and its unique challenges, are yet to be thoroughly defined or clarified. **Priority:** High **Recommendation**: Convene a subcommittee or working group in one standards development organization (SDO) which includes technical experts in in-process flaw *and* post-fabrication AM defect categorization, to draft standard terminology. Consider as an appendix or addendum to existing standards on post-fabrication defects.

8. Summary and conclusions

The cost-effective fabrication of complex high-value components in small batches with significantly reduced lead times makes AM an excellent candidate for manufacturing nuclear power plant components. However, challenges associated with excessive variability of AM processes necessitate more rigorous monitoring, control, and inspection of both processes and built parts. In-process monitoring and in-process NDE methods and associated standards are being developed by the AM research community and industry to meet these challenges. In this report, we have provided technical summaries of the two most common metal AM technologies, L-PBF and L-DED, reviewed the latest developments related to various in-process monitoring and in-process NDE methods and instruments (including thermography, machine vision, acoustics, ultrasonics, and electromagnetics), provided a list of existing relevant standards as well as the ones currently being developed, and identified knowledge gaps to be focused on in the near future by the AM community to reliably incorporate in-process monitoring and in-process NDE methods and tools into the overall AM process and part qualification frameworks.

The knowledge gaps, categorized as AM process knowledge, measuring instrumentation design and integration, and data acquisition and management, indicate that the level of maturity of using in-process monitoring and in-process NDE measurements for process and part qualification efforts is relatively low. In other words, they are not currently relied on as principal sources of evidence for qualification in safety-significant applications. Concerted efforts by the AM community to fill these gaps should be among the highest priorities. Better understanding of the relationships among process signatures, influencing factors, and resulting part defects is a key prerequisite to any further developments and improvements of in-process monitoring and in-process NDE methods. More specific and useful in-process monitoring and in-process NDE standards for process and part qualification are only possible upon achieving such understanding.

References

[1] Wohlers Associates (2021) *Wohlers report 2021 – 3D printing and additive manufacturing global state of the industry* (Wohlers Associates, Inc. Fort Collins, CO).

[2] S. Jedlan, et al., (2022) Utilization of Additive Manufacturing in Nuclear Power Industry, *Proceedings of the IEEE 8th Youth Conference on Energy (IYCE)* **DOI:** 10.1109/IYCE54153.2022.9857541

[3] J. Simpson, et al., (2019) Considerations for application of additive manufacturing to nuclear reactor core components, ORNL/TM-2019/1190

[4] M. Mani, et al. (2017) A review on measurement science needs for real-time control of additive manufacturing powder bed Fusion processes. *Int'l Journal of Production Research*, 55/5 pp 1400-1418. https://doi.org/10.1080/00207543.2016.1223378

[5] America Makes & ANSI Additive Manufacturing Standardization Collaborative (AMSC), (2023) *Standardization Roadmap for Additive Manufacturing*. Available at https://www.ansi.org/standards-coordination/collaboratives-activities/additive-manufacturing-collaborative#.ZCMxZnbMKUk

[6] S. Kenderian, et al., (2009) A general overview of some Nondestructive Evaluation (NDE) techniques for materials characterization, *Proceedings of SPIE 7425, Optical Materials and Structures Technologies IV*, 742506

[7] R. Jacob, et al., (2020) *Survey of pre-service and in-service nondestructive evaluation techniques of AMT-fabricated components*, PNNL-30759

[8] WH Woodall, DC Montgomery, (1999) Research issues and ideas in statistical process control, *J of Quality Technology*, 31/4, pp 376-386

[9] A. Matsubara, K. Nagaoka, T. Fujita (2011) Model-reference feedforward controller design for high-accuracy contouring control of machine tool axes, *CIRP Annals – Manufacturing Technology*, 60/1 pp 415-418.

[10] V.R. Gervasi (1997) Statistical process control for solid freeform fabrication processes. In: *8th Solid Free. Fabr. Symp.* University of Texas at Austin, Austin, pp 141–148

[11] H. Luan et al., (2017) Statistical Process Control of In-Plane Shape Deformation for Additive Manufacturing, *13th IEEE Conference on Automation Science and Engineering (CASE)* Xi'an, China, pp 1274-1279

[12] ASTM International (2022) *ASTM E1316-22a Standard terminology for nondestructive examinations* (ASTM International, W. Conshohocken, PA).

[13] ASTM International (2022) *ASTM E3353-22 Standard Guide for In-Process Monitoring Using Optical and Thermal Methods for Laser Powder Bed Fusion* (ASTM International, W. Conshohocken, PA).

[14] ASTM International (2021) *ISO/ASTM 52900:2021 Additive manufacturing – General principles – Terminology* (ASTM International, West Conshohocken, PA,).

[15] I. Gibson, D.W. Rosen, and B. Stucker (2015) *Additive manufacturing technologies*, vol. 17, Springer.

[16] W.J. Sames, F.A. List, S. Pannala, R.R. Dehoff, and S.S. Babu, (2016) The metallurgy and processing science of metal additive manufacturing, *Int. Mater. Rev.*, vol. 61, no. 5, pp. 315–360, Jul. 2016, doi: 10.1080/09506608.2015.1116649.

[17] M. Van Elsen, (2007) Complexity of selective laser melting : a new optimisation approach, Doctoral Dissertation, Katholieke Universiteit Leuven. Accessed: Nov. 18, 2022. [Online]. Available: https://lirias.kuleuven.be/1746431

[18] J.S. Weaver *et al.*, (2021) The effects of particle size distribution on the rheological properties of the powder and the mechanical properties of additively manufactured 17-4 PH stainless steel, *Addit. Manuf.*, vol. 39, p. 101851, Mar. 2021, doi: 10.1016/j.addma.2021.101851.

[19] J. Karlsson, A. Snis, H. Engqvist, and J. Lausmaa, (2013) Characterization and comparison of materials produced by Electron Beam Melting (EBM) of two different Ti–6Al–4V powder fractions, *J. Mater. Process. Technol.*, vol. 213, no. 12, pp. 2109–2118, Dec. 2013, doi: 10.1016/j.jmatprotec.2013.06.010.

[20] Y. Liu, Y. Yang, S. Mai, D. Wang, and C. Song, (2015) Investigation into spatter behavior during selective laser melting of AISI 316L stainless steel powder, *Mater. Des.*, vol. 87, pp. 797–806, Dec. 2015, doi: 10.1016/j.matdes.2015.08.086.

[21] S.E. Brika, M. Letenneur, C.A. Dion, and V. Brailovski, (2019) Influence of particle morphology and size distribution on the powder flowability and laser powder bed fusion manufacturability of Ti-6Al-4V alloy, *Addit. Manuf.*, vol. 31, p. 100929, Jan. 2020, doi: 10.1016/j.addma.2019.100929.

[22] J.A. Slotwinski and E.J. Garboczi, (2015) Metrology Needs for Metal Additive Manufacturing Powders, *JOM*, vol. 67, no. 3, pp. 538–543, Mar. 2015, doi: 10.1007/s11837-014-1290-7.

[23] L.P. Lefebvre, J. Whiting, B. Nijikovsky, S.E. Brika, H. Fayazfar, and O. Lyckfeldt, (2020) Assessing the robustness of powder rheology and permeability measurements, *Addit. Manuf.*, vol. 35, p. 101203, Oct. 2020, doi: 10.1016/j.addma.2020.101203.

[24] J.G. Whiting, E.J. Garboczi, V.N. Tondare, J.H.J. Scott, M.A. Donmez, and S.P. Moylan, (2021) A comparison of particle size distribution and morphology data acquired using lab-based and commercially available techniques: Application to stainless steel powder, *Powder Technol.*, vol. 396, pp. 648–662, Jan. 2022, doi: 10.1016/j.powtec.2021.10.063.

[25] S. Das, (2003) "Physical Aspects of Process Control in Selective Laser Sintering of Metals, *Adv. Eng. Mater.*, vol. 5, no. 10, pp. 701–711, 2003, doi: 10.1002/adem.200310099.

[26] V. Seyda, N. Kaufmann, and C. Emmelmann, (2012) Investigation of Aging Processes of Ti-6Al-4 V Powder Material in Laser Melting, *Phys. Procedia*, vol. 39, pp. 425–431, Jan. 2012, https://doi.org/10.1016/j.phpro.2012.10.057

[27] B.A. Hann, (2016) Powder Reuse and Its Effects on Laser Based Powder Fusion Additive Manufactured Alloy 718, *SAE Int. J. Aerosp.*, vol. 9, no. 2, Art. No. 2016-01–2071, Sep. 2016, doi: 10.4271/2016-01-2071.

[28] J.A. Slotwinski, E.J. Garboczi, P.E. Stutzman, C.F. Ferraris, S.S. Watson, and M.A. Peltz, (2014) Characterization of metal powders used for additive manufacturing, *J. Res. Natl. Inst. Stand. Technol.*, vol. 119, p. 460.

[29] P. Moghimian *et al.*, (2021) Metal powders in additive manufacturing: A review on reusability and recyclability of common titanium, nickel and aluminum alloys, *Addit. Manuf.*, vol. 43, p. 102017, Jul. 2021, doi: 10.1016/j.addma.2021.102017.

[30] ASTM International (2022) ASTM F3456 – 22 Standard Guide for Powder Reuse Schema in Powder Bed Fusion Processes for Medical Applications for Additive Manufacturing Feedstock Materials (ASTM International, West Conshohocken, PA).

[31] Z. Snow, A.R. Nassar, and E.W. Reutzel, (2020) Review of the formation and impact of flaws in powder bed fusion additive manufacturing, *Addit. Manuf.*, vol. 36, p. 101457, Dec. 2020, doi: 10.1016/j.addma.2020.101457.

[32] S. Hall, A. Chrostek-Mroz, and J. Dawes, (2020) Developing Storage and Handling Guidelines for Additive Manufacturing Metal Powder Feedstock, in *Progress in Additive Manufacturing 2020*, pp. 1–12. http://doi.org/10.1520/STP163720210005.

[33] L. Cordova, T. Bor, M. de Smit, M. Campos, and T. Tinga, (2020) Measuring the spreadability of pre-treated and moisturized powders for laser powder bed fusion, *Addit. Manuf.*, vol. 32, p. 101082, Mar. 2020, doi: 10.1016/j.addma.2020.101082.

[34] M.K. Thompson *et al.*, (2016) Design for Additive Manufacturing: Trends, opportunities, considerations, and constraints, *CIRP Ann.-Manuf. Technol.*, vol. 65, no. 2, Art. No. 2, 2016, doi: 10.1016/j.cirp.2016.05.004

[35] H. Budinoff and S. McMains, (2018) Prediction and visualization of achievable orientation tolerances for additive manufacturing, *Procedia CIRP*, vol. 75, pp. 81–86.

[36] P. Das, R. Chandran, R. Samant, and S. Anand, (2015) Optimum Part Build Orientation in Additive Manufacturing for Minimizing Part Errors and Support Structures, *Procedia Manuf.*, vol. 1, pp. 343–354, Jan. 2015, doi: 10.1016/j.promfg.2015.09.041.

[37] S. Abolmaali, A. Vinel, J. Fox, J. Liu, D. Silva, and N. Shamsaei, (2022) Location and Orientation Dependency in Surface Roughness Of Nickel Super Alloy 625 Parts: Statistical and Distributional Analysis, *NIST*, Aug. 2021, Accessed: Nov. 21, 2022. [Online]. Available: https://www.nist.gov/publications/location-and-orientation-dependency-surface-roughness-nickel-super-alloy-625-parts

[38] G. Strano, L. Hao, R.M. Everson, and K.E. Evans, (2013) Surface roughness analysis, modelling and prediction in selective laser melting, *J. Mater. Process. Technol.*, vol. 213, no. 4, pp. 589–597, Apr. 2013, doi: 10.1016/j.jmatprotec.2012.11.011.

[39] L. Cheng and A. To, (2014) Part-scale build orientation optimization for minimizing residual stress and support volume for metal additive manufacturing: Theory and experimental validation, *Comput.-Aided Des.*, vol. 113, pp. 1–23, Aug. 2019, https://doi.org/10.1016/j.cad.2019.03.004

[40] J. Berez, L. Sheridan, and C. Saldaña, (2022) Extreme variation in fatigue: Fatigue life prediction and dependence on build volume location in laser powder bed fusion of 17-4 stainless steel, *Int. J. Fatigue*, vol. 158, p. 106737, May 2022, https://doi.org/10.1016/j.ijfatigue.2022.106737

[41] R. Wauthle *et al.*, (2015) Effects of build orientation and heat treatment on the microstructure and mechanical properties of selective laser melted Ti6Al4V lattice structures, *Addit. Manuf.*, vol. 5, pp. 77–84.

[42] J. Jiang, X. Xu, and J. Stringer, (2018) Support Structures for Additive Manufacturing: A Review, *J. Manuf. Mater. Process.*, vol. 2, no. 4, Art. No. 4, Dec. 2018, doi: 10.3390/jmmp2040064.

[43] J.J. Beaman, D.L. Bourell, C.C. Seepersad, and D. Kovar, (2020) Additive Manufacturing Review: Early Past to Current Practice, *J. Manuf. Sci. Eng.*, vol. 142, no. 11, Sep. 2020, doi: 10.1115/1.4048193.

[44] ASTM International (2019) ISO/ASTM 52911-1:2019 Additive manufacturing — Design — Part 1: Laser-based powder bed fusion of metals (ASTM International, West Conshohocken, PA).

[45] J. Beuth *et al.*, (2013) Process Mapping for Qualification Across Multiple Direct Metal Additive Manufacturing Processes, in *Proceedings of the 2013 International Solid Freeform Fabrication Symposium*, 2013. http://dx.doi.org/10.26153/tsw/15590

[46] H. Gong, K. Rafi, H. Gu, T. Starr, and B. Stucker, (2014) Analysis of defect generation in Ti–6Al–4V parts made using powder bed fusion additive manufacturing processes, *Addit. Manuf.*, vol. 1–4, pp. 87–98, Oct. 2014, doi: 10.1016/j.addma.2014.08.002.

[47] J.-P. Kruth, L. Froyen, J. Van Vaerenbergh, P. Mercelis, M. Rombouts, and B. Lauwers, (2004) Selective laser melting of iron-based powder, *J. Mater. Process. Technol.*, vol. 149, no. 1, pp. 616–622, Jun. 2004, doi: 10.1016/j.jmatprotec.2003.11.051.

[48] L. Thijs, F. Verhaeghe, T. Craeghs, J.V. Humbeeck, and J.-P. Kruth, (2010) A study of the microstructural evolution during selective laser melting of Ti–6Al–4V, *Acta Mater.*, vol. 58, no. 9, pp. 3303–3312, May 2010, doi: 10.1016/j.actamat.2010.02.004.

[49] J.V. Gordon *et al.*, (2020) Defect structure process maps for laser powder bed fusion additive manufacturing, *Addit. Manuf.*, vol. 36, p. 101552, Dec. 2020, doi: 10.1016/j.addma.2020.101552.

[50] M. Tang, P.C. Pistorius, and J.L. Beuth, (2017) Prediction of lack-of-fusion porosity for powder bed fusion, *Addit. Manuf.*, vol. 14, pp. 39–48, Mar. 2017, https://doi.org/10.1016/j.addma.2016.12.001

[51] M. Bayat *et al.*, (2019) Keyhole-induced porosities in Laser-based Powder Bed Fusion (L-PBF) of Ti6Al4V: High-fidelity modelling and experimental validation, *Addit. Manuf.*, vol. 30, p. 100835, Dec. 2019, doi: 10.1016/j.addma.2019.100835.

[52] W.E. King *et al.*, (2014) Observation of keyhole-mode laser melting in laser powder-bed fusion additive manufacturing, *J. Mater. Process. Technol.*, vol. 214, no. 12, pp. 2915–2925, Dec. 2014, doi: 10.1016/j.jmatprotec.2014.06.005.

[53] N.K. Tolochko *et al.*, (2004) Balling processes during selective laser treatment of powders, *Rapid Prototyp. J.*, vol. 10, no. 2, pp. 78–87, Apr. 2004, doi: 10.1108/13552540410526953.

[54] E. Abele, H.A. Stoffregen, K. Klimkeit, H. Hoche, and M. Oechsner, (2015) Optimisation of process parameters for lattice structures, *Rapid Prototyp. J.*, vol. 21, no. 1, Art. No. 1, 2015, doi: 10.1108/Rpj-10-2012-0096.

[55] B. Lane *et al.*, (2020) Measurements of Melt Pool Geometry and Cooling Rates of Individual Laser Traces on IN625 Bare Plates, *Integrating Mater. Manuf. Innov.*, vol. 9, no. 1, pp. 16–30, Mar. 2020, doi: 10.1007/s40192-020-00169-1.

[56] G. Ameta, R. Lipman, S. Moylan, and P. Witherell, (2015) Investigating the Role of Geometric Dimensioning and Tolerancing in Additive Manufacturing, *J. Mech. Des.*, vol. 137, no. 11, Art. No. 11, Nov. 2015, doi: Artn 111401 10.1115/1.4031296.

[57] V. Viale, J. Stavridis, A. Salmi, F. Bondioli, and A. Saboori, (2022) Optimisation of downskin parameters to produce metallic parts via laser powder bed fusion process: an overview, *Int. J. Adv. Manuf. Technol.*, vol. 123, no. 7, pp. 2159–2182, Dec. 2022, doi: 10.1007/s00170-022-10314-z.

[58] E. Abele and M. Kniepkamp, (2015) Analysis and optimization of vertical surface roughness in micro selective laser melting, *Surf. Topography: Metrology. And Prop.*, vol. 3, no. 3, p. 034007, Sep. 2015, doi: 10.1088/2051-672X/3/3/034007.

[59] H. Yeung, B. Lane, and J. Fox, (2019) Part geometry and conduction-based laser power control for powder bed fusion additive manufacturing, *Addit. Manuf.*, vol. 30, p. 100844. https://doi.org/10.1016/j.addma.2019.100844

[60] Z. Yang, Y. Lu, H. Yeung, and S. Krishnamurty, (2020) From Scan Strategy to Melt Pool Prediction: A Neighboring-Effect Modeling Method, *J. Comput. Inf. Sci. Eng.*, vol. 20, no. 5, Apr. 2020, doi: 10.1115/1.4046335.

[61] H. Yeung *et al.*, (2021) Effect of spiral scan strategy on microstructure for additively manufactured stainless steel 17–4, *Manuf. Lett.*, vol. 29, pp. 1–4, Aug. 2021, https://doi.org/10.1016/j.mfglet.2021.04.005

[62] Z.A. Young *et al.*, (2020) Types of spatter and their features and formation mechanisms in laser powder bed fusion additive manufacturing process, *Addit. Manuf.*, vol. 36, p. 101438, Dec. 2020, doi: 10.1016/j.addma.2020.101438.

[63] S. Ly, A. M. Rubenchik, S.A. Khairallah, G. Guss, and M.J. Matthews, (2017) Metal vapor micro-jet controls material redistribution in laser powder bed fusion additive manufacturing, *Sci. Rep.*, vol. 7, no. 1, Art. No. 1, Jun. 2017, doi: 10.1038/s41598-017-04237-z.

[64] S.A. Khairallah, A.T. Anderson, A. Rubenchik, and W.E. King, (2016) Laser powder-bed fusion additive manufacturing: Physics of complex melt flow and formation mechanisms of pores, spatter, and denudation zones, *Acta Mater.*, vol. 108, pp. 36–45, Apr. 2016, doi: 10.1016/j.actamat.2016.02.014.

[65] M. Simonelli *et al.*, (2015) A Study on the Laser Spatter and the Oxidation Reactions During Selective Laser Melting of 316L Stainless Steel, Al-Si10-Mg, and Ti-6Al-4V, *Metall. Mater. Trans. A*, vol. 46, no. 9, pp. 3842–3851, Sep. 2015, doi: 10.1007/s11661-015-2882-8.

[66] Q. Guo *et al.*, (2018) Transient dynamics of powder spattering in laser powder bed fusion additive manufacturing process revealed by in-situ high-speed high-energy x-ray imaging, *Acta Mater.*, vol. 151, pp. 169–180, Jun. 2018, doi: 10.1016/j.actamat.2018.03.036.

[67] M.J. Heiden *et al.*, (2019) Evolution of 316L stainless steel feedstock due to laser powder bed fusion process, *Addit. Manuf.*, vol. 25, pp. 84–103, Jan. 2019, doi: 10.1016/j.addma.2018.10.019.

[68] C. Rock *et al.*, (2020) Analysis of Self-Organized Patterned Surface Oxide Spots on Ejected Spatter Produced during Laser Powder Bed Fusion, *Addit. Manuf.*, vol. 35, p. 101320, Oct. 2020, https://doi.org/10.1016/j.addma.2020.101320

[69] R. Esmaeilizadeh, U. Ali, A. Keshavarzkermani, Y. Mahmoodkhani, E. Marzbanrad, and E. Toyserkani, (2019) On the effect of spatter particles distribution on the quality of Hastelloy X parts made by laser powder-bed fusion additive manufacturing, *J. Manuf. Process.*, vol. 37, pp. 11–20.

[70] Z. Chen, A. Raza, and E. Hryha, (2022) Influence of part geometry on spatter formation in laser powder bed fusion of Inconel 718 alloy revealed by optical tomography, *J. Manuf. Process.*, vol. 81, pp. 680–695, Sep. 2022, doi: 10.1016/j.jmapro.2022.07.031

[71] Z. Snow, L. Scime, A. Ziabari, B. Fisher, and V. Paquit, (2022) Observation of Spatter-Induced Stochastic Lack-of–Fusion in Laser Powder Bed Fusion Using In Situ Process Monitoring, *Addit. Manuf.*, p. 103298, Nov. 2022, https://doi.org/10.1016/j.addma.2022.103298

[72] C. Schwerz, A. Raza, X. Lei, L. Nyborg, E. Hryha, and H. Wirdelius, (2021) In-situ detection of redeposited spatter and its influence on the formation of internal flaws in laser powder bed fusion, *Addit. Manuf.*, vol. 47, p. 102370, Nov. 2021, doi: 10.1016/j.addma.2021.102370

[73] M.J. Matthews, G. Guss, S.A. Khairallah, A.M. Rubenchik, P.J. Depond, and W.E. King, (2016) Denudation of metal powder layers in laser powder bed fusion processes, *Acta Mater.*, vol. 114, pp. 33–42, Aug. 2016, doi: 10.1016/j.actamat.2016.05.017

[74] C. Tenbrock, T. Kelliger, N. Praetzsch, M. Ronge, L. Jauer, and J.H. Schleifenbaum, (2021) Effect of laser-plume interaction on part quality in multi-scanner Laser Powder Bed Fusion, *Addit. Manuf.*, vol. 38, p. 101810, Feb. 2021, doi: 10.1016/j.addma.2020.101810.

[75] R. Mertens, S. Dadbakhsh, J.V. Humbeeck, and J.-P. Kruth, (2018) Application of base plate preheating during selective laser melting, *Procedia CIRP*, vol. 74, pp. 5–11, Jan. 2018, doi: 10.1016/j.procir.2018.08.002.

[76] K. Godineau, S. Lavernhe, and C. Tournier, (2019) Calibration of galvanometric scan heads for additive manufacturing with machine assembly defects consideration, *Addit. Manuf.*, vol. 26, pp. 250–257, Mar. 2019, doi: 10.1016/j.addma.2019.02.003.

[77] K. Godineau, S. Lavernhe, and C. Tournier, (2019) Influence of the opto-mechanical chain on the energy provided by the laser spot to the material in laser powder bed fusion processes, in *Proceedings of Joint Special Interest Group meeting between euspen and ASPE Advancing Precision in Additive Manufacturing*, Ecole Centrale de Nantes, France, Sep. 2019, p. 5.

[78] S.P. Moylan, J.A. Slotwinski, A.L. Cooke, K.K. Jurrens, and M.A. Donmez, (2014) An Additive Manufacturing Test Artifact, *NIST J. of Research*, Oct. 2014, Accessed: Dec. 01, 2022. [Online]. Available: https://www.nist.gov/publications/additive-manufacturing-test-artifact

[79] F. Kim, H. Yeung, and E. Garboczi, (2021) Characterizing the effects of laser control in laser powder bed fusion on near-surface pore formation via combined analysis of in-situ melt pool monitoring and X-ray computed tomography, *Additive Manufacturing*, vol. 48, Oct. 2021,

[80] J. Berez, M. Praniewicz, and C. Saldana, (2021) Assessing laser powder bed fusion system geometric errors through artifact-based methods, *Procedia Manuf.*, vol. 53, pp. 395–406, Jan. 2021, doi: 10.1016/j.promfg.2021.06.042.

[81] L. Dowling, J. Kennedy, S. O'Shaughnessy, and D. Trimble, (2020) A review of critical repeatability and reproducibility issues in powder bed fusion, *Mater. Des.*, vol. 186, p. 108346, Jan. 2020, doi: 10.1016/j.matdes.2019.108346.

[82] H. Yeung and S. Grantham, (2022) Laser Calibration for Powder Bed Fusion Additive Manufacturing Process, *Proceedings of the Solid Freeform Fabrication Symposium 2022*, Jul. 2022. Accessed: Feb. 28, 2023. [Online]. Available: https://www.nist.gov/publications/laser-calibration-powder-bed-fusion-additive-manufacturing-process

[83] K. Kempen, L. Thijs, B. Vrancken, S. Buls, J. Van Humbeeck, and J.-P. Kruth, (2013) Producing Crack-Free, High Density M2 HSS Parts by Selective Laser Melting: Pre-Heating the Baseplate, *Proceedings of the 2013 International Solid Freeform Fabrication Symposium*, Austin, TX, USA, Aug. 2013, pp. 131–139. Doi: 10.26153/tsw/15419.

[84] P. Edwards, A. O'Conner, and M. Ramulu, (2013) Electron Beam Additive Manufacturing of Titanium Components: Properties and Performance, *J. Manuf. Sci. Eng.*, vol. 135, no. 6, Nov. 2013, doi: 10.1115/1.4025773.

[85] J.L. Bartlett and X. Li, (2019) An overview of residual stresses in metal powder bed fusion, *Addit. Manuf.*, vol. 27, pp. 131–149, May 2019, doi: 10.1016/j.addma.2019.02.020.

[86] H. Shen, P. Rometsch, X. Wu, and A. Huang, (2020) Influence of Gas Flow Speed on Laser Plume Attenuation and Powder Bed Particle Pickup in Laser Powder Bed Fusion, *JOM*, vol. 72, no. 3, pp. 1039–1051, Mar. 2020, doi: 10.1007/s11837-020-04020-y.

[87] D. Deisenroth, J. Neira, J. Weaver, and H. Yeung, (2020) "Effects of shield gas flow on meltpool variability and signature in scanned laser melting, *Proceedings of the ASME 2020 15th International Manufacturing Science and Engineering Conference. Volume 1: Additive Manufacturing; Advanced Materials Manufacturing; Biomanufacturing; Life Cycle Engineering; Manufacturing Equipment and Automation*, https://doi.org/10.1115/MSEC2020-8410

[88] J. Weaver, A. Schlenoff, D. Deisenroth, and S.P. Moylan, (2021) Inert Gas Flow Speed Measurements in Laser Powder Bed Fusion Additive Manufacturing, *NIST AMS 100-43*, https://doi.org/10.6028/NIST.AMS.100-43

[89] L. Wang, A. Yu, E. Li, H. Shen, and Z. Zhou, (2021) Effects of spreader geometry on powder spreading process in powder bed additive manufacturing, *Powder Technol.*, vol. 384, pp. 211–222, May 2021, doi: 10.1016/j.powtec.2021.02.022.

[90] M. Soulier, A. Burr, V. Bonnefoy, and R. Laucournet, (2022) Relationship between powder properties and powder layer quality in powder-bed-based additive manufacturing processes, *the World PM2022*, Oct. 2022, p. 5368597. Accessed: Dec. 27, 2022. [Online]. Available: https://hal-cea.archives-ouvertes.fr/cea-03864909

[91] "Rethinking doctor blades and counter-rotating rollers," *Aerosint*, Jan. 30, 2020. https://aerosint.com/rethinking-doctor-blades-and-counter-rotating-rollers/ (accessed Dec. 27, 2022).

[92] Z. Snow, R. Martukanitz, and S. Joshi, (2019) On the development of powder spreadability metrics and feedstock requirements for powder bed fusion additive manufacturing, *Addit. Manuf.*, vol. 28, pp. 78–86, Aug. 2019, doi: 10.1016/j.addma.2019.04.017.

[93] L.C. Capozzi, A. Sivo, and E. Bassini, (2022) Powder spreading and spreadability in the additive manufacturing of metallic materials: A critical review, *J. Mater. Process. Technol.*, vol. 308, p. 117706, Oct. 2022, https://doi.org/10.1016/j.jmatprotec.2022.117706

[94] S. Vock, B. Klöden, A. Kirchner, T. Weißgärber, and B. Kieback, (2019) Powders for powder bed fusion: a review, *Prog. Addit. Manuf.*, vol. 4, no. 4, pp. 383–397, Dec. 2019, doi: 10.1007/s40964-019-00078-6.

[95] Y.S. Lee and W. Zhang, (2015) Mesoscopic Simulation of Heat Transfer and Fluid Flow in Laser Powder Bed Additive Manufacturing, *the 2015 International Solid Freeform Fabrication Symposium*, Accessed: Dec. 27, 2022. [Online]. Available: https://repositories.lib.utexas.edu/handle/2152/89408

[96] L. Scime and J. Beuth, (2018) Anomaly detection and classification in a laser powder bed additive manufacturing process using a trained computer vision algorithm, *Addit. Manuf.*, vol. 19, pp. 114–126, Jan. 2018, https://doi.org/10.1016/j.addma.2017.11.009

[97] A. Phua, P.S. Cook, C.H.J. Davies, and G.W. Delaney, (2022) Powder spreading over realistic laser melted surfaces in metal additive manufacturing, *Addit. Manuf. Lett.*, vol. 3, p. 100039, Dec. 2022, https://doi.org/10.1016/j.addlet.2022.100039

[98] ASTM International (2022) *ASTM F3522-22: Standard Guide for Additive Manufacturing of Metals — Feedstock Materials —Assessment of Powder Spreadability* (ASTM International West Conshohocken, PA).

[99] P.A. Hooper, (2018) Melt pool temperature and cooling rates in laser powder bed fusion, *Addit. Manuf.*, vol. 22, pp. 548–559, Aug. 2018, doi: 10.1016/j.addma.2018.05.032.

[100] B.K. Foster, E.W. Reutzel, A.R. Nassar, B.T. Hall, S.W. Brown, and C.J. Dickman, (2015) Optical, Layerwise Monitoring of Powder Bed Fusion, *Proceedings of the 2015 International Solid Freeform Fabrication Symposium*, 2015. Accessed: Nov. 21, 2022. [Online]. Available: https://repositories.lib.utexas.edu/handle/2152/89328

[101] J. zur Jacobsmühlen, S. Kleszczynski, D. Schneider, and G. Witt, (2013) High resolution imaging for inspection of laser beam melting systems, *2013 IEEE International Instrumentation and Measurement Technology Conference (I2MTC)*, May 2013, pp. 707–712. Doi: 10.1109/I2MTC.2013.6555507.

[102] M. Abdelrahman, E.W. Reutzel, A.R. Nassar, and T.L. Starr, (2017) Flaw detection in powder bed fusion using optical imaging, *Addit. Manuf.*, vol. 15, pp. 1–11, May 2017, doi: 10.1016/j.addma.2017.02.001.

[103] C. Gobert, E.W. Reutzel, J. Petrich, A.R. Nassar, and S. Phoha, (2018) Application of supervised machine learning for defect detection during metallic powder bed fusion additive manufacturing using high resolution imaging, *Addit. Manuf.*, vol. 21, pp. 517–528, May 2018, doi: 10.1016/j.addma.2018.04.005.

[104] H. Krauss, T. Zeugner, and M.F. Zaeh, (2014) Layerwise Monitoring of the Selective Laser Melting Process by Thermography, *Phys. Procedia*, vol. 56, pp. 64–71, Jan. 2014, https://doi.org/10.1016/j.phpro.2014.08.097

[105] A. Dickins *et al.*, (2020) Multi-view fringe projection system for surface topography measurement during metal powder bed fusion, *JOSA A*, vol. 37, no. 9, pp. B93–B105, Sep. 2020, doi: 10.1364/JOSAA.396186.

[106] H. Zhang, C.K.P. Vallabh, Y. Xiong, and X. Zhao, (2022) A systematic study and framework of fringe projection profilometry with improved measurement performance for in-situ LPBF process monitoring, *Measurement*, vol. 191, p. 110796, Mar. 2022, https://doi.org/10.1016/j.measurement.2022.110796

[107] A. Remani *et al.*, (2022) Multi-sensor measurement for in-situ defect identification in metal laser powder bed fusion, *Proceedings of the 2022 ASPE and euspen Summer Topical Meeting – Advancing Precision in Additive Manufacturing*, Knoxville, TN, USA, Jul. 2022.

[108] L. Scime and J. Beuth, (2018) A multi-scale convolutional neural network for autonomous anomaly detection and classification in a laser powder bed fusion additive manufacturing process, *Addit. Manuf.*, vol. 24, pp. 273–286, Dec. 2018, doi: 10.1016/j.addma.2018.09.034.

[109] ASTM International (2021) ISO/ASTM52900:2021: Additive manufacturing — General principles — Fundamentals and vocabulary (ASTM International, West Conshohocken, PA). https://doi.org/10.1520/F3177-21

[110] D-G Ahn (2021) Directed energy deposition (DED) process: state of the art. *International Journal of Precision Engineering and Manufacturing-Green Technology* 8(2):703-742.

[111] P. Kumar , N.K. Jain (2020) Effect of material form on deposition characteristics in micro-plasma transferred arc additive manufacturing process, *CIRP Journal of Manufacturing Science and Technology* 30:195-205. https://doi.org/10.1016/j.cirpj.2020.05.008

[112] M. Dalaee, et al., (2020) Feasibility study in combined direct metal deposition (DMD) and plasma transfer arc welding (PTA) additive manufacturing. *The International Journal of Advanced Manufacturing Technology* 106(9):4375-4389. https://doi.org/10.1007/s00170-019-04917-2

[113] D. Jafari, T.H.J. Vaneker, I. Gibson, (2021) Wire and arc additive manufacturing: Opportunities and challenges to control the quality and accuracy of manufactured parts. *Materials & Design* 202:109471. https://doi.org/10.1016/j.matdes.2021.109471

[114] J. Ding, et al., (2015) Development of a laminar flow local shielding device for wire+arc additive manufacture. *Journal of Materials Processing Technology* 226:99-105. https://doi.org/10.1016/j.jmatprotec.2015.07.005

[115] D. Ding, Z. Pan, D. Cuiuri, H. Li (2015) Wire-feed additive manufacturing of metal components: technologies, developments and future interests. *The International Journal of Advanced Manufacturing Technology* 81(1):465-481.

[116] N. Kumar N, et al., (2022) Wire Arc Additive Manufacturing–A revolutionary method in additive manufacturing. *Mater Chem Phys*:126144.

[117] J. Schaible, et al., (2021) Development of a high-speed laser material deposition process for additive manufacturing. *Journal of Laser Applications* 33(1):012021.
[118] J. Schaible, D. Hausch, T. Schopphoven, C. Häfner (2022) Deposition strategies for generating cuboid volumes using extreme high-speed directed energy deposition. *Journal of Laser Applications* 34(4):042034.
[119] G.Y. Chen, et al., (2022) Multi-energy source (MES) configuration for bead shape control in wire-based directed energy deposition (w-DED). *Journal of Materials Processing Technology* 304. https://doi.org/10.1016/j.jmatprotec.2022.117549
[120] American Welding Society (2019) *AWS D20.1:2019 Specification for fabrication of metal components using additive manufacturing* (American Welding Society, Miami, FL)
[121] ASTM International (2016) *ASTM F3187-16 Standard Guide for Directed Energy Deposition of Metals* (ASTM International, West Conshohocken, PA). https://doi.org/10.1520/F3187-16
[122] ASTM International (2019) *ASTM F3413e1 Guide for Additive Manufacturing — Design — Directed Energy Deposition* (ASTM International, West Conshohocken, PA). https://doi.org/10.1520/F3413-19E01
[123] S.M. Thompson, L. Bian, N. Shamsaei, A. Yadollahi (2015) An overview of Direct Laser Deposition for additive manufacturing; Part I: Transport phenomena, modeling and diagnostics. *Additive Manufacturing* 8:36-62. https://doi.org/10.1016/j.addma.2015.07.001
[124] D. Feenstra, et al., (2021) Critical review of the state of the art in multi-material fabrication via directed energy deposition. *Current Opinion in Solid State and Materials Science* 25(4):100924.
[125] J.L. Dávila, et al., (2020) Hybrid manufacturing: a review of the synergy between directed energy deposition and subtractive processes. *The International Journal of Advanced Manufacturing Technology* 110(11):3377-3390.
[126] A. Saboori, et al., (2019) Application of directed energy deposition-based additive manufacturing in repair. *Applied Sciences* 9(16):3316.
[127] A. Singh, S. Kapil, M. Das (2020) A comprehensive review of the methods and mechanisms for powder feedstock handling in directed energy deposition. *Additive Manufacturing* 35:101388. https://doi.org/10.1016/j.addma.2020.101388
[128] W.U.H. Syed, A.J. Pinkerton, L. Li (2005) A comparative study of wire feeding and powder feeding in direct diode laser deposition for rapid prototyping. *Applied Surface Science* 247(1):268-276. https://doi.org/10.1016/j.apsusc.2005.01.138
[129] R.M. Mahamood, E.T. Akinlabi (2016) Processing parameters optimization for material deposition efficiency in laser metal deposited titanium alloy. *Lasers in Manufacturing and Materials Processing* 3(1):9-21.
[130] S. Alya , R. Singh (2021) Discrete phase modeling of the powder flow dynamics and the catchment efficiency in laser directed energy deposition with inclined coaxial nozzles. *Journal of Manufacturing Science and Engineering* 143(8).
[131] J.W. Murray, et al., (2021) Unprocessed machining chips as a practical feedstock in directed energy deposition. *International Journal of Machine Tools and Manufacture* 169:103803. https://doi.org/10.1016/j.ijmachtools.2021.103803
[132] W.U.H. Syed, A.J. Pinkerton, L. Li (2006) Combining wire and coaxial powder feeding in laser direct metal deposition for rapid prototyping. *Applied Surface Science* 252(13):4803-4808. https://doi.org/10.1016/j.apsusc.2005.08.118
[133] A.D. Iams, M.Z. Gao, A. Shetty, T.A. Palmer (2022) Influence of particle size on powder rheology and effects on mass flow during directed energy deposition additive manufacturing. *Powder Technology* 396:316-326. https://doi.org/10.1016/j.powtec.2021.10.059
[134] J. Bennett, et al., (2022) Powder-borne porosity in directed energy deposition. *Journal of Manufacturing Processes* 80:69-74. https://doi.org/10.1016/j.jmapro.2022.04.036
[135] T. Zhao, et al., (2021) Some factors affecting porosity in directed energy deposition of AlMgScZr-alloys. *Optics & Laser Technology* 143:107337. https://doi.org/10.1016/j.optlastec.2021.107337
[136] Y. Chen, X. Zhang, M.M. Parvez, F. Liou (2020) A review on metallic alloys fabrication using elemental powder blends by laser powder directed energy deposition process. *Materials* 13(16):3562.
[137] S. Karnati, F.F. Liou, J.W. Newkirk (2019) Characterization of copper–nickel alloys fabricated using laser metal deposition and blended powder feedstocks. *The International Journal of Advanced Manufacturing Technology* 103:239-250.
[138] W. Cui, et al., (2018) Fabrication of AlCoCrFeNi high-entropy alloy coating on an AISI 304 substrate via a CoFe2Ni intermediate layer. *Entropy* 21(1):2.
[139] W. Li, S. Karnati, Y. Zhang, F. Liou (2018) Investigating and eliminating powder separation in pre-mixed powder supply for laser metal deposition process. *Journal of Materials Processing Technology* 254:294-301. https://doi.org/10.1016/j.jmatprotec.2017.11.045
[140] T. Mukherjee, J.S. Zuback, A. De, T. DebRoy (2016) Printability of alloys for additive manufacturing. *Scientific Reports* 6(1):19717. https://doi.org/10.1038/srep19717
[141] F. Kaji, et al., (2022) Process planning for additive manufacturing of geometries with variable overhang angles using a robotic laser directed energy deposition system. *Additive Manufacturing Letters* 2:100035. https://doi.org/10.1016/j.addlet.2022.100035
[142] B.T. Gibson, et al., (2022) Controls and process planning strategies for 5-axis laser directed energy deposition of Ti-6Al-4V using an 8-axis industrial robot and rotary motion. *Additive Manufacturing* 58:103048. https://doi.org/10.1016/j.addma.2022.103048

[143] J. Xu, X. Gu, D. Ding, Z. Pan, K. Chen (2018) A review of slicing methods for directed energy deposition based additive manufacturing. *Rapid Prototyping Journal* 24(6):1012-1025. https://doi.org/10.1108/RPJ-10-2017-0196
[144] N. Shamsaei, A. Yadollahi, L. Bian, S.M. Thompson (2015) An overview of Direct Laser Deposition for additive manufacturing; Part II: Mechanical behavior, process parameter optimization and control. *Additive Manufacturing* 8:12-35. https://doi.org/10.1016/j.addma.2015.07.002
[145] T. DebRoy, et al., (2018) Additive manufacturing of metallic components – Process, structure and properties. *Progress in Materials Science* 92:112-224. https://doi.org/10.1016/j.pmatsci.2017.10.001
[146] S. Kersten, M. Praniewicz, T. Kurfess, C. Saldana (2020) Build Orientation Effects on Mechanical Properties of 316SS Components Produced by Directed Energy Deposition. *Procedia Manufacturing* 48:730-736. https://doi.org/10.1016/j.promfg.2020.05.106
[147] A. Dass , A. Moridi (2019) State of the art in directed energy deposition: From additive manufacturing to materials design. *Coatings* 9(7):418.
[148] S.M. Yusuf, N. Gao (2017) Influence of energy density on metallurgy and properties in metal additive manufacturing. *Materials Science and Technology* 33(11):1269-1289. https://doi.org/10.1080/02670836.2017.1289444
[149] D.R. Feenstra, A. Molotnikov, N. Birbilis (2021) Utilisation of artificial neural networks to rationalise processing windows in directed energy deposition applications. *Materials & Design* 198:109342. https://doi.org/10.1016/j.matdes.2020.109342
[150] S. Webster, K. Ehmann, J. Cao (2020) Energy Density Comparison via Highspeed, In-situ Imaging of Directed Energy Deposition. *Procedia Manufacturing* 48:691-696. https://doi.org/10.1016/j.promfg.2020.05.101
[151] S.J. Wolff, et al., (2021) In-situ observations of directed energy deposition additive manufacturing using high-speed x-ray imaging. *Jom* 73(1):189-200
[152] J. Kummailil J, et al., (2005) Effect of select LENS™ processing parameters on the deposition of Ti-6Al-4V. *Journal of manufacturing processes* 7(1):42-50.
[153] M. Liu, A. Kumar, S. Bukkapatnam, M. Kuttolamadom (2021) A Review of the Anomalies in Directed Energy Deposition (DED) Processes & Potential Solutions – Part Quality & Defects. *Procedia Manufacturing* 53:507-518. https://doi.org/10.1016/j.promfg.2021.06.093
[154] J.C. Haley, et al., (2019) Working distance passive stability in laser directed energy deposition additive manufacturing. *Materials & Design* 161:86-94. https://doi.org/10.1016/j.matdes.2018.11.021
[155] J. Xiong , G. Zhang (2014) Adaptive control of deposited height in GMAW-based layer additive manufacturing. *Journal of Materials Processing Technology* 214(4):962-968. https://doi.org/10.1016/j.jmatprotec.2013.11.014
[156] K.S. Ribeiro, F.E. Mariani, R.T. Coelho (2020) A study of different deposition strategies in direct energy deposition (DED) processes. *Procedia Manufacturing* 48:663-670.
[157] M. Köhler,et al., (2021) Comparative study of deposition patterns for DED-Arc additive manufacturing of Al-4046. *Materials & Design* 210:110122. https://doi.org/10.1016/j.matdes.2021.110122
[158] D. Svetlizky, et al., (2021) Directed energy deposition (DED) additive manufacturing: Physical characteristics, defects, challenges and applications. *Materials Today* 49:271-295. https://doi.org/10.1016/j.mattod.2021.03.020
[159] S-G Chen, H-J Gao, Y-D Zhang, Q. Wu, Z-H Gao, X. Zhou (2022) Review on residual stresses in metal additive manufacturing: formation mechanisms, parameter dependencies, prediction and control approaches. *Journal of Materials Research and Technology* 17:2950-2974. https://doi.org/10.1016/j.jmrt.2022.02.054
[160] C.R. Cunningham, et al., (2018) Strategies and processes for high quality wire arc additive manufacturing. *Additive Manufacturing* 22:672-686. https://doi.org/10.1016/j.addma.2018.06.020
[161] K-H Kim, C-H Jung, D-Y Jeong, S-K Hyun (2021) Preventing Evaporation Products for High-Quality Metal Film in Directed Energy Deposition: A Review. *Metals* 11(2):353.
[162] K. Kamimuki, et al., (2002) Prevention of welding defect by side gas flow and its monitoring method in continuous wave Nd: YAG laser welding. *Journal of Laser applications* 14(3):136-145.
[163] J. Zou, W. Yang, S. Wu, Y. He, R. Xiao (2016) Effect of plume on weld penetration during high-power fiber laser welding. *Journal of Laser Applications* 28(2):022003.
[164] J.F. Wang, et al., (2016) Effect of location on microstructure and mechanical properties of additive layer manufactured Inconel 625 using gas tungsten arc welding. *Materials Science and Engineering: A* 676:395-405. https://doi.org/10.1016/j.msea.2016.09.015
[165] Y.C. Yeoh, et al., (2021) Multiscale microstructural heterogeneity and mechanical property scatter in Inconel 718 produced by directed energy deposition. *Journal of Alloys and Compounds* 887:161426. https://doi.org/10.1016/j.jallcom.2021.161426
[166] S. Kou (2021) Predicting susceptibility to solidification cracking and liquation cracking by CALPHAD. *Metals* 11(9):1442.
[167] Z. Zhou, et al., (2018) Causes analysis on cracks in nickel-based single crystal superalloy fabricated by laser powder deposition additive manufacturing. *Materials & Design* 160:1238-1249. https://doi.org/10.1016/j.matdes.2018.10.042
[168] S. Kou (2003) Solidification and liquation cracking issues in welding. *JOM* 55(6):37-42. https://doi.org/10.1007/s11837-003-0137-4

[169] W. Cong, F. Ning (2017) A fundamental investigation on ultrasonic vibration-assisted laser engineered net shaping of stainless steel. *International Journal of Machine Tools and Manufacture* 121:61-69.
[170] Y. Ding, et al., (2016) Microstructure and mechanical property considerations in additive manufacturing of aluminum alloys. *MRS Bulletin* 41(10):745-751.
[171] Y. Chi, et al., (2022) Wire-Arc Directed Energy Deposition of Aluminum Alloy 7075 with Dispersed Nanoparticles. *Journal of Manufacturing Science and Engineering*:1-14
[172] J. Xu, et al., (2017) The effect of preheating on microstructure and mechanical properties of laser solid forming IN-738LC alloy. *Materials Science and Engineering: A* 691:71-80. https://doi.org/10.1016/j.msea.2017.03.046
[173] N. Chen, et al., (2020) Microstructural characteristics and crack formation in additively manufactured bimetal material of 316L stainless steel and Inconel 625. *Additive Manufacturing* 32:101037. https://doi.org/10.1016/j.addma.2020.101037
[174] N. Lu, et al., (2020) Hot cracking behavior and mechanism of a third-generation Ni-based single-crystal superalloy during directed energy deposition. *Additive Manufacturing* 34:101228. https://doi.org/10.1016/j.addma.2020.101228
[175] E. Plancher, et al., (2019) Tracking pores during solidification of a Ni-based superalloy using 4D synchrotron microtomography. *Acta Materialia* 181:1-9. https://doi.org/10.1016/j.actamat.2019.09.040
[176] Y. Yu, W. Yan, F. Lin (2022) Understanding the formation process of shrinkage pores with a 3D dendrite growth model: from casting to additive manufacturing. *Computational Mechanics* 69(1):133-149. https://doi.org/10.1007/s00466-021-02086-2
[177] J. Fu, H. Li, X. Song, M.W. Fu (2022) Multi-scale defects in powder-based additively manufactured metals and alloys. *Journal of Materials Science & Technology* 122:165-199. https://doi.org/10.1016/j.jmst.2022.02.015
[178] A. Guner, et al., (2022) Nozzle designs in powder-based direct laser deposition: A review. *International Journal of Precision Engineering and Manufacturing* 23(9):1077-1094.
[179] Y. Nalam, et al., (2021) Gas flow study for development of a novel shielding gas nozzle for directed energy deposition processes using computational fluid dynamic simulations. *IOP Conference Series: Materials Science and Engineering* 1135(1):012016. https://doi.org/10.1088/1757-899X/1135/1/012016
[180] B. Silwal, et al., (2022) Altering the Supply of Shielding Gases to Fabricate Distinct Geometry in GMA Additive Manufacturing. *Applied Sciences-Basel* 12(7). https://doi.org/10.3390/app12073679
[181] A. Aversa, et al., (2020) The role of Directed Energy Deposition atmosphere mode on the microstructure and mechanical properties of 316L samples. *Additive Manufacturing* 34:101274. https://doi.org/10.1016/j.addma.2020.101274
[182] Y.K. Bandari, S.W. Williams, J. Ding, F. Martina (2015) Additive manufacture of large structures: robotic or CNC systems? *2014 International Solid Freeform Fabrication Symposium*, (University of Texas at Austin)
[183] P. Urhal, A. Weightman, C. Diver, P. Bartolo (2019) Robot assisted additive manufacturing: A review. *Robotics and Computer-Integrated Manufacturing* 59:335-345. https://doi.org/10.1016/j.rcim.2019.05.005
[184] Z-J Tang, et al., (2020) A review on in situ monitoring technology for directed energy deposition of metals. *The International Journal of Advanced Manufacturing Technology* 108(11):3437-3463.
[185] E.W. Reutzel, A.R. Nassar (2015) A survey of sensing and control systems for machine and process monitoring of directed-energy, metal-based additive manufacturing. *Rapid Prototyping Journal*, 21(2):159–167. https://doi.org/10.1108/RPJ-12-2014-0177
[186] S.K. Everton, et al., (2016) Review of in-situ process monitoring and in-situ metrology for metal additive manufacturing. *Materials & Design* 95:431-445. https://doi.org/10.1016/j.matdes.2016.01.099
[187] G.Tapia , A. Elwany (2014) A review on process monitoring and control in metal-based additive manufacturing. *Journal of Manufacturing Science and Engineering* 136(6).
[188] M. Grasso, et al., (2021) In-situ measurement and monitoring methods for metal powder bed fusion: an updated review. *Measurement Science and Technology* 32(11):112001. https://doi.org/10.1088/1361-6501/ac0b6b
[189] D.S. Egan, K. Jones, D.P. Dowling (2020) Selective laser melting of Ti-6Al-4V: Comparing µCT with in-situ process monitoring data. *CIRP Journal of Manufacturing Science and Technology* 31:91–98. https://doi.org/10.1016/j.cirpj.2020.10.004
[190] Y. Mao, et al., (2022) A deep learning framework for layer-wise porosity prediction in metal powder bed fusion using thermal signatures. *Journal of Intelligent Manufacturing*. https://doi.org/10.1007/s10845-022-02039-3
[191] T. Kolb, P. Gebhardt, O. Schmidt, J. Tremel, M. Schmidt (2018) Melt Pool Monitoring for Laser Beam Melting of Metals: Assistance for Material Qualification for the Stainless Steel 1.4057. *Procedia CIRP* 74:116–121. https://doi.org/10.1016/j.procir.2018.08.058
[192] T. Reutzel, et al., (2014) Comparison of Thermal Imaging Measurements with FEA Modeling of Heat Flows in Directed Energy Laser Deposition. (ASM International, Orlando, FL).
[193] X. Xie, et al., (2021) Mechanistic data-driven prediction of as-built mechanical properties in metal additive manufacturing. *Npj Computational Materials* 7(1):1–12. https://doi.org/10.1038/s41524-021-00555-z
[194] J. Mazumder, D. Dutta, N. Kikuchi, A. Ghosh (2000) Closed loop direct metal deposition: art to part. *Optics and Lasers in Engineering* 34:397–414.

[195] W. Cai, et al., (2020) Application of sensing techniques and artificial intelligence-based methods to laser welding real-time monitoring: A critical review of recent literature. *Journal of Manufacturing Systems* 57:1–18. https://doi.org/10.1016/j.jmsy.2020.07.021

[196] A. Fernandez, R. Felice, C.A.Terrazas-Nájera, R. Wicker (2021) Implications for accurate surface temperature monitoring in powder bed fusion: Using multi-wavelength pyrometry to characterize spectral emissivity during processing. *Additive Manufacturing* 46:102138. https://doi.org/10.1016/j.addma.2021.102138

[197] C-G Ren, Y-L Lo, H-C Tran, M-H Lee (2019) Emissivity calibration method for pyrometer measurement of melting pool temperature in selective laser melting of stainless steel 316L. *The International Journal of Advanced Manufacturing Technology*. https://doi.org/10.1007/s00170-019-04193-0

[198] S. Coeck, M. Bisht, J. Plas, F. Verbist (2019) Prediction of lack of fusion porosity in selective laser melting based on melt pool monitoring data. *Additive Manufacturing* 25:347–356. https://doi.org/10.1016/j.addma.2018.11.015

[199] G. Repossini, V. Laguzza, M. Grasso, B.M. Colosimo (2017) On the use of spatter signature for in-situ monitoring of Laser Powder Bed Fusion. *Additive Manufacturing* 16:35–48. https://doi.org/10.1016/j.addma.2017.05.004

[200] L.E. Criales, et al., (2017) Laser powder bed fusion of nickel alloy 625: Experimental investigations of effects of process parameters on melt pool size and shape with spatter analysis. *International Journal of Machine Tools and Manufacture* 121:22–36. https://doi.org/10.1016/j.ijmachtools.2017.03.004

[201] H. Zheng, et al., (2021) Observation of Vapor Plume Behavior and Process Stability at Single-Track and Multi-Track Levels in Laser Powder Bed Fusion Regime. *Metals* 11(6):937. https://doi.org/10.3390/met11060937

[202] B.M. Lane, D.C. Deisenroth (2023) Thermography of Metals-based Additive Manufacturing. *ASM Handbook Volume 24A: Additive Manufacturing Design and Applications*, ASM Handbook. (Materials Park, OH), Vol. 24A.

[203] M. Seleznev, et al., (2022) In situ detection of cracks during laser powder bed fusion using acoustic emission monitoring. *Additive Manufacturing Letters*:100099. https://doi.org/10.1016/j.addlet.2022.100099

[204] N. Eschner, L. Weiser, B. Häfner, G. Lanza (2018) Development of an acoustic process monitoring system for selective laser melting (SLM). *Proceedings of the Solid Freeform Fabrication Symposium* (Austin, TX).

[205] D. Kouprianoff, et al., (2017) On-line monitoring of laser powder bed fusion by acoustic emission: Acoustic emission for inspection of single tracks under different powder layer thickness. *2017 Pattern Recognition Association of South Africa and Robotics and Mechatronics (PRASA-RobMech)*, pp 203–207. https://doi.org/10.1109/RoboMech.2017.8261148

[206] D. Kouprianoff, et al., (2021) Monitoring of Laser Powder Bed Fusion by Acoustic Emission: Investigation of Single Tracks and Layers. *Frontiers in Mechanical Engineering* 7. Available at https://www.frontiersin.org/articles/10.3389/fmech.2021.678076

[207] V. Pandiyan, et al., (2020) Analysis of time, frequency and time-frequency domain features from acoustic emissions during Laser Powder-Bed fusion process. *Procedia CIRP* 94:392–397. https://doi.org/10.1016/j.procir.2020.09.152

[208] K. Wasmer, et al., (2018) Laser processing quality monitoring by combining acoustic emission and machine learning: a high-speed X-ray imaging approach. *Procedia CIRP* 74:654–658. https://doi.org/10.1016/j.procir.2018.08.054

[209] C.S. Lough, et al., (2020) In-situ optical emission spectroscopy of selective laser melting. *Journal of Manufacturing Processes* 53:336–341. https://doi.org/10.1016/j.jmapro.2020.02.016

[210] A.R. Nassar, T.J.Spurgeon, E.W. Reutzel (2014) Sensing Defects during Directed-Energy Additive Manufacturing of Metal Parts using Optical Emissions Spectroscopy. (University of Texas at Austin). https://doi.org/10.26153/tsw/15684

[211] T.R. Allen, et al., (2020) Energy-Coupling Mechanisms Revealed through Simultaneous Keyhole Depth and Absorptance Measurements during Laser-Metal Processing. *Physical Review Applied* 13(6):064070. https://doi.org/10.1103/PhysRevApplied.13.064070

[212] B. Lane, et al., (2020) Transient laser energy absorption, co-axial melt pool monitoring, and relationship to melt pool morphology. *Additive Manufacturing* 36:101504. https://doi.org/10.1016/j.addma.2020.101504

[213] D. Deisenroth, S. Mekhontsev, B. Lane (2020) Measurement of mass loss, absorbed energy, and time-resolved reflected power for laser powder bed fusion. *Laser 3D Manufacturing VII*, eds Helvajian H, Gu B, Chen H (SPIE, San Francisco, United States), p 20. https://doi.org/10.1117/12.2547491

[214] W.E. King, et al., (2015) Laser powder bed fusion additive manufacturing of metals; physics, computational, and materials challenges. *Applied Physics Reviews* 2(4):041304. https://doi.org/10.1063/1.4937809

[215] C. Zhao C, et al., (2017) Real-time monitoring of laser powder bed fusion process using high-speed X-ray imaging and diffraction. *Scientific Reports* 7(1):3602. https://doi.org/10.1038/s41598-017-03761-2

[216] P. Bidare, et al., (2018) Fluid and particle dynamics in laser powder bed fusion. *Acta Materialia* 142:107–120. https://doi.org/10.1016/j.actamat.2017.09.051

[217] H. Yeung, B. Lane (2020) A residual heat compensation based scan strategy for powder bed fusion additive manufacturing. *Manufacturing Letters* 25:56–59. https://doi.org/10.1016/j.mfglet.2020.07.005

[218] L. Caprio, A.G. Demir, B. Previtali (2020) Observing molten pool surface oscillations during keyhole processing in laser powder bed fusion as a novel method to estimate the penetration depth. *Additive Manufacturing*:101470. https://doi.org/10.1016/j.addma.2020.101470

[219] M. Grasso, B.M. Colosimo (2017) Process defects and in situ monitoring methods in metal powder bed fusion: a review. *Measurement Science and Technology* 28(4):044005. https://doi.org/10.1088/1361-6501/aa5c4f
[220] J.C. Fox, S.P. Moylan, B.M. Lane (2016) Effect of process parameters on the surface roughness of overhanging structures in laser powder bed fusion additive manufacturing. *Procedia CIRP* 45:131–134.
[221] D. Wang, Y. Yang, Z. Yi, X. Su (2013) Research on the fabricating quality optimization of the overhanging surface in SLM process. *The International Journal of Advanced Manufacturing Technology* 65(9):1471–1484. https://doi.org/10.1007/s00170-012-4271-4
[222] P. Shcheglov (2012) Study of Vapour-plasma plume during high power fiber laser beam influence on metals. Candidate of Science (Bundesanstalt für Materialforschung und -prüfung (BAM), Berlin, Germany). Available at https://opus4.kobv.de/opus4-bam/files/70/diss88_vt.pdf
[223] T. Kolb, L. Müller, J. Tremel, M. Schmidt (2018) Melt Pool Monitoring for Laser Beam Melting of Metals: Inline-Evaluation and Remelting of Surfaces. *Procedia CIRP* 74:111–115. https://doi.org/10.1016/j.procir.2018.08.052
[224] B.A. Fisher, B. Lane, H. Yeung, J. Beuth (2018) Toward determining melt pool quality metrics via coaxial monitoring in laser powder bed fusion. *Manufacturing Letters* 15:119–121. https://doi.org/10.1016/j.mfglet.2018.02.009
[225] G. Mohr, et al., (2020) In-situ defect detection in laser powder bed fusion by using thermography and optical tomography—comparison to computed tomography. *Metals* 10(1). https://doi.org/10.3390/met10010103
[226] Z. Li, et al., (2022) A Review of Spatter in Laser Powder Bed Fusion Additive Manufacturing: In Situ Detection, Generation, Effects, and Countermeasures. *Micromachines* 13(8):1366. https://doi.org/10.3390/mi13081366
[227] W. Zhang, H. Ma, Q. Zhang, S. Fan (2022) Prediction of powder bed thickness by spatter detection from coaxial optical images in selective laser melting of 316L stainless steel. *Materials & Design* 213:110301. https://doi.org/10.1016/j.matdes.2021.110301
[228] D. Wang, et al., (2017) Mechanisms and characteristics of spatter generation in SLM processing and its effect on the properties. *Materials & Design* 117:121–130. https://doi.org/10.1016/j.matdes.2016.12.060
[229] D.M. Seltzer, et al., (2015) System Identification and Feedback Control for Directed-Energy, Metal-Based Additive Manufacturing. *Proceedings of the Solid Freeform Fabrication Symposium* (Austin, TX). Available at https://repositories.lib.utexas.edu/handle/2152/89361
[230] H. Wang, et al., (2020) Review on adaptive control of laser-directed energy deposition. *Optical Engineering* 59(7):070901. https://doi.org/10.1117/1.OE.59.7.070901
[231] Z. Sun, W. Guo, L. Li (2020) In-process measurement of melt pool cross-sectional geometry and grain orientation in a laser directed energy deposition additive manufacturing process. *Optics & Laser Technology* 129:106280. https://doi.org/10.1016/j.optlastec.2020.106280
[232] G. Piscopo, E. Atzeni, A. Salmi (2019) A hybrid modeling of the physics-driven evolution of material addition and track generation in laser powder directed energy deposition. *Materials* 12(17):2819. https://doi.org/10.3390/ma12172819
[233] F. Wirth, S. Arpagaus, K. Wegener (2018) Analysis of melt pool dynamics in laser cladding and direct metal deposition by automated high-speed camera image evaluation. *Additive Manufacturing* 21:369–382. https://doi.org/10.1016/j.addma.2018.03.025
[234] H.S. Prasad, F. Brueckner, A.F.H. Kaplan (2020) Powder incorporation and spatter formation in high deposition rate blown powder directed energy deposition. *Additive Manufacturing* 35:101413. https://doi.org/10.1016/j.addma.2020.101413
[235] Y. Kawahito, N. Matsumoto, M. Mizutani, S. Katayama (2008) Characterisation of plasma induced during high power fibre laser welding of stainless steel. *Science and Technology of Welding and Joining* 13(8):744–748. https://doi.org/10.1179/136217108X329313
[236] C.L. Chan, J. Mazumder (1987) One-dimensional steady-state model for damage by vaporization and liquid expulsion due to laser-material interaction. *Journal of Applied Physics* 62(11):4579–4586. https://doi.org/10.1063/1.339053
[237] S. Donadello, M. Motta, A.G. Demir, B. Previtali (2019) Monitoring of laser metal deposition height by means of coaxial laser triangulation. *Optics and Lasers in Engineering* 112:136–144. https://doi.org/10.1016/j.optlaseng.2018.09.012
[238] Z. Smoqi, et al., (2022) Closed-loop control of meltpool temperature in directed energy deposition. *Materials & Design* 215:110508. https://doi.org/10.1016/j.matdes.2022.110508
[239] J.L. Bennett, et al., (2017) Thermal effect on clad dimension for laser deposited Inconel 718. *Journal of Manufacturing Processes* 28:550–557. https://doi.org/10.1016/j.jmapro.2017.04.024
[240] S.J. Wolff, et al., (2019) Experimentally validated predictions of thermal history and microhardness in laser-deposited Inconel 718 on carbon steel. *Additive Manufacturing* 27:540–551. https://doi.org/10.1016/j.addma.2019.03.019
[241] A. Kramida, Y. Ralchenko, J. Reader, NIST ASD Team (2022) NIST Atomic Spectra Database (version 5.10). *National Institute of Standards and Technology*. Available at https://physics.nist.gov/asd
[242] L. Song, J. Mazumder (2012) Real Time Cr Measurement Using Optical Emission Spectroscopy During Direct Metal Deposition Process. *IEEE Sensors Journal* 12(5):958–964. https://doi.org/10.1109/JSEN.2011.2162316
[243] W. Ya, et al., (2015) Spectroscopic monitoring of metallic bonding in laser metal deposition. *Journal of Materials Processing Technology* 220:276–284. https://doi.org/10.1016/j.jmatprotec.2015.01.026

[244] J. Shin, J. Mazumder (2018) Composition monitoring using plasma diagnostics during direct metal deposition (DMD) process. *Optics & Laser Technology* 106:40–46. https://doi.org/10.1016/j.optlastec.2018.03.020

[245] C.B. Stutzman, A.R. Nassar, E.W. Reutzel (2018) Multi-sensor investigations of optical emissions and their relations to directed energy deposition processes and quality. *Additive Manufacturing* 21:333–339. https://doi.org/10.1016/j.addma.2018.03.017

[246] C. Kledwig, et al., (2019) Analysis of Melt Pool Characteristics and Process Parameters Using a Coaxial Monitoring System during Directed Energy Deposition in Additive Manufacturing. *Materials* 12(2):308. https://doi.org/10.3390/ma12020308

[247] R.B. Dinwiddie RB, et al., (2013) Thermographic in-situ process monitoring of the electron-beam melting technology used in additive manufacturing. *Proceedings of the SPIE,* Vol. 8705, pp 87050K-87050K–9. *http://dx.doi.org/10.1117/12.2018412*

[248] J. Berez, C. Saldaña, (2022) Laser Line Profile Scanning for Powder Bed Topography Measurement, in: 2022 *Int. Solid Free. Fabr. Symposium*.

[249] S. Barua, F. Liou, J. Newkirk, T. Sparks, (2014) Vision-based defect detection in laser metal deposition process, *Rapid Prototyp. J*. 20 (2014) 77–85. https://doi.org/10.1108/RPJ-04-2012-0036

[250] C. Millon C, et al., (2018) Development of laser ultrasonics inspection for online monitoring of additive manufacturing. *Welding in the World* 62(3):653–661. https://doi.org/10.1007/s40194-018-0567-9

[251] J. Whiting, A. Springer, F. Sciammarella (2018) Real-time acoustic emission monitoring of powder mass flow rate for directed energy deposition, *Add. Mfg* 23:312–318. https://doi.org/10.1016/j.addma.2018.08.015

[252] L. Pagani, M. Grasso, P.J. Scott, B.M. Colosimo, (2020) Automated layerwise detection of geometrical distortions in laser powder bed fusion, *Add. Mfg.* 36 101435. https://doi.org/10.1016/j.addma.2020.101435

[253] R.Y. Ilieva, M.A. Nikolov, (2020) The Impact of Machine Vision in Additive Manufacturing, in: *2020 XI Natl. Conf. Int. Particip. Electron.*, IEEE, Sofia, Bulgaria,: pp. 1–4. https://doi.org/10.1109/ELECTRONICA50406.2020.9305112

[254] R. McCann, M.A. Obeidi, C. Hughes, É. McCarthy, D.S. Egan, R.K. Vijayaraghavan, A.M. Joshi, V. Acinas Garzon, D.P. Dowling, P.J. McNally, D. Brabazon, (2021) In-situ sensing, process monitoring and machine control in Laser Powder Bed Fusion: A review, *Add. Manuf*. 45 102058. https://doi.org/10.1016/j.addma.2021.102058.

[255] T. Sahar, M. Rauf, A. Murtaza, L.A. Khan, H. Ayub, S.M. Jameel, I.U. Ahad, (2023) Anomaly detection in laser powder bed fusion using machine learning: A review, *Results Eng*. 17 100803. https://doi.org/10.1016/j.rineng.2022.100803

[256] G.K. Sarkon, B. Safaei, M.S. Kenevisi, S. Arman, Q. Zeeshan, (2022) State-of-the-Art Review of Machine Learning Applications in Additive Manufacturing; from Design to Manufacturing and Property Control, *Arch. Comput. Methods Eng*. 29 5663–5721. https://doi.org/10.1007/s11831-022-09786-9.

[257] Y. AbouelNour, N. Gupta, (2022) In-situ monitoring of sub-surface and internal defects in additive manufacturing: A review, *Mater. Des*. 111063.

[258] B. Lane, H. Yeung, Z. Yang (2022) Statistical and spatio-temporal data features in melt pool monitoring of additive manufacturing. *Proceedings of the 2022 IISE Annual Conference (Seattle, WA). Available at https://tsapps.nist.gov/publication/get_pdf.cfm?pub_id=934033*

[259] D. Svetlizky, M. Das, B. Zheng, A.L. Vyatskikh, S. Bose, A. Bandyopadhyay, J.M. Schoenung, E.J. Lavernia, N. Eliaz, (2021) Directed energy deposition (DED) additive manufacturing: Physical characteristics, defects, challenges and applications, *Mater. Today*. 49 271–295. https://doi.org/10.1016/j.mattod.2021.03.020.

[260] P.J. DePond, G. Guss, S. Ly, N.P. Calta, D. Deane, S. Khairallah, M.J. Matthews, In situ measurements of layer roughness during laser powder bed fusion additive manufacturing using low coherence scanning interferometry, *Mater. Des*. (n.d.). https://doi.org/10.1016/j.matdes.2018.05.050.

[261] B. Zhang, J. Ziegert, F. Farahi, A. Davies, (2016) In situ surface topography of laser powder bed fusion using fringe projection, *Addit. Manuf*. 12 100–107. https://doi.org/10.1016/j.addma.2016.08.001.

[262] R.K. Leach, D. Bourell, S. Carmignato, A. Donmez, N. Senin, W. Dewulf, (2019) Geometrical metrology for metal additive manufacturing, *CIRP Ann*. 68 677–700. https://doi.org/10.1016/j.cirp.2019.05.004.

[263] N. Senin, A. Thompson, R. Leach, (2018) Feature-based characterization of signature topography in laser powder bed fusion of metals, *Meas. Sci. Technol.* 29 045009. https://doi.org/10.1088/1361-6501/aa9e19.

[264] J. Fox, A. Allen, B. Mullany, E. Morse, R. Isaacs, M. Lata, A. Sood, C. Evans, (2021) Surface topography process signatures in nickel superalloy 625 additive manufacturing, in: *Proc. Jt. Spec. Interest Group Meet. Euspen ASPE*, St. Gallen, Switzerland, 2021.

[265] A. Mostafaei, C. Zhao, Y. He, S. Reza Ghiaasiaan, B. Shi, S. Shao, N. Shamsaei, Z. Wu, N. Kouraytem, T. Sun, J. Pauza, J.V. Gordon, B. Webler, N.D. Parab, M. Asherloo, Q. Guo, L. Chen, A.D. Rollett, (2022) Defects and anomalies in powder bed fusion metal additive manufacturing, *Curr. Opin. Solid State Mater. Sci.* 26 100974. https://doi.org/10.1016/j.cossms.2021.100974

[266] Y. Zhang, W. Yan, (2022) Applications of machine learning in metal powder-bed fusion in-process monitoring and control: status and challenges, *J. Intell. Manuf*. https://doi.org/10.1007/s10845-022-01972-7.

[267] Y. Fu, A.R.J. Downey, L. Yuan, T. Zhang, A. Pratt, Y. Balogun, (2022) Machine learning algorithms for defect detection in metal laser-based additive manufacturing: A review, *J. Manuf. Process*. 75 693–710. https://doi.org/10.1016/j.jmapro.2021.12.061.

[268] M. Gronle, M. Grasso, E. Granito, F. Schaal, B.M. Colosimo, (2022) Open data for open science in Industry 4.0: In-situ monitoring of quality in additive manufacturing, *J. Qual. Technol*. 0 1–13.

[269] F. Meriaudeau, F. Truchetete, C. Dumont, E. Renier, P. Bolland, (1996) Acquisition and image processing system able to optimize laser cladding process, in: *Proc. Third Int. Conf. Signal Process*. ICSP96, IEEE, Beijing, China,: pp. 1628–1631. https://doi.org/10.1109/ICSIGP.1996.571205.

[270] D. Becker, S. Boley, R. Eisseler, T. Stehle, H.-C. Möhring, V. Onuseit, M. Hoßfeld, T. Graf, (2021) Influence of a closed-loop controlled laser metal wire deposition process of S Al 5356 on the quality of manufactured parts before and after subsequent machining, *Prod. Eng*. 15 489–507. https://doi.org/10.1007/s11740-021-01030-w.

[271] M. Iravani-Tabrizipour, E. Toyserkani, (2007) An image-based feature tracking algorithm for real-time measurement of clad height, *Mach. Vis. Appl*. 18 343–354. https://doi.org/10.1007/s00138-006-0066-7.

[272] X. Zhang, W. Shen, V. Suresh, J. Hamilton, L.-H. Yeh, X. Jiang, Z. Zhang, Q. Li, B. Li, I.V. Rivero, H. Qin, (2021) In situ monitoring of direct energy deposition via structured light system and its application in remanufacturing industry, *Int. J. Adv. Manuf. Technol*. 116 959–974. https://doi.org/10.1007/s00170-021-07495-4.

[273] C. Stehmar, M. Gipperich, M. Kogel-Hollacher, A. Velazquez Iturbide, R.H. Schmitt, (2022) Inline Optical Coherence Tomography for Multidirectional Process Monitoring in a Coaxial LMD-w Process, *Appl. Sci*. 12 2701. https://doi.org/10.3390/app12052701.

[274] E.H. Glaessgen et al., (2021) NASA/NIST/FAA Technical Interchange Meeting on Computational Materials Approaches for Qualification by Analysis for Aerospace Applications, NASA/TM-20210015175, https://ntrs.nasa.gov/citations/20210015175

[275] AZO Sensors, An Introduction to Laser Triangulation Sensors, (n.d.).

[276] M. Liu, N. Senin, R. Su, R. Leach, (2022) Measurement of laser powder bed fusion surfaces with light scattering and unsupervised machine learning, *Meas. Sci. Technol*. 33 074006.

[277] ASTM Center of Excellence (CoE), NASA Marshall Space Flight Center, America Makes (2023) Strategic Guide: Additive Manufacturing In-Situ Technology Readiness. (Huntsville, AL), ASTM CoE Specialty Workshop. Available at https://amcoe.org/in-situtechnologyreadiness/ (Accessed 09/07/2024)

[278] ISO/ASTM TR 52906-EB: Additive Manufacturing—Nondestructive Testing—Intentionally Seeding Flaws in Metallic Parts. https://doi.org/10.1520/ISO/ASTMTR52906-EB

[279] Department of Energy, 2011, Technology Readiness Assessment Guide, https://www.directives.doe.gov/directives-documents/400-series/0413.3-Eguide-04a-admchg1/@@images/file

[280] Z. Chen, C. Han, M. Gao, S.Y. Kandukuri, K. Zhou, (2022) A review on qualification and certification for metal additive manufacturing, *Virtual Phys. Prototyp*. 17 382–405.

[281] H. Rieder, et al., (2014) Online monitoring of additive manufacturing processes using ultrasound. *Proceedings of the 11th European Conference on Non-destructive testing*, pp 2194-2201.

[282] H. Rieder H, et al., (2016) On- and offline ultrasonic characterization of components built by SLM additive manufacturing. *AIP Conference Proceedings* 1706(1):130002. https://doi.org/10.1063/1.4940605

[283] H. Sohn, P/ Liu, (2016) Non-contact laser ultrasonics for SHM in aerospace structures. *Structural Health Monitoring (SHM) in Aerospace Structures*, ed Yuan F-G (Woodhead Publishing), pp 325-352.

[284] M. Johansmann, G. Wirth (2012) Laser Doppler vibrometry for measuring vibration in ultrasonic transducers. *Ultrasonic Transducers*, ed Nakamura K (Woodhead Publishing), pp 277-313.

[285] S. Everton S, et al., (2018) Using Laser Ultrasound to Detect Subsurface Defects in Metal Laser Powder Bed Fusion Components. *JOM* 70(3):378-383. https://doi.org/10.1007/s11837-017-2661-7

[286] D. Pieris D, et al., (2020) Laser Induced Phased Arrays (LIPA) to detect nested features in additively manufactured components. *Materials & Design* 187:108412. https://doi.org/10.1016/j.matdes.2019.108412

[287] R.J. Smith, et al., (2014) Spatially resolved acoustic spectroscopy for rapid imaging of material microstructure and grain orientation. *Measurement Science and Technology* 25(5):055902. https://doi.org/10.1088/0957-0233/25/5/055902

[288] M.G. Somekh, G.A.D Briggss, C. Ilett (1984) The effect of elastic anisotropy on contrast in the scanning acoustic microscope. *Philosophical Magazine A* 49(2):179-204. https://doi.org/10.1080/01418618408234922

[289] R.J. Smith, et al., (2016) Spatially resolved acoustic spectroscopy for selective laser melting. *Journal of Materials Processing Technology* 236:93-102. https://doi.org/10.1016/j.jmatprotec.2016.05.005

[290] M. Hirsch, et al., (2017) Assessing the capability of in-situ nondestructive analysis during layer based additive manufacture. *Additive Manufacturing* 13:135-142. https://doi.org/10.1016/j.addma.2016.10.004

[291] O. Matsuda, et al., (2015) Fundamentals of picosecond laser ultrasonics. *Ultrasonics* 56:3-20. https://doi.org/10.1016/j.ultras.2014.06.005

[292] P. Liu, K. Yi, I. Jeon, H. Sohn (2021) Porosity inspection in directed energy deposition additive manufacturing based on transient thermoreflectance measurement. *NDT & E International* 122:102491. https://doi.org/10.1016/j.ndteint.2021.102491
[293] S-H. Park, et al., (2021) Mechanical properties estimation of additively manufactured metal components using femtosecond laser ultrasonics and laser polishing. *International Journal of Machine Tools and Manufacture* 166:103745. https://doi.org/10.1016/j.ijmachtools.2021.103745
[294] H. Sohn H, et al., (2022) Real-time porosity reduction during metal directed energy deposition using a pulse laser. *Journal of Materials Science & Technology* 116:214-223. https://doi.org/10.1016/j.jmst.2021.12.013
[295] H. Yoon, et al., (2022) Pulsed laser-assisted additive manufacturing of Ti-6Al-4V for in-situ grain refinement. *Scientific Reports* 12(1):22247. https://doi.org/10.1038/s41598-022-26758-y
[296] R.K.W. Vithanage, et al., (2022) Development of a phased array ultrasound roller probe for inspection of wire + arc additive manufactured components. *Journal of Manufacturing Processes* 80:765-774. https://doi.org/10.1016/j.jmapro.2022.06.045
[297] R. Zimermann, et al., (2022) Collaborative Robotic Wire + Arc Additive Manufacture and Sensor-Enabled In-Process Ultrasonic Non-Destructive Evaluation. *Sensors (Basel)* 22(11). https://doi.org/10.3390/s22114203
[298] N. Eschner, et al., (2020) Classification of specimen density in Laser Powder Bed Fusion (L-PBF) using in-process structure-borne acoustic process emissions. *Additive Manufacturing* 34:101324. https://doi.org/10.1016/j.addma.2020.101324
[299] T. Hauser, et al., (2022) Acoustic emissions in directed energy deposition processes. *The International Journal of Advanced Manufacturing Technology* 119(5):3517-3532. https://doi.org/10.1007/s00170-021-08598-8
[300] E. Todorov, P. Boulware, K. Gaah (2018) *Demonstration of array eddy current technology for real-time monitoring of laser powder bed fusion additive manufacturing process* (SPIE), Vol. 10599.
[301] M.A. Spurek, et al., (2022) In-situ monitoring of powder bed fusion of metals using eddy current testing. *Additive Manufacturing* 60:103259. https://doi.org/10.1016/j.addma.2022.103259
[302] K. Taherkhani, E. Sheydaeian, C. Eischer, M. Otto, E. Toyserkani, (2021) Development of a defect-detection platform using photodiode signals collected from the melt pool of laser powder-bed fusion, *Additive Manufacturing*. 46 102152. https://doi.org/10.1016/j.addma.2021.102152.
[303] P. Witherell, (2018) "Emerging Datasets and Analytics Opportunities in Metals Additive Manufacturing." In *Direct Digital Manufacturing Conference*.
[304] K. Bi, et al., (2021) "Additive manufacturing embraces big data." *Progress in Additive Manufacturing* 6: 181-197.
[305] D.B. Kim, P. Witherell, R. Lipman, and S. C. Feng. (2015) "Streamlining the additive manufacturing digital spectrum: A systems approach." *Additive Manufacturing* 5: 20-30.
[306] R. Bonnard, J-Y Hascoët, and P. Mognol. (2019) "Data model for additive manufacturing digital thread: State of the art and perspectives." *International Journal of Computer Integrated Manufacturing* 32, no. 12: 1170-1191.
[307] P. Witherell, et al., (2014) "Toward metamodels for composable and reusable additive manufacturing process models." *Journal of Manufacturing Science and Engineering* 136, no. 6.
[308] M.M. Francois, et al. (2017) "Modeling of additive manufacturing processes for metals: Challenges and opportunities." *Current Opinion in Solid State and Materials Science* 21, no. 4: 198-206.
[309] https://ammd.nist.gov/
[310] https://mmpds.org/
[311] S.S. Razvi, et al., (2019) "A review of machine learning applications in additive manufacturing." In *International design engineering technical conferences and computers and information in engineering conference*, vol. 59179, p. V001T02A040. American Society of Mechanical Engineers.
[312] Y. Gui, et al., (2022) "Detection, classification and prediction of internal defects from surface morphology data of metal parts fabricated by powder bed fusion type additive manufacturing using an electron beam." *Additive Manufacturing* 54: 102736.
[313] V.W.H. Wong, M. Ferguson, K.H. Law, Y.T.T. Lee, and P. Witherell, (2021). Automatic volumetric segmentation of additive manufacturing defects with 3D U-Net. *arXiv preprint arXiv:2101.08993*.
[314] L. Scime, D. Siddel, S. Baird, and V. Paquit. (2020) "Layer-wise anomaly detection and classification for powder bed additive manufacturing processes: A machine-agnostic algorithm for real-time pixel-wise semantic segmentation." *Additive Manufacturing* 36: 101453.
[315] J. Petrich, Z. Snow, D. Corbin, and E.W. Reutzel. (2021) "Multi-modal sensor fusion with machine learning for data-driven process monitoring for additive manufacturing." *Additive Manufacturing* 48: 102364.
[316] J. Zenisek, et al., (2022) "Machine learning based data stream merging in additive manufacturing." *Procedia Computer Science* 200: 1422-1431.
[317] G. Box, (1976) "Science and statistics." *Journal of the American Statistical Association* 71, no. 356: 791-799.
[318] Y. Qin, et al., (2019) "Status, comparison, and future of the representations of additive manufacturing data." *Computer-Aided Design* 111: 44-64.

[319] M. Seifi, A. Salem, J. Beuth, O. Harrysson, J.J. Lewandowski, (2016) Overview of materials qualification needs for metal additive manufacturing. *JOM*. 68(3):747-64.

[320] R. Russell, et al., (2019) Qualification and certification of metal additive manufactured hardware for aerospace applications. *Additive Manufacturing for the Aerospace Industry*, 33-66**,** doi:10.1016/B978-0-12-814062-8.00003-0.

[321] Marshall Space Flight Center (2017) *MSFC-SPEC-3717 (2017), Specification for control and qualification of laser powder bed fusion metallurgical processes* (MSFC, Huntsville, AL). Available at https://www.nasa.gov/sites/default/files/atoms/files/msfcspec3717baseline.pdf.

[322] Marshall Space Flight Center (2017) MSFC-STC-3716 (2017), Standard for additively manufactured spaceflight hardware by laser powder bed fusion in metals, (MSFC, Huntsville, AL).

[323] SAE International (1999) *SAE AS 9100 (1999) Quality Systems – Aerospace – Model for Quality Assurance in Design, Development, Production, Installation and Servicing* (Warrendale, PA). Available at https://www.sae.org/standards/content/as9100/

[324] National Aeronautics and Space Administration (2021) *NASA-STD-6030 (2021) Additive Manufacturing Requirements for Spaceflight Systems* (NASA, Washington, D.C.). https://standards.nasa.gov/standard/NASA/NASA-STD-6030

[325] Aerospace Industries Association (2020), *Recommended guidance for certification of AM component* (AIA, Arlington, VA). Available at https://www.aia-aerospace.org/wpcontent/uploads/2020/02/AIA-Additive-Manufacturing-Best-Practices-Report-Final-Feb2020.pdf

[326] U.S. Food and Drug Administration (2017), *Technical considerations for additive manufactured medical devices – Guidance for industry and food and drug administration staff* (FDA, Silver Spring, MD). Available at https://www.fda.gov/regulatory-information/search-fdaguidance-documents/technical-considerations-additive-manufactured-medicaldevices

[327] American Petroleum Institute (2012) *API STD 20S Additively Manufactured Metallic Components for Use in the Petroleum and Natural Gas Industries,* American Petroleum Institute, Washington, D.C.). Available at http://apiwebstore.org/standards/20S

[328] ASTM Committee E07 Nondestructive Testing. Available at https://www.astm.org/get-involved/technical-committees/committee-e07/subcommittee-e07

[329] ASTM International (2020) *ASTM E3166-20e1* Standard Guide for Nondestructive Examination of Metal Additively Manufactured Aerospace Parts After Build (ASTM International West Conshohocken, PA).

[330] J. Mazumder, (2015) Design for metallic additive manufacturing machine with capability for "Certify as you build," *Procedia CIRP* 36, 187-192

[331] L.P. Swiler, et al,. (2018) Data analysis for the Born Qualified LDRD project, Sandia report SAND2018-11244. https://www.osti.gov/servlets/purl/1481602

[332] S.A. Motaman, et al., (2020) Optimal design for metal additive manufacturing: an integrated computational materials engineering (ICME) approach. *JOM*. 72(3):1092-104

[333] A. Huning, et al., (2022) Advancement of Certification Methods and Applications for Industrial Deployments of Components Derived from Advanced Manufacturing Technologies, ORNL/TM-2022/2654

[334] S. Clijsters, et al. (2014) In situ quality control of the selective laser melting process using a high-speed, real-time melt pool monitoring system. *Int J Adv Manuf Technol* 75, 1089–1101. https://doi.org/10.1007/s00170-014-6214-8

[335] Q. Y. Lu and C. H. Wong (2018) Additive manufacturing process monitoring and control by non-destructive testing techniques: challenges and in-process monitoring, *Virtual and Physical Prototyping*, 13:2, 39-48, DOI: 10.1080/17452759.2017.1351201

[336] L. Scime, et al., (2020) Report on progress of in-situ and ex-situ data and the use of artificial intelligence to predict defects, ORNL/TM-2020/1748.

[337] M.D. Wilkinson, et al., (2016). The FAIR Guiding Principles for scientific data management and stewardship. *Scientific Data*, 3, Article 160018

[338] JCGM 200 (2012) International vocabulary of metrology – Basic and general concepts and associated terms (VIM) (ISO/IEC Guide 99), 3rd ed., Joint Committee for Guides in Metrology, BIPM.

[339] D. Deisenroth, et al., (2021) Measurement Uncertainty of Surface Temperature Distributions for Laser Powder Bed Fusion Processes, *Journal of Research of the National Institute of Standards and Technology*, v126, Article number 126013. https://doi.org/10.6028/jres.126.013

[340] L. Schild, et al., (2019) Uncertainty Evaluation of Pore Analysis for Additively Manufactured Parts using Cross Sections, *9th Conference on Industrial Computed Tomography, Padova, Italy (iCT 2019)*.